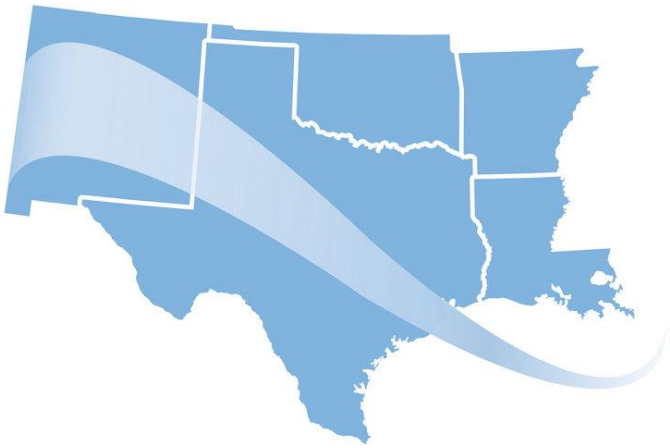

SOUTHERN PLAINS
TRANSPORTATION CENTER

Impact of Severe Drought on the Compacted Expansive Clays (Subgrade) in Northern Louisiana

JAY X. WANG, Ph.D., P.E.
MD ADNAN KHAN, Ph.D., EIT
BERJEES ANISA IKRA, M.S.

SPTC14.1-76-F

Southern Plains Transportation Center
201 Stephenson Parkway, Suite 4200
The University of Oklahoma
Norman, Oklahoma 73019

DISCLAIMER

The contents of this report reflect the views of the authors, who are responsible for the facts and accuracy of the information presented herein. This document is disseminated under the sponsorship of the Department of Transportation University Transportation Centers Program, in the interest of information exchange. The U.S. Government assumes no liability for the contents or use thereof.

TECHNICAL REPORT DOCUMENTATION PAGE

1. REPORT NO.	2. GOVERNMENT ACCESSION NO.	3. RECIPIENTS CATALOG NO.
SPTC 14.1-76		

4. TITLE AND SUBTITLE	5. REPORT DATE
Impact of Severe Drought on the Compacted Expansive Clays (Subgrade) in Northern Louisiana	July 31, 2017
	6. PERFORMING ORGANIZATION CODE

7. AUTHOR(S)	8. PERFORMING ORGANIZATION REPORT
Jay X. Wang, Ph.D., P.E. Md Adnan Khan, Ph.D., EIT Berjees Anisa Ikra, M.S.	

9. PERFORMING ORGANIZATION NAME AND ADDRESS	10. WORK UNIT NO.
Programs of Civil Engineering and Construction Engineering Technology Louisiana Tech University 600 Dan Reneau Dr., Ruston, LA 71272	11. CONTRACT OR GRANT NO.

12. SPONSORING AGENCY NAME AND ADDRESS	13. TYPE OF REPORT AND PERIOD COVERED
Southern Plains Transportation Center 201 Stephenson Pkwy, Suite 4200 The University of Oklahoma Norman, OK 73019	FINAL MAY 2015 - MAY 2017
	14. SPONSORING AGENCY CODE

15. SUPPLEMENTARY NOTES

University Transportation Center

16. ABSTRACT

Understanding unsaturated expansive soil has always been a major challenge for soil scientists and engineers. Due to presence of high quantity of montmorillonite mineral in the Moreland clay in northern Louisiana, structural damage due to soil heave/shrinkage has always been a key concern for geotechnical engineers. In this research, a state-of-the-art characterization of the Moreland clay is presented. It includes the identification of its swell-shrink properties, soil index property measurement, plotting of the soil water characteristics curve (SWCC) to understand the water retention capacity of the clay, development of an empirical equation for its unsaturated shear strength, establishment of its three-dimensional constitutive surface, and the soil heave predictions. The characterization indicated that the Moreland Clay is highly expansive.

An analytical method is developed to analyze the heave/shrinkage-induced stresses in pavement. To get the closed-form solutions, a virtual load concept is proposed to analyze a pavement that is assumed as a beam resting on expansive soil, integrating the heave/shrinkage of expansive soil in the Winkler's soil model. Field observations from a country road in Texas on expansive soil indicated that initiation and propagation of the cracks in the road had a good match with the location where the maximum bending moment was found. Preliminary results have demonstrated that the closed-form solutions could provide a reliable prediction for the bending moment and shear force in the pavement. As compared with the finite element models, the analytical model is significantly simple and more easily implemented. All the equations and calculations are incorporated in the Excel spreadsheet, which is easily handled in pavement design.

In this research, expansive soil stabilization is investigated by employing geo-polymer concrete (GPC) and cement as stabilizers, respectively. Three batches of the soil were stabilized with GPC (5-20%) to establish a base line. Results were then compared with the soil stabilized using one batch of cement (10%). It was concluded that even though cement is by far the best soil stabilizer the application of higher percentage of GPC, a satisfactory level of soil stabilization can be achieved as well.

17. KEY WORDS	18. DISTRIBUTION STATEMENT
Expansive soil, Moreland clay, Louisiana, Characterization, SWCC, Constitutive surface, Pavement, Winkler's soil model, Virtual load, Closed-form solution, Excel spread sheet.	No restrictions. This publication is available at www.sptc.org and from the NTIS.

19. SECURITY CLASSIF. (OF THIS REPORT)	20. SECURITY CLASSIF. (OF THIS PAGE)	21. NO. OF PAGES	22. PRICE
Unclassified	Unclassified	118 + cover	

SI* (MODERN METRIC) CONVERSION FACTORS

APPROXIMATE CONVERSIONS TO SI UNITS

SYMBOL	WHEN YOU KNOW	MULTIPLY BY	TO FIND	SYMBOL
		LENGTH		
in	inches	25.4	millimeters	mm
ft	feet	0.305	meters	m
yd	yards	0.914	meters	m
mi	miles	1.61	kilometers	km
		AREA		
in^2	square inches	645.2	square millimeters	mm^2
ft^2	square feet	0.093	square meters	m^2
yd^2	square yard	0.836	square meters	m^2
ac	acres	0.405	hectares	ha
mi^2	square miles	2.59	square kilometers	km^2
		VOLUME		
fl oz	fluid ounces	29.57	milliliters	mL
gal	gallons	3.785	liters	L
ft^3	cubic feet	0.028	cubic meters	m^3
yd^3	cubic yards	0.765	cubic meters	m^3
		NOTE: volumes greater than 1000 L shall be		
		MASS		
oz	ounces	28.35	grams	g
lb	pounds	0.454	kilograms	kg
T	short tons (2000 lb)	0.907	megagrams (or "metric ton")	Mg (or "t")
		TEMPERATURE (exact degrees)		
^oF	Fahrenheit	5 (F-32)/9 or (F-32)/1.8	Celsius	^oC
		ILLUMINATION		
fc	foot-candles	10.76	lux	lx
fl	foot-Lamberts	3.426	$candela/m^2$	cd/m^2
		FORCE and PRESSURE or STRESS		
lbf	poundforce	4.45	newtons	N
lbf/in^2	poundforce per square inch	6.89	kilopascals	kPa

APPROXIMATE CONVERSIONS FROM SI UNITS

SYMBOL	WHEN YOU KNOW	MULTIPLY BY	TO FIND	SYMBOL
		LENGTH		
mm	millimeters	0.039	inches	in
m	meters	3.28	feet	ft
m	meters	1.09	yards	yd
km	kilometers	0.621	miles	mi
		AREA		
mm^2	square millimeters	0.0016	square inches	in^2
m^2	square meters	10.764	square feet	ft^2
m^2	square meters	1.195	square yards	yd^2
ha	hectares	2.47	acres	ac
km^2	square kilometers	0.386	square miles	mi^2
		VOLUME		
mL	milliliters	0.034	fluid ounces	fl oz
L	liters	0.264	gallons	gal
m^3	cubic meters	35.314	cubic feet	ft^3
m^3	cubic meters	1.307	cubic yards	yd^3
		MASS		
g	grams	0.035	ounces	oz
kg	kilograms	2.202	pounds	lb
Mg (or "t")	megagrams (or "metric ton")	1.103	short tons (2000 lb)	T
		TEMPERATURE (exact degrees)		
^oC	Celsius	1.8C+32	Fahrenheit	^oF
		ILLUMINATION		
lx	lux	0.0929	foot-candles	fc
cd/m^2	$candela/m^2$	0.2919	foot-Lamberts	fl
		FORCE and PRESSURE or STRESS		
N	newtons	0.225	poundforce	lbf
kPa	kilopascals	0.145	poundforce per square inch	lbf/in^2

*SI is the symbol for the International System of Units. Appropriate rounding should be made to comply with Section 4 of ASTM E380. (Revised March 2003)

ACKNOWLEDGMENTS

The research presented in this report was sponsored by the Southern Plains Transportation Center (SPTC) under contract No. SPTC14.1-76. The authors would like to express their gratitude to Mr. Harold "Skip" Paul of former LTRC director, Mr. Daniel Thompson at Aillet, Fenner, Jolly & McClelland, Mr. Gary Hubbard at Greater Bossier Economic Development Foundation, and Shams Arafat at Louisiana Tech University for their assistances in collecting boring logs, locating soil sampling sites, and taking soil samples.

IMPACT OF SEVERE DROUGHT ON THE COMPACTED EXPANSIVE CLAYS (SUBGRADE) IN NORTHERN LOUISIANA

Final Report

July 2017

Jay X. Wang, Ph.D., P.E.

Md Adnan Khan, Ph.D., EIT

Berjees Anisa Ikra, M.S.

Southern Plains Transportation Center

201 Stephenson Pkwy, Suite 4200

The University of Oklahoma

Norman, OK 73019

Table of Contents

List of Figures

List of Tables

EXECUTIVE SUMMARY

Highways in Louisiana have been affected by the widely spread expansive soils. In north Louisiana especially, pavements often get longitudinal cracks due to the expansive subgrade soil. In this SPTC-sponsored research project, one of the major types of expansive soils, which is called the Moreland clay, is investigated to understand the swell-shrink properties. The research started with the characterization of the Moreland clay by performing a series of laboratory tests. As a by-product, a GIS-based swelling potential map of expansive soil in Louisiana is developed. It is concluded from the characterization that the Moreland clay is one of the most expansive soils in the world.

In the research, an easily implementable model is developed based on the theory of beam on elastic foundation, in which the mechanism of soil strength mathematically considered. The predicted heave or shrinkage of expansive soils below a pavement is integrated in the model as the beam deflection. In the proposed method, pavement is simplified as a beam with a virtual load expressed in a form of Fourier series applied on top of the beam to mimic the heave/settlement caused by the volume change of expansive soils. The virtual load is determined by making the predicted subgrade soil heave/settlement equal to the beam deflection. Finally, a closed-form solution of the beam's deflection, rotation, bending moment and shear force is developed. The deflection is caused by the heave/shrinkage of the expansive soil below the pavement. Field observations from a country road (FM 2) on expansive soil in Texas indicated that initiation and propagation of the cracks in the road had a good match with the location where the maximum bending moment is found. Compared with the traditional finite element models, the analytical model is significantly simpler and more easily implemented. The closed-form solutions make pavement stress analyses and soil heave predictions separate. All the equations and calculations are incorporated in the Excel spreadsheet. The Excel-based software package will be the only required tool for design calculations. As a part of the expansive soil research, using different soil stabilizers (e.g., geopolymer cement (GPC) and cement) to stabilize the expansive soil is also investigated. It may be concluded that cement is a better soil stabilizer than GPC. However, the application of higher percentage of GPC, a satisfactory level of soil stabilization can be achieved as well.

1. INTRODUCTION

Moisture in the expansive clay soil has been the cause of distress for engineers for many years. For the geotechnical engineers, it is the constant worry about the uplift of expansive soil on the foundation by the soil's volume change, where for the pavement engineers the concern is about the longitudinal cracks of pavements if placed on expansive subgrade. For years, the north Louisiana has been suffering because of the presence of Moreland clay in abundance. Moreland clay is well known for its expansive in nature which is one of the major reasons for the structural and pavement damage in the north Louisiana. In this study, a comprehensive understanding of swell-shrink properties of expansive soil and its implication on causing pavement stress and finally a solution to this problem tried to be find out.

1.1 EXPANSIVE SOIL- THE HIDDEN DISASTER

Expansive soil refers to any soil whose volume can change significantly when its moisture content varies. Generally, when expansive soil gets wet its volume increases and when it dries it shrinks. Because of its seasonal volume change it might create structural failure, if not considered during the design of the structure. Many researchers tried to find the consequences of expansive soil on structures. Jones and Holtz (1973) reported that, in the United States alone, "each year, shrinking and swelling soils inflict at least $2.3 billion in damages to houses, buildings, roads, and pipelines more than twice the damage from floods, hurricanes, tornadoes, and earthquakes!". They also concluded that 60% of the new houses built in the United States will experience minor damage during their useful lives and 10% will experience significant damage some beyond repair. Krohn and Slosson (1980) estimated that $7 billion is spent each year in the United States as a result of damage to all types of structures built on expansive soils. Snethen (1986) stated: "While few people have ever heard of expansive soils and even fewer realize the magnitude of the damage they cause, more than one fifth of American families live on such soils and no state is immune from the problem they cause. Expansive soils have been called the 'hidden disaster': while they do not cause loss of life, economically these soils have become one of the United States costliest natural hazards". Fredlund (1979) mentioned there are two main reasons behind the development for unsaturated soils: (1) Insufficient science with theoretical background. The stress condition and mechanics involved in an unsaturated expansive soil did not properly understood and (2) financial recovery for engineers seems insufficient.

Especially in expansive soil the possible liability to the engineer is often large relative to the financial remuneration. Consultants might find other areas of geotechnical engineering more profitable. To have more structurally sound and economical design is possible if volume change behavior of expansive soil can be reliably estimated (Fredlund 1979; Fredlund *et al.* 2012).

1.2 BACKGROUND

Expansive soil is considered as one of the most common causes of pavement and/or building distresses. Depending upon the moisture content level, expansive soil will experience changes in volume due to moisture fluctuations from seasonal variations (Al-Homoud *et al.* 1995; Chen 1975; Erzin and Erol 2007; Groenevelt and Grant 2004; Ng *et al.* 2003; Nwaiwu and Nuhu 2006; Post Tensioning Institute 2008; Zhan *et al.* 2007). During periods of high moisture content expansive soil swells underneath the pavement structure and during periods of very dry season soil shrinks and reduces its volume. These cycles of swell and/or shrinkage can lead to highway pavement cracking. The effect also has negative impact on shallow foundation of buildings. If the soil underneath the concrete slab experiences a change in volume, the slab will distort into either a center lift mode (sometimes termed as edge drying) or an edge lift mode (also termed as edge drying) (Post Tensioning Institute 2008). In many places of northern Louisiana, there is a presence of expansive soil with high groundwater table (GWT) (Dhakal 2009).

Louisiana Department of Transportation and Development (LADOTD)/Louisiana Transportation Research Center (LTRC) conducted or sponsored a few research projects relevant to expansive soil, and the special treatments of weak/flexible base and subgrade soil. Notable research included laboratory correlation of soil swelling potential, various techniques to stabilize soil, and usage of geogrid in flexible pavements to compensate the heave of soil (Abu-Farsakh *et al.* 2012; Abu-Farsakh and Nazzal 2009; Melancon 1979; Rupnow *et al.* 2011; Wang 2002; Wu *et al.* 2011). Literature review revealed that the research for swelling/shrinkage of Louisiana expansive clay has not been remarkably performed. A comprehensive characterization of northern Louisiana's expansive soil and its heave potential has not been well addressed or corresponding research has not been well documented in Louisiana.

1.3 OBJECTIVES

1. A complete understanding of the swell-shrink properties of the Moreland clay is acquired. A series of regular soil experiments and experiments which are exclusive for the expansive soil are performed. Using the experimental results, the constitutive surface of the Moreland clay is developed which will give a better understanding of its volume change behavior.
2. It is necessary to understand the distributions of the Moreland clay and other expansive soils in Louisiana and their degrees of free potential heaves. A state-of-the art GIS map of Louisiana's soil map based on the swelling potential is produced.
3. An analytical model is developed to predict heave/shrinkage-induced stresses on pavement, which frequently cause cracks in pavement. As compared with the finite element models, the developed analytical model is significantly simple and more easily implemented. All the equations and calculations are incorporated in the Excel spreadsheet, which is easily implementable in pavement design.
4. As a remedy of expansive soil's volume change stabilizing with geopolymer cement (GPC) is evaluated. A series of stabilized soil samples are tested with different concentrations of GPC and cement, and under different curing time.

1.4 SCOPE

The project began with a literature review to search for any documents recording the knowledge of the expansive soils in northern Louisiana, and methods that are being used to analyze and design pavements on expansive subgrades by engineers around the world. Then as the second step, rich expansive soil sites were identified and located around Bossier city near Shreveport with the help received from local industry. Expansive soil samples (disturbed and undisturbed) were acquired, and transported to the Geotechnical Lab at Louisiana Tech University. Various laboratory tests were conducted to characterize the expansive soil, and practical methods to predict soil heaves under pavement were identified. Soil stabilization was studied as well using geopolymer cement (GPC) as the stabilizer. Finally, a mathematical model was developed to analyze the induced stress in pavement that are caused by the heave or shrinkage of expansive soils underlying the pavement. Through the entire research project, in-situ field sampling and

laboratory experiments were performed. Research effort was also focused on experimental data analyses and mathematical model development.

1.5 TECHNOLOGY TRANSFER

From the very beginning, the research team has stayed closely with Louisiana Transportation Research Center (LTRC), and/or Louisiana Department of Transportation and Development (LADOTD) for special helps in the duration of the project, such as field monitoring and testing data. Local industry has been contacted to identify the location of the Moreland expansive clay sites. Presentations to disseminate the preliminary and final achievements have been made in LTRC/LADOTD and international conferences to find potential application of the research achievements. The potential technology implementation in industry will be implemented together with the LTRC/LADOTD engineers if a need comes up. If necessary, a detailed steps and sample calculations will be documented for the easy deployment of the achieved results. Partial results were presented in November 2016 at the second Climate Conference at the SPTC at Norman, Oklahoma. Conference and journal papers have been published, reviewed or prepared.

2. DEVELOPMENT OF THE EXPANSIVE SOIL MAP OF LOUISIANA

Locating expansive soil is a key step for a successful design and construction of any highway pavements through the expansive soil area. There have been some expansive soil maps available in the USA (Olive *et al.* 1989; Snethen *et al.* 1975; Tourtelot 1973). In 1990, LTRC, along with Louisiana Tech University developed an expansive soil distribution map for Louisiana (Burns *et al.* 1990). These early maps only showed locations of expansive soils, but never indicated degrees of their potential expansion or heave. In engineering design, which requires an elaboration of the knowledge of the expansive soil below the pavement to be constructed, a map would be helpful to include not only the location, but a numerical value to understand the severity of the expansive soil that is being dealt with. For this purpose, a state-of-the-art expansive soil map based on its heave potential was created using the ArcGIS software. One of

the simplest ways to measure the severity of swelling potential is to calculate the swelling potential index (SP) from the plasticity index (PI) as described in Eq. 1 (Seed *et al.* 1962).

$$SP = 0.00216 * PI^{2.44} \quad (1)$$

The PI is especially useful when soil data are very limited. Fundamental soil data including the PI values from website of the United States Department of Agriculture (USDA) were for found for any location in the USA (USDA 2013). To plot the contour map of potential swelling over the state of Louisiana, one data set was obtained from the USDA website for each of the 64 parishes (counties) in Louisiana. Fig. 1 shows the degrees of soil expansion over Louisiana in terms of the plotted swelling potential (SP) contours. It shows that the soil expansion issue in southern Louisiana is more severe than in northern Louisiana. However, it must be noted that Eq. 1 was developed to measure the swell potential with the moisture content increased from the optimum moisture content (W_{OPT}) to the saturated moisture content (W_{SAT}). As in most cases the in-situ moisture content is not the optimum in southern Louisiana. For example, from Fig. 1 the swelling potential in New Orleans is around 50%. However, due to the high ground water table, the soil in New Orleans most likely has a moisture content above its W_{OPT}, which implies that the soil has already achieved most of its heave potential. Interpretation of Fig. 1 should be done very carefully and engineering judgment should be applied. The objective to plot Fig. 1 is not to give a real measurement of soil heave, but to have a general idea regarding the distribution of expansive soils based on swelling degree in Louisiana.

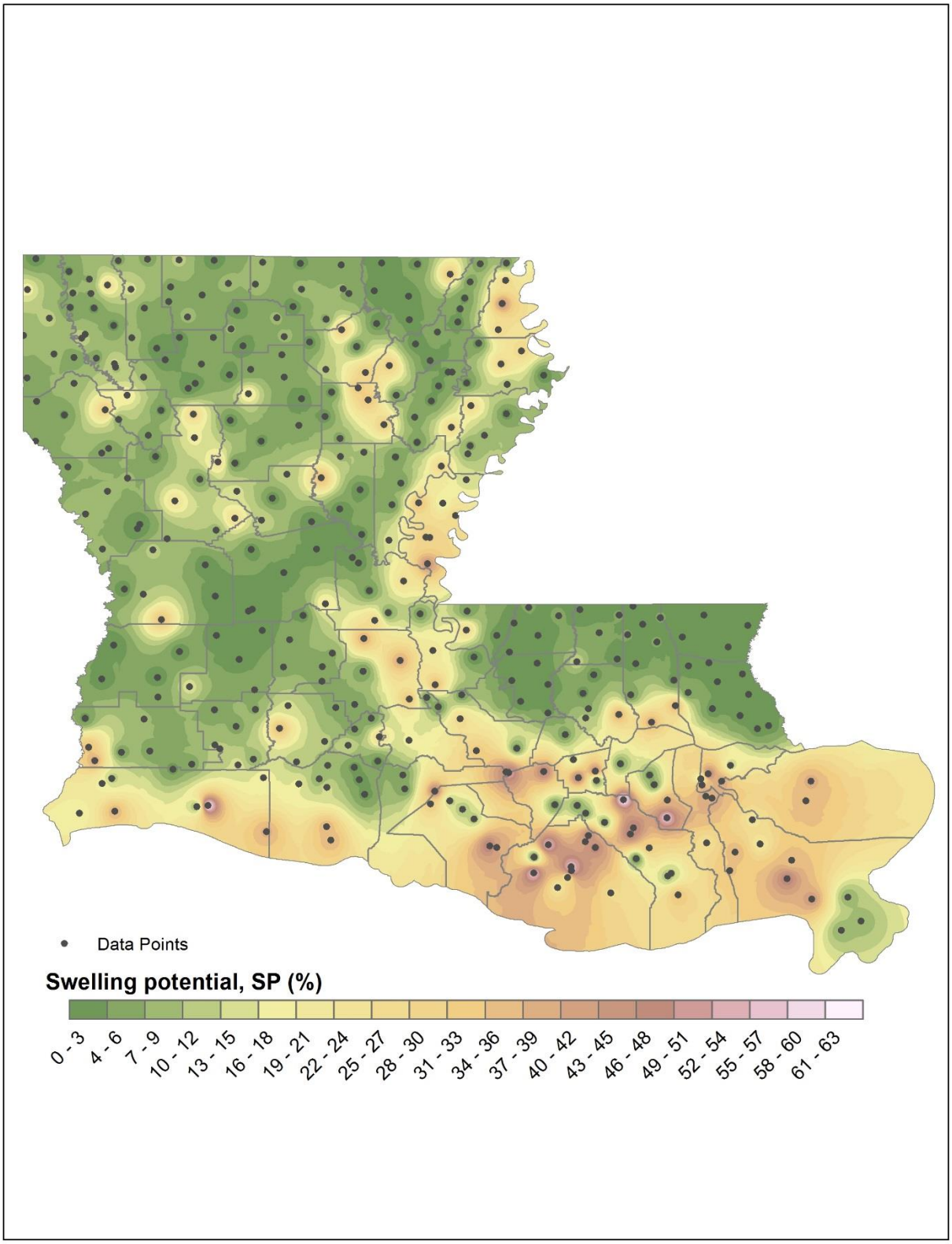

Figure 1 SP Map of Louisiana (Ikra 2017a, adapted from Khan 2017)

In this research, the main focus is on Moreland Clay which is found mostly in northern part of Louisiana, some parts in Arkansas and Oklahoma. According to USDA soil taxonomy classification it is Moreland clay which is very fine, Very-fine, smectitic, thermic Oxyaquic Hapluderts, very poor as construction and road fill materials and expansive in nature. The USDA website also shows detail information about the location and distribution of Moreland clay in the USA. Of the total 4872710 acres of Moreland clay, Table 1 shows the distribution of Moreland clay by each Parish/County in these three states (USDA 2013). Fig. 2 shows the mapping of these areas which was produced using the "websoil survey" tool in the USDA website.

Table 1 Distribution of Moreland clay in USA

Soil Survey Area	Soil Acres	Soil Survey Area	Soil Acres
Avoyelles Parish, LA	116293	Perry County, AR	3081
Rapides Parish, LA	99700	Wagoner County, OK	2677
Natchitoches Parish, LA	86815	DeSoto Parish, LA	2602
Caddo Parish, LA	43580	Catahoula Parish, LA	1672
Bossier Parish, LA	31781	Yell County, AR	1429
Red River Parish, LA	26548	Winn Parish, LA	1384
Grant Parish, LA	16687	Logan County, AR	1241
Evangeline Parish, LA	12727	Pope County, AR	1122
Pulaski County, AR	11985	Johnson County, AR	789
Conway County, AR	10046	Franklin County, AR	595
LeFlore County, OK	5716	Bienville Parish, LA	327
Faulkner County, AR	4400	West Feliciana Parish, LA	225
Lonoke and Prairie Counties, AR	3845	East Feliciana Parish, LA	4

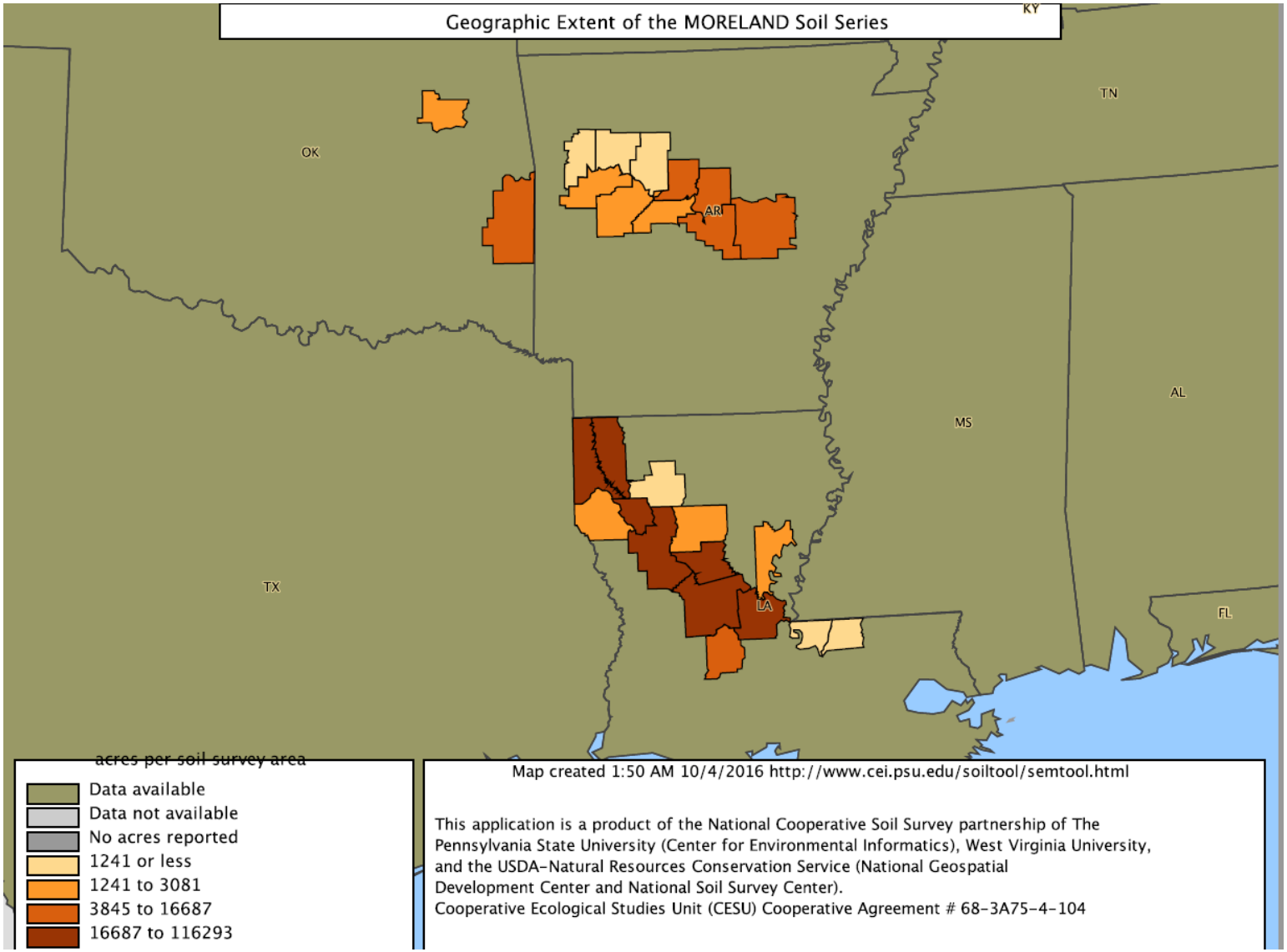

Figure 2 The Moreland Clay Map of Louisiana

3. FIELD INVESTIGATION, LABORATORY EXPERMIENTS AND DATA ANALYSIS

3.1 INTRODUCTION

In order to investigate the structural damage by expansive Moreland clay, its expansive nature has to be investigated first. Soil property including the regular soil tests and tests which are done exclusively for the expansive soil has been performed. After a brief discussion with the local engineers and field visits buildings and pavements in Caddo Parish and Bossier Parish found being suffered a lot due to the Moreland clay. Figs. 3 and 4 shows some of the catastrophic damages to pavements and structures in that region. Fig. 3 was taken from the "The Pentecostals of Bossier City" church in Bossier City and Fig. 4 was taken from Tacoma Boulevard road in Caddo Parish which is close to the church. Interestingly, the Tacoma Boulevard road is a geosynthetic-reinforced road which is still suffering from its subgrade expansive soil. Once the initial investigation is complete to get the Moreland clay samples from Bossier parish of northern Louisiana a permitted site was selected near road I-220, next to the Pentecostals of Bossier City church as illustrated in Fig. 5. To make sure the soil is the Moreland clay even before the lab experiments, the USDA "websoil survey" was used. Fig. 6 was produced using the "websoil survey" tool and it clearly marked the site location as "MoA" which is the Moreland clayey soil.

(a) (b)

Figure 3 (a) Structural damage in the slab column joint (b) closed-up picture of the crack

Figure 4 Longitudal cracks in roads in Caddo Parish, LA

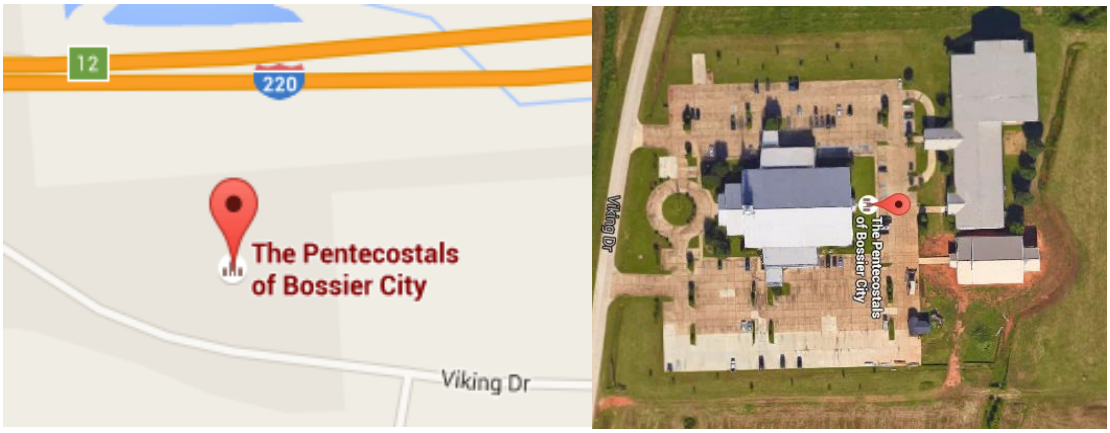

Figure 5 Location of the soil sampling site using google map

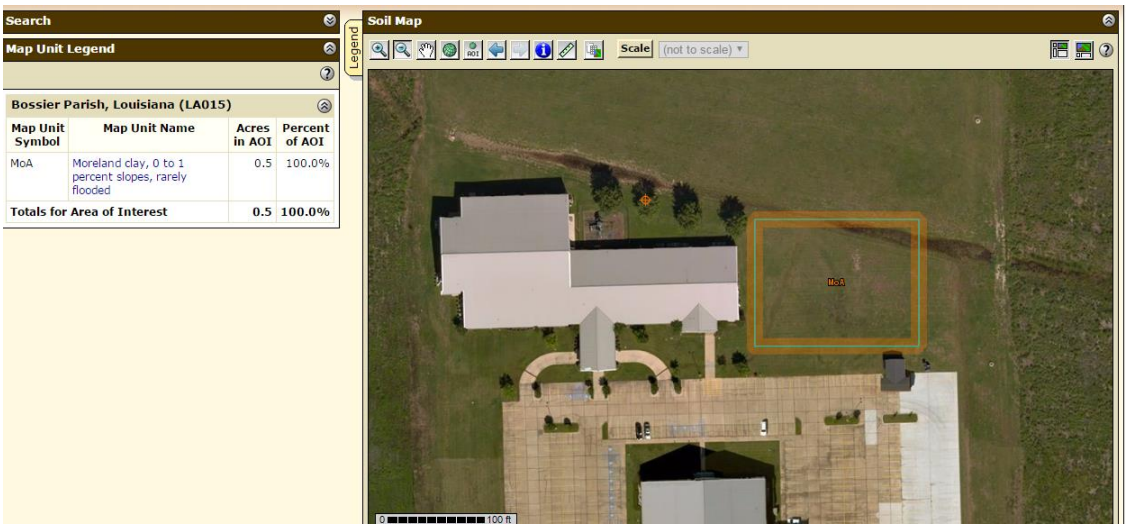

Figure 6 Soil investigation using USDA web soil survey tool

3.2 ENGINEERING IDENTIFICATION PROCESS OF EXPANSIVE SOIL

To understand the volume change intensity of an expansive soil engineers and researchers around the world tried to relate expansivity of a soil with its experimentally found geotechnical index properties. There are couples of ways to identify expansiveness of clay soils. The most notable one can be based on any of the following laboratory tests: 1) the plasticity index test; 2) the free swell test; 3) the potential volume change test, the expansion index test (EI); 4) the coefficient of linear extensibility (COLE) test; 5) the standard absorption moisture content (SAMC) test; 6) the cation exchange capacity (CEC) test; 7) the specific surface area (SSA) test, and 7) the total potassium (TP) test (Nelson *et al.* 2015). In this research project results from the plasticity index test and the expansion index test are used to identify expansive soils.

Table 2 The Expansion Potential of Soil Based on the Plasticity Index (Peck *et al.* 1974)

Plasticity Index, PI (%)	**Expansion Potential**
0-15	Low
0-35	Medium
20-55	High
> 35	Very High

Table 3 The Skempton Classification of Expansive Soil (Skempton 1953)

Activity (A_C)	**Soil Type**
< 0.75	Inactive
0.75 – 1.25	Normal
> 1.25	Active

Table 4 Expansion Potential Based on the Expansion Index (Uniform Building Code 1997)

Expansion Index, EI	Expansion Potential
0-20	Very Low
21-50	Low
51-90	Medium
91-130	High
Above 130	Very High
Note: Table 29-C from the Uniform Building Code and Standards (1991)	

3.3 SOIL SAMPLING

Expansive soil samples were collected from the open pit at the church construction site in Bossier city, Louisiana, which was shown in Fig. 6. Hand auger and Shelby tube samplers were used to retrieve the soil samples. Disturbed soil samples were obtained in accordance with ASTM D1452-09 (ASTM 2009) and undisturbed soil samples obtained following ASTM D1587/D1587M-15 (ASTM 2015). The samples were retrieved in sealed container and transported to the Geotechnical Engineering Laboratory at Louisiana Tech University.

3.4 LABORATORY EXPERMIENTS

Laboratory experiments were done following ASTM standard and other suggested methods. To understand the volume change behavior of expansive soil, both the load induced and moisture content change induced volume change was measured. This gave the most comprehensive understanding of Moreland clay swell-shrink behavior.

3.4.1 GENERAL PROPERTIES

The average initial void ratio was 1.27, the activity was 1.37, liquid limit (LL) 79, plasticity index (PI) 51 with a field moisture content 32%, and a saturated moisture content 52% (ASTM 2010a; ASTM 2010b).

3.4.2 SPECIFIC GRAVITY (G_S)

The specific gravity was measured following ASTM D854-14 and it was found to be 2.75 (ASTM 2014).

3.4.3 SIEVE ANALYSIS

Using ASTM D422-63 the grain size distribution was performed. The soil was found extremely fine with 99% passing the 0.075mm sieve (#200) (ASTM 2007). Skempton (1953) provided a relationship between plasticity index and clay fraction (< 2 micron) for different soils. Among the soils, the closest soil to Louisiana's fat clay was chosen and with its Skempton (1953) provided relationship the activity was found to be 1.27.

3.4.4 SOIL CLASSIFICATION

Soil classification was completed using the Unified Soil Classification System (ASTM D2487-11) and the soil was classified as Fat Clay (CH) (ASTM 2011b).

3.4.5 STANDARD PROCTOR TEST

The soil compaction tests were conducted according to ASTM D698-12 (Method A) (Materials 2012) using the standard compactive effort. A known quantity of water was added to a known amount of clay and the mix was covered using plastic wrap. The mix was compacted in three layers using 25 blows per layer in the mold after an equilibration time of about 24 h. The gravimetric water content (w) was determined by ASTM D2216-10 (ASTM 2010a) and used in conjunction with the measured sample weight and volume to determine the dry density (ρ_d) using the basic weight-volume relationships. From Fig. 7 it was found the maximum dry density is 14.52 kN/m^3 and optimum moisture content is 27%. The optimum moisture content is within the range of ±5% of the plastic limit (Marinho and Oliveira 2012), which can be used to verify the plastic limit result.

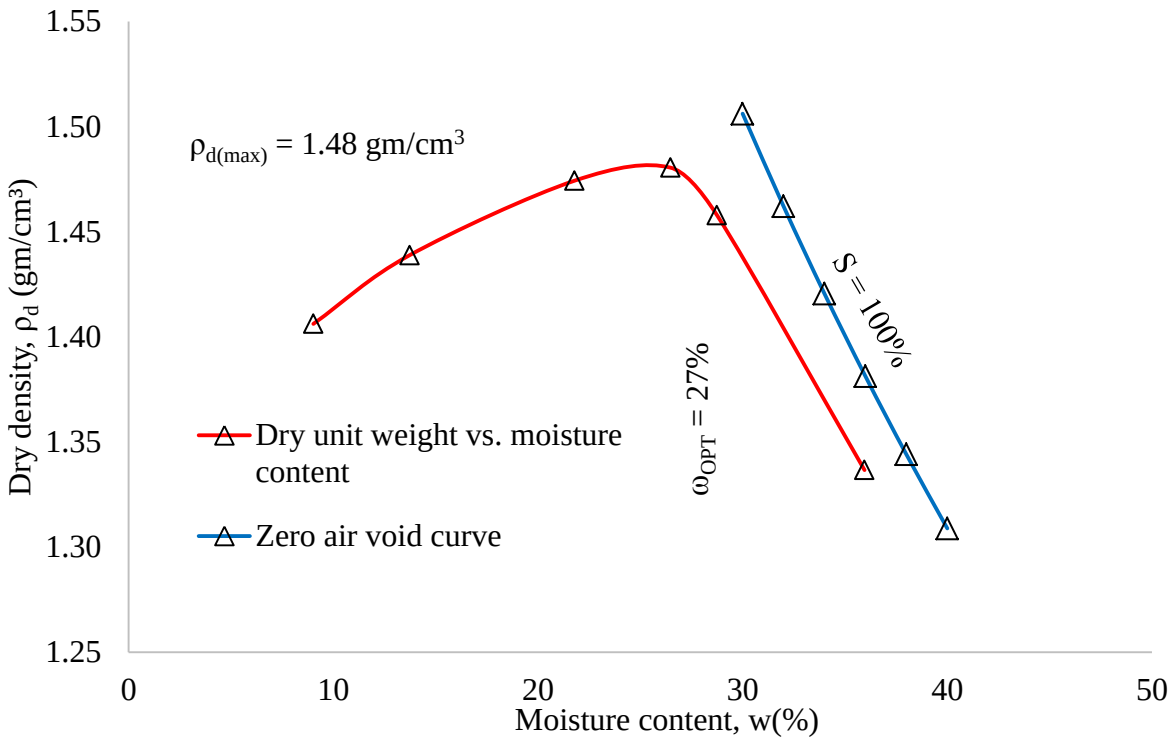

Figure 7 The dry unit weight vs. moisture content curve

3.4.6 SOIL WATER CHARACTERISTIC CURVE (SWCC)

The SWCC defines the relationship between soil water retention and soil suction. The SWCC is used to determine the unsaturated soil property functions as it refers to the potential energy state of water in soil (Fredlund *et al.* 2012; Jury *et al.* 1991). In-depth soil test showed a strong correlation between unsaturated soil properties with the SWCC. It has been a very common practice to predict any unsaturated soil property empirically using the SWCC and the same soil property (e.g., permeability function, shear strength) in saturated condition (Fredlund *et al.* 2012; Marshall 1958; Mualem 1986; Van Genuchten 1980). The SWCC was created for the sampled northern Louisiana's expansive clay using two methods. An impact corer was used to collect three cores from the sample site at a depth of 10 m. The aluminum cylinder inside the corer was five-cm in length and 4.8 cm in inner diameter. Soil cores in the cylinders were trimmed in the field exactly to the cylinder length, and the cylinders were immediately capped at both ends, and transported to the geotechnical laboratory. Uncapped cylinders were placed on a 1-bar ceramic

pressure plate, which was inundated for 48 hours. Water was placed on the ceramic plate, and the cylinders were saturated from the bottom for 72 hours. The cylinders were removed from the saturated ceramic plate and weighed, followed by placing them back on the plate for an additional 48 hours. As illustrated in Fig. 8a, the saturated ceramic plate and cylinders were placed in a pressure plate apparatus and pressure was increased to 33 kPa, and maintained for 48 hours (Dane and Hopmans 2002). The cylinders and their soils were then weighed, and placed in an oven at 110°C for 48 hours. After that, they were moved in a desiccator, and then weighed again. These measurements of gravimetric soil water content at 0 kPa (saturation) and 33 kPa (field capacity) represent the wetter points on the SWCC. Bulk density (Grossman and Reinsch 2002) of the cores were calculated based on the cylinder volumes and the oven dry soil weights, and it was used to calculate volumetric moisture content of the soil cores.

The second method used to create the SWCC was the chilled mirror dew point technique (Scanlon *et al.* 2002) using the WP4-T Dewpoint Potentiometer by Decagon Devices on disturbed soil samples as shown in Fig. 8b. Approximately 15 grams of the crushed soil passing through a 2mm diameter sieve was placed into stainless steel sample cups. Thirteen soil samples were prepared by varying moisture contents. Sample cups were made temperature equilibration by placing them on the upper surface of the WP4-T. Each sample cup was placed into the Dewpoint Potentiometer for the water potential measurement. Drier samples had one measurement, but the wetter 6 samples had three or four measurements of water potential. After the water potential measurements, samples were placed into an oven, and maintained at 110°C for 24 hours, and then were placed in a desiccator for one hour before being weighed to the nearest 0.0001 g. Bulk density of the undisturbed soil samples was measured by placing crushed, sieved (<0.002 mm diameter) soil into the stainless steel cups, which had an inner height of 1-cm, and an inner diameter of 3.75 cm. Various moisture levels were dropped into 19 sample cups, and the samples were left to equilibrate for 48 hours. If a sample swelled beyond the sample cup's volume, the soil was trimmed to the cup's height. The samples were then placed in an oven at 110°C for 48 hours, followed by cooling in a desiccator for one hour, and then weighing to the nearest 0.01g. Bulk density was calculated as the soil volume (cm^3) divided by the oven dried soil weight (g). Finally, a complete SWCC curve was plotted as illustrated in Fig. 9.

(a)

Figure 7 (a) Pressure Plate Test and (b) WP4-T Test to Construct the SWCC Curve

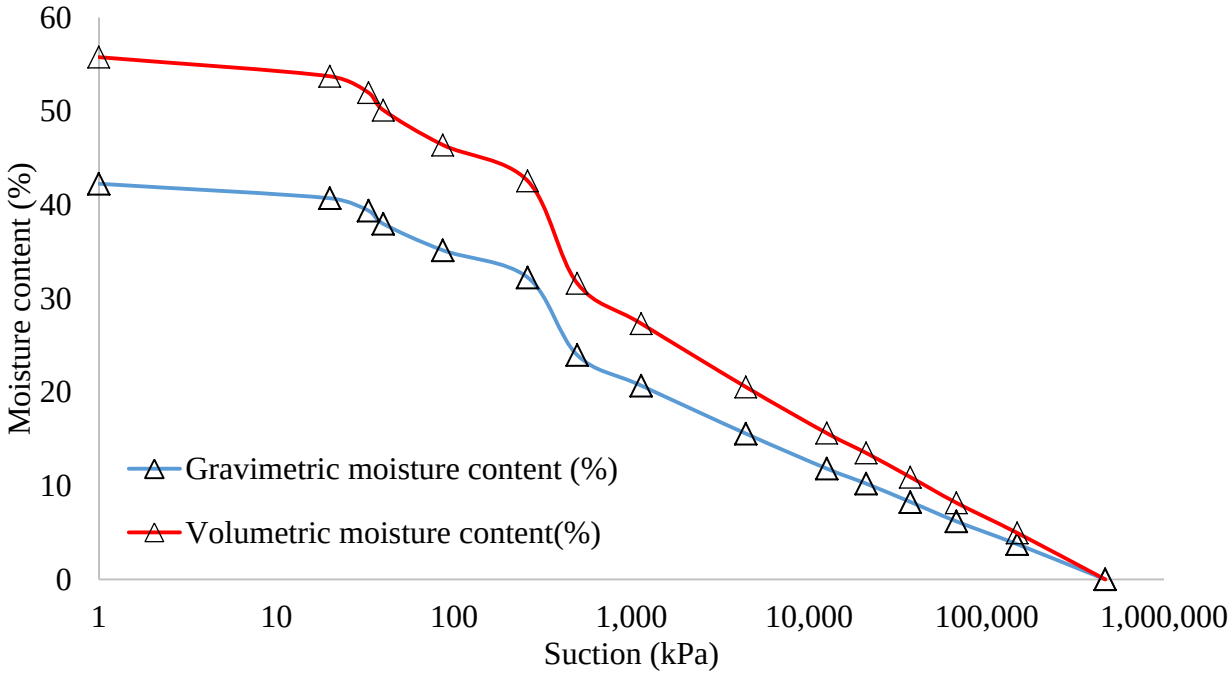

Figure 8 The SWCC Curve for Northern Louisiana's Expansive Soil

3.4.7 THE CONSOLIDATION TEST

In order to understand the loading and unloading behavior of Moreland clay a consolidation test was performed using ASTM D2435/D2435M-11 (ASTM 2010c) to measure the compression index, swelling index and swelling pressure. These indexes later will be later used to measure the free heave of expansive soil using heave equations. Three undisturbed soil samples were tested to get the initial void ratio. An average of the three values, which is 1.26, is used to represent the soil's void ratio. From Fig. 10, it was found that the swelling pressure corresponding to the initial void ratio is 120 kPa. Disturbances in soil structures in extracting soil samples from the field may result into a reduction of the swelling pressure and a correction is needed using a graphical procedure (Fredlund 1969; Fredlund *et al.* 2012; Nelson *et al.* 2015). The corrected swelling pressure was finally determined to be 180 kPa.

The compression index (C_c) and the swelling index (C_s) were determined from the slope of the loading curve and the rebound curve in Fig. 10, and they are 0.36 and 0.11, respectively. The C_s fell within the range typical of inorganic silty clays, which is in between 1/4 or 1/5 of C_c (Das 2010). The relatively high C_s/C_c ratio indicates the expansive soil in the field was stiff in nature.

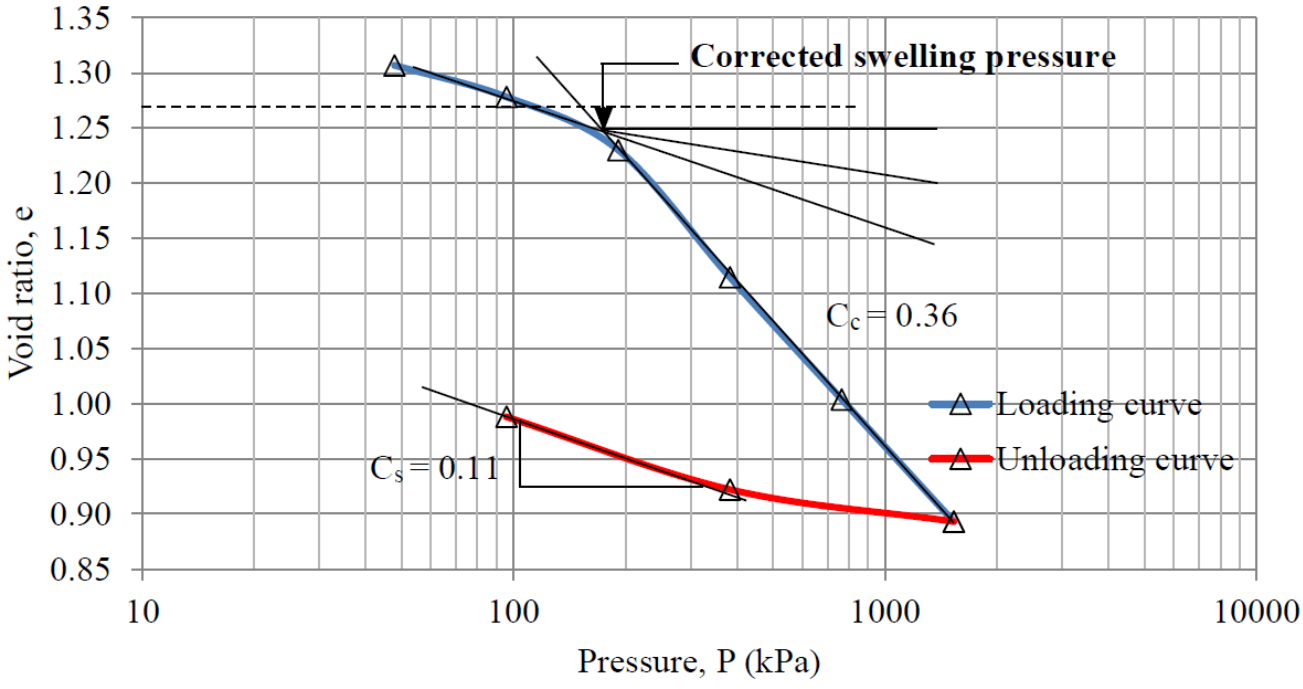

Figure 9 Void Ratio vs. Pressure from the Consolidation Test

3.4.8 THE SHRINKAGE CURVE OF THE EXPANSIVE SOIL

The shrinkage curve is significant in the sense that it shows the direct relationship between the changes in void ratio with the change in moisture content. Briaud *et al.* (2003) proposed a simple method to obtain the shrinkage curve. It was followed in the research. A soil sample with a recommended dimension of 75 mm in diameter × 150 mm in height was used in the test. After measuring a minimum of three times for initial heights and diameters at a circular interval of 120^0, the sample was weighed, and then the soil sample was air dried. Readings were taken at the times with a one-hour interval for the first eight hours. After that, based on Briaud's recommendations, the time interval was increased to every four hour and continuous measurements were taken for two days. Once the last reading was taken, it was oven dried and the weight was measured once again. Finally, a shrinkage curve as presented in Fig. 11 was generated for the northern Louisiana clay.

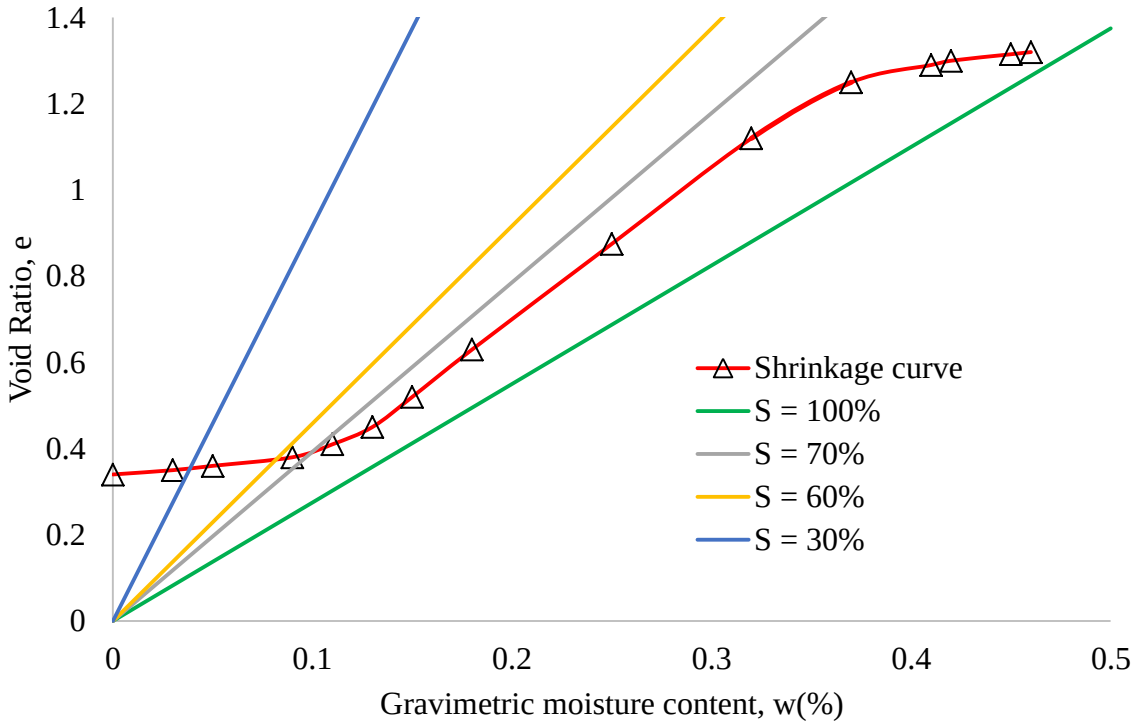

Figure 10 The Shrinkage Curve for the Northern Louisiana Clay

In the process of conducting tests for the shrinkage graph following the method described above, cracks and fissures occurred in the soil samples as the soil moisture content decreased below the shrinkage limit. As a result, it was difficult to accurately measure the deformed

sample sizes. Zhang (2004) proposed a simple method to eliminate the problem by taking a constant void ratio for the soil samples after the water contents are below the shrinkage limit. Using Zhang's method, a modified shrinkage curve was produced as presented in Fig. 12.

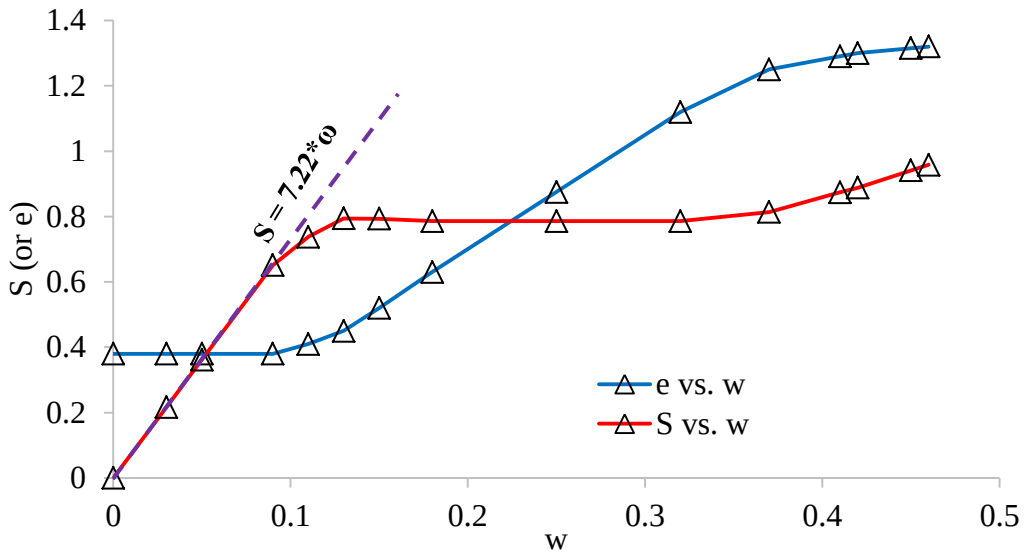

Figure 11 The Modified Shrinkage Curve

3.4.9 THE DIRECT SHEAR TEST

To characterizing shear strength of the unsaturated expansive soil three undisturbed soil samples were taken from the field and they were kept in water bath inside a shear box until they were fully saturated. Fully saturated soil sample was achieved in four days. Three different normal stresses (75 kPa, 150 kPa and 250 kPa) were applied on the soil samples with a very slow strain rate, respectively. ASTM D3080/D3080M-11 (ASTM 2011a) was followed and the shear strain rate was kept below 5×10^{-3} mm/min to avoid the generation of excess pore water pressure in the soil samples (Khan *et al.* 2017). Fig. 13 shows the soil sample preparation and Fig. 14 illustrates the relationship between shear stress and normal stress from the tested soil samples.

Figure 12 Direct Shear Test Preparations for Saturated Soil Samples

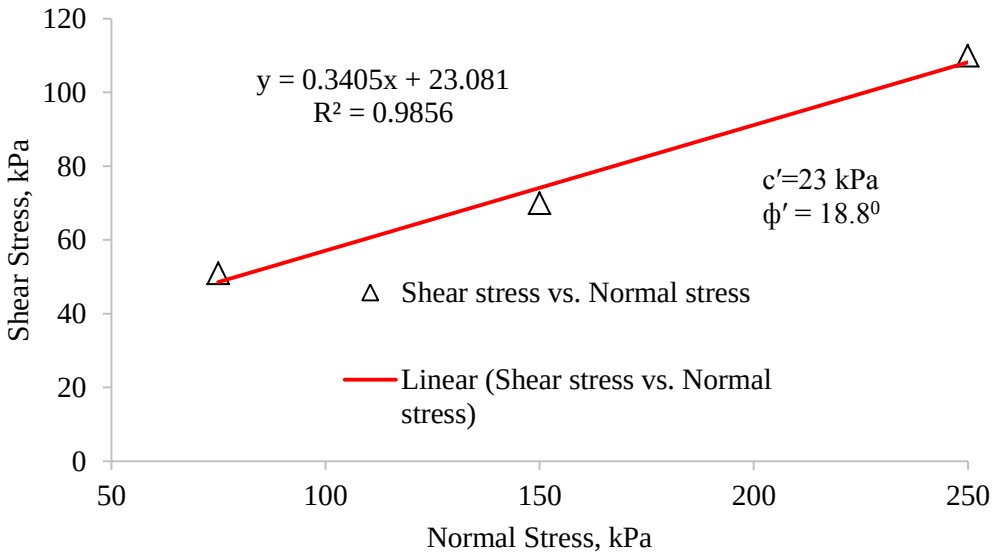

Figure 13 Shear Stress vs. Normal Stress for the Undisturbed Saturated Soil

Measuring the shear strength of unsaturated soils can be directly completed by conducting the triaxial test or the modified direct shear test. Both tests are time consuming, and require a long period to complete. For this reason, empirical equations were proposed to predict the shear strength of unsaturated soil, as saturated soil is considered an extension of unsaturated soil (Fredlund *et al.* 2012; Zhang 2004). Eq. 2 (Terzaghi *et al.* 1996), which follows the well-known Mohr-Coulomb criterion, is to evaluate the shear strength of saturated soil, and Eq. 3 (Fredlund *et al.* 1978; Vanapalli *et al.* 1996) is for unsaturated soil. In Eq. 3 the value of ϕ^b is the slope angle of shear stress vs. matric suction line. Most of the regular geotechnical labs are not

equipped with a direct shear test machine that is capable of controlling soil suction during a direct shear test. The use of Eq. 4 (Vanapalli *et al.* 1996) eliminates the need of finding the ϕ^b value experimentally and it can be predicted using the SWCC. The fitting parameter κ can be estimated from the plasticity index by following the procedure described in the section 3.4.10.

$$\tau = c' + (\sigma - ua) \tan\phi' \quad (2)$$

$$\tau = c' + (\sigma - ua) \tan\phi' + (u_a - u_w) \tan\phi^b \quad (3)$$

$$\tan\phi^b = (\theta_w/\theta_s)^\kappa \tan\phi' \quad (4)$$

Here,

τ = Shear stress at failure

c' = Cohesion of the soil

$\sigma - u_a$ = Effective normal stress at failure

ϕ' = Friction angle of saturated samples

$u_a - u_w$ = Suction at failure measured from suction measurement device

ϕ^b = Friction angle due to suction

θ_w = Volumetric water content (= $\omega * \gamma_d/\gamma\omega$), γ_d is the dry unit weight, which is obtained from the soil compaction curve.

θ_s = Saturated volumetric water content obtained from the soil water characteristic curve

κ = Fitting parameter from the PI versus κ plot

3.4.10 PROCEDURE OF MEASURING FITTING PARAMETER (κ)

Garven and Vanapalli (2006) gave an empirical equation relating fitting parameter and plasticity index using nine different soil samples. Although the relation has been modified couple of times, the latest was given in Fig. 15. Chowdhury (2013) provided a different equation from five other soil samples as showed in Fig. 16.

$$\kappa = -0.0016*PI^2 + 0.0975*PI + 1 \quad (5)$$

$$\kappa = -0.001*PI^2 + 0.0874*PI + 0.98 \quad (6)$$

Eq. 5 gave fitting parameter (κ) value 1.81 for Louisiana soil (PI = 51), where using Eq. 6 the k value was found 2.84. Either one of them or the average of the values 2.33 can be used. So, the shear strength of unsaturated soil of Louisiana can be found using Eq. 7, while volumetric water content can be found from Eq. 8.

$$\tau = 23 + (\sigma - u_a) *0.34 + (u_a - u_w) (\theta_w/\theta_s)^{2.33} *0.34 \quad (7)$$

$$\theta_w = w*(\gamma_d/\gamma_w) \quad (8)$$

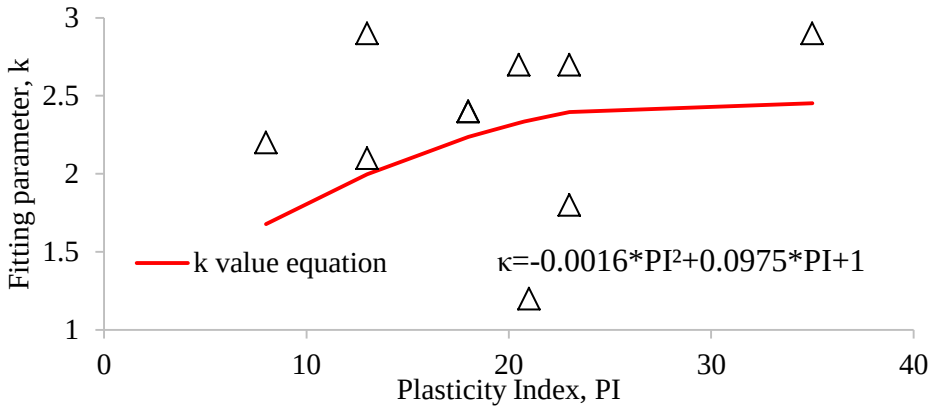

Figure 14 Relationship between k and PI(Modified after Fredlund *et al.* (2012))

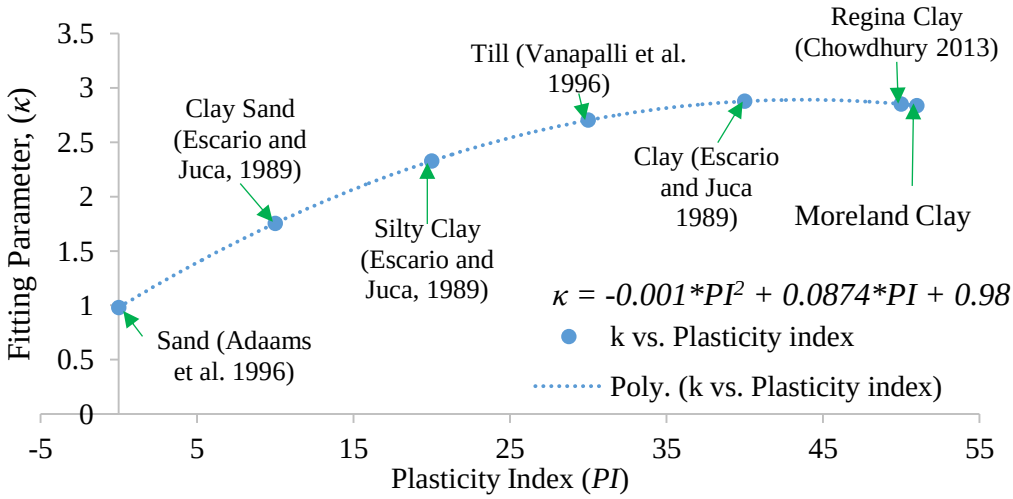

Figure 15 Relationship between k and PI (Modified after Chowdhury (2013))

4. SUMMARY OF THE MORELAND CLAY PROPERTIES

Summary of the soil properties are given in Table 5. In chapter five these properties will be used to predict the free heave using different methods.

Table 5 Summary of the laboratory tests

Soil Properties	Value	Soil Properties	Value
USDA soil taxonomy classification	Very-fine, smectitic, thermic Oxyaquic Hapluderts	Bulk Density, gm/cm³	1.24
USCS soil classification	Fat clay	Bulk volume moisture content	41.04
USCS soil symbol	CH	Free soil swelling, in	0.101
Specific Gravity, G_s	2.75	Expansion Index, EI	101
# 200 passing (%)	99	Activity of clay, Ac	1.37
Liquid limit, LL	79	Compression Index, C_c	0.36
Plastic limit, PL	28	Swell Index, C_s	0.11
Shrinkage limit, SL	9 %	Corrected Swelling Pressure, KPa	180
Plasticity Index, PI	51	Avg. Field Moisture content (%)	32
Opt moisture Content	27%	Avg. Saturated Moisture content (%)	52
Max dry unit weight (kN/m³)	14.52	Saturated unit weight (kN/m³)	19.70
Average field void Ratio, e_0	1.27	Field unit weight (kN/m³)	17.11

5. HEAVE PREDICTION FOR 1-M DEPTH OF MORELAND CLAY

The soil properties are summarized in Table 5. The properties were employed to predict the heave of 1 meter of expansive soil layer with the schematic diagram shown in Fig. 17.

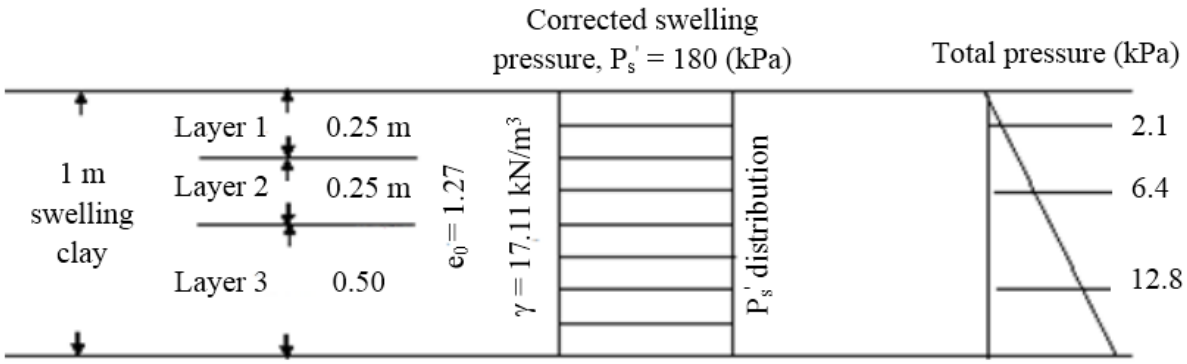

Figure 16 Schematic diagram of the example problem

The methods available to predict the soil heave can be mainly divided into three sub-sections: the empirical method using the geotechnical index properties, the oedometer test-based method (constant volume or free swell test), and the suction-based method (SWCC test). In this study, a total of 5 methods were selected from the 3 categories to evaluate the Moreland clay heave as an example problem. Regarding the selection of the expansive soil depth for the heave prediction, the following factors are considered.

A field research project was conducted by TxDOT on highly expansive soils below highway pavements at Grimes County, TX. Researchers installed a group of sensors at different depths below the drainage ditch, and recorded the moisture content data for an entire year (Gupta 2009; Zornberg *et al.* 2010), showing that moisture content varied only within the 1-m depth from the ground surface. In the absence of any published data regarding seasonal variation of moisture content in the ground in Moreland clay, a depth of 1-m was selected for the example problem. In addition, a few researchers (Azam and Chowdhury 2013; Fredlund *et al.* 2012) published heave prediction results for 2-m and 1-m depth expansive soils. Comparison with these predictions will be enable interpretation of Moreland clay heave.

In engineering practice, moisture content decreases with time due to environmental changes such as evaporation, thus increasing negative pore water pressure in the soil. For simplicity, it was assumed that the negative pore water pressure increased to zero throughout the 1-m zone, decreasing moisture content change for the entire depth of the zone.

Table 6 shows the predicted heaves that were calculated from three layers (0.25 m, 0.25 m and 0.50 m) using different methods, and were reproduced after Azam and Chowdhury (2013). The range of the predicted heaves was between 67 mm and 80 mm. An oedometer-based heave was predicted to be 69 mm by Fredlund *et al.* (2012). Lu and Vanapalli (2012) empirically predicted heave was 75 mm, whereas the suction-based Dhowian (1990) method suggested heave of 80 mm, which was the most conservative prediction. Other suction-based methods such as Snethen (1980) predicted 70 mm. Briaud *et al.* (2003) used the shrink-swell modulus and shrinkage ratio, and estimated heave of 67 mm. Table 6 shows that the average heave was 72.2 mm in the one-meter deep soil layer, which gave the swelling potential (SP) of 7.22%. In Table 7, the swelling potential of Moreland clay is compared to those of the expansive soils found in other places, and it showed that the expansive soil in northern Louisiana is one of the highest expansive soils in the USA and around the world (Azam and Chowdhury 2013; Chao 2007; Puppala *et al.* 2016; Tu and Vanapalli 2015).

Table 6 Heave Predictions of the 1-m Deep Expansive Clay Using Different Methods (Briaud *et al.* 2003; Dhowian 1990; Fredlund *et al.* 2012; Lu and Vanapalli 2012; Snethen 1980)

Methods	**Parameters**	**Heave (mm)**	**Comment**	**Eq.**
$\Delta H = C_s \frac{H}{1+e_0} \log(\frac{P_f}{P_s'})$	Swelling index, C_s= 0.11 Initial void ratio, e_0= 1.27 Final stress state, P_f = iterative calculated for each layer Moist unit weight γ = 17.11 kN/m^3 Corrected swelling pressure, Corrected P_S'= 180 kPa	69	Odometer based method	(9)
$\Delta H = C_s \frac{H}{1+e_0} \log\left(\frac{kP_f}{10^{(\frac{C_s}{C_w}\Delta w)}}\right)$ $k = 0.0039 * e^{0.64 I_p}$ $C_w = 0.019 * e^{0.64(\Delta w)}$	Correction parameter, k = 0.004 Suction modulus ratio, C_w = 0.019 Change in water content, Δw = 0.2 Plasticity Index, PI = 51%	75	Empirical based method	(10)
$\Delta H = HC_w (w_f - w_i)$ $C_w = \frac{\alpha G_s}{1+e_0}$	Volumetric compressibility factor, α = 0.33 Specific gravity, G_s = 2.75 Initial void ratio, e_0= 1.27 Water content change = 0.2 Suction Index, C_w = 0.4	80	Suction based method	(11)
$\Delta H = \sum_{i=1}^{n} (h_i f_i \Delta w_i / E_{wi})$	Water content change Δw = 0.2 Shrink swell modulus, E_w = 0.45 Shrinkage ratio, f = 0.13	67	Suction based method	(12)
$\Delta H = H \frac{C_\tau}{1+e_0} \log\left(\frac{\tau_{m_i^0}}{\tau_{m_f^0}}\right)$ $\log \tau_{m_i^0} = A - Bw$ $\tau_{m_f^0} = \alpha_0 \sigma_f - u_{wf}$ $C_\tau = \frac{\alpha G_s}{100B}$	Compressibility factor α = 1 as PI>40 Suction index, C_τ = 0.25 Y intercept of gravimetric SWCC, A= 5.1 Slope of gravimetric SWCC, B= 0.11 Final suction,$\tau_{m_f^0} = 0$ kPa Final pressure, σ_f = 17.11 kPa Specific gravity, G_s = 2.75 Initial moisture content, w_0 = 0.32	70	Suction based method	(13)

Table 7 Comparison of expansive soil based on swell percent (Azam and Chowdhury 2013; Chao 2007; Puppala *et al.* 2016; Tu and Vanapalli 2015)

Predominant Soil Type	% Swell	Results/Location
Moreland clay (CH)	7.22	Predicted value/north Louisiana
Regina clay (CH)	7.78	Predicted value/Regina, Canada
Grayson	9.8	Lab test
Colorado	8.2	Lab test
San Antonio	7.3	Lab test
Oklahoma	3.8	Lab test
San Diego	3.4	Lab test
Denver	6.5-7.4	Lab test
Pierre Shale	3.1-5.7	Lab test
London clay (CH)	2.12	Predicted value/Chattenden, Kent, UK
Maryland clay (CH)	3.56	Predicted value/Newcastle, Australia
Kenswick clay (CH)	1.76	Predicted value/Adelaide, Australia
Arlington clay (CL-CH)	1.35	Predicted value/Arlington, Texas, US
Al-Ghat shale(CH)	3.53	Predicted value/Al-Ghat, Riyadh, Saudi Arabia
Zaoyang soil (CL-CH)	1.03	Zaoyang, Hubei, China

6. THE CONSTITUTIVE SURFACES FOR UNSTAURATED SOILS

6.1 INTRODUCTION

The constitutive relation of a soil correlates deformation state variables to stress state variables. The mathematical equations relating the total volume and the water content state variables to the stress variables are called the volume-mass constitutive equations. When these equations are used to plot a three-dimensional surface, this surface is called the constitutive surface. This surface helps to visualize the behavior of an unsaturated soil under the change of net mean stress and/or soil matric suction. Soil volume changes are due to two reasons. The first one is the mechanical stress change and the second one is the change in the matric suction. For an unsaturated soil where multiple phases may be present (e.g., solid, water and air), and this relation is very complicated. Generally, a saturated soil is considered as a special case to the unsaturated soil. The constitutive surface can also be created by correlating moisture content

change with the two-state change, once the correlation between the void ratio change and the two-stress state change is known. In this section only the first type of the constitutive surface will be plotted for the Moreland clay following the six-boundary condition as described by Zhang (2004). Sign convention of the stress state is very important and will be discussed before developing the constitutive surface.

6.2 STRESS STATE VARIABLES SIGN CONVENTIONS

The compressibility form for the unsaturated constitutive equation is given in Eq.14 and water phase of the constitutive equation is showed in Eq.15. m_1^S, m_2^S, m_1^w and m_2^w are different according to various loading conditions.

$$d\varepsilon_V = m_1^S d\,(\sigma_{mean} - U_a) + m_2^S d\,(U_a - U_w) \tag{14}$$

$$\frac{dV_w}{V_0} = m_1^w d\,(\sigma_{mean} - U_a) + m_2^w d\,(U_a - U_w) \tag{15}$$

Where,

m_1^S= Coefficient of volume change with respect to net normal stress

m_2^S= Coefficient of volume change with respect to matric suction

m_1^w= Coefficient of water volume change with respect to net normal stress

m_2^w= Coefficient of water volume change with respect to matric suction

Consider a case where load is applied, stress increases, volume decreases, stress increases and strain decreases, according to the classical soil mechanics where compression is taken as positive, and the Young's modulus becomes negative. Eq.16 shows the expression

$$\mathrm{E}(-) = \frac{\mathrm{d}\sigma(-)}{\mathrm{d}\varepsilon(+)} \tag{16}$$

However, according to Zhang (2004) the confusion comes up when the pore water pressure gets increased, which causes a decrease in effective stress and an increase in volume. This will cause positive Young's modulus as showed in Eq.17.

$$\mathrm{E}(+) = \frac{\mathrm{d}\sigma(-)}{\mathrm{d}\varepsilon(-)} \tag{17}$$

From Eqs. 16 and 17 it can be seen modulus of elasticity or Young's modulus for the soil structure has a reverse sign for an increase in net mechanical stress and an increase in pore water pressure. Same confusion comes up in the water phase modulus, too. To avoid this confusion Zhang (2004) suggested taking (u_a-u_w) as a whole to be the stress state variable for unsaturated soils when two stress state variables are used. Fig. 18 illustrates the stress state variables as a nonlinear curve for the soil.

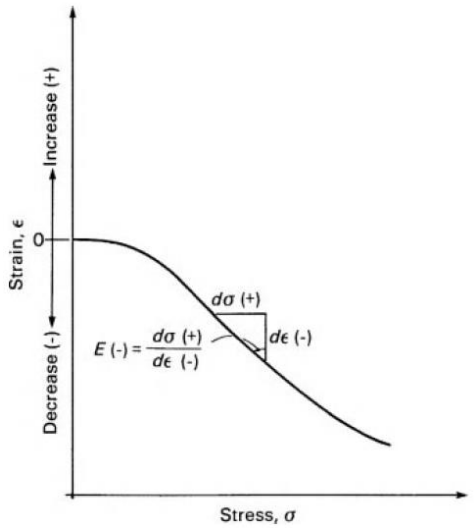

Figure 17 Definition of variables for a nonlinear stress-strain curve for a soil (Fredlund *et al.* 2012)

6.3 THE CONSTITUTIVE SURFACE FOR UNSATURATED SOILS

Matyas and Radhakrishna (1968) showed how to find the constitutive surface of a soil experimentally using 80% flint powder and 20% kaolin as shown in Fig. 19. This process was very lengthy and needed sophisticated experimental equipment. Below a simple mathematical process is described where using some boundary conditions a very close shape of actual constitutive surface of any soil can be found.

The effective stress of a soil exclusively defines its degree of compression. The effective stress is the difference between total stress and pore water pressure. Eq. 18 shows the relation between void ratio and its stress state.

$$e = f(\sigma') = f(\sigma - u_w) = f(\sigma - u_a) + f(u_a - u_w) \quad (18)$$

Fig. 20 shows the constitutive surface for a saturated soil while Fig. 21 shows the constitutive surface for an unsaturated soil. When the soil is saturated the constitutive surface looks like AGFD, and when the soil becomes unsaturated the surface will change to ABEDI. Axis OS shows the pore water pressure, axis OI shows the matric suction and axis OD shows the compressive stress. Curve AD represents the void ratio versus net normal stress when there is no suction where curve AI represents the void ratio versus matric suction when there is no net normal stress. AI is found by rotating curve AD by 90^0 anticlockwise. Please note that for unsaturated soil the effective stress principle ($\sigma' = \sigma - u_w$) does not work. For this reason, instead of AP, AI represents the zero-net normal stress curve. As mentioned before using boundary conditions the constitutive surface will be constructed as shown by Fredlund *et al.* (2012) and Zhang (2004). Fig. 22 shows all the six boundary curves needed for constructing the constitutive surface.

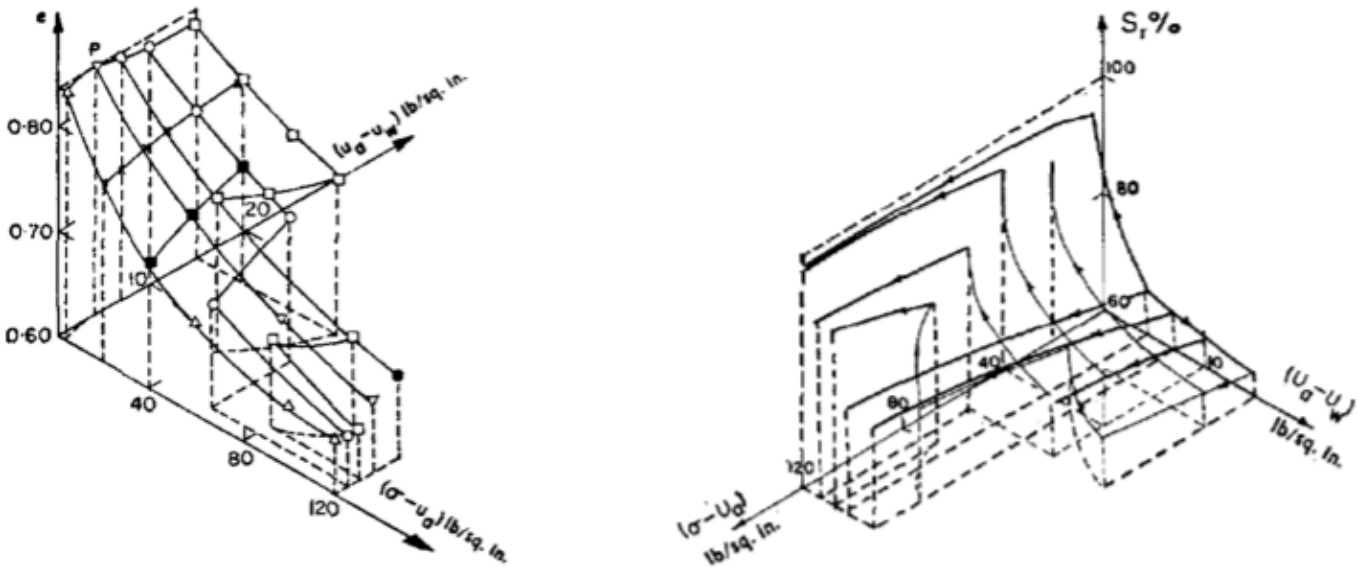

Figure 18 (a) void ratio constitutive surface; (b) degree-of-saturation constitutive surface (after Matyas and Radhakrishna (1968))

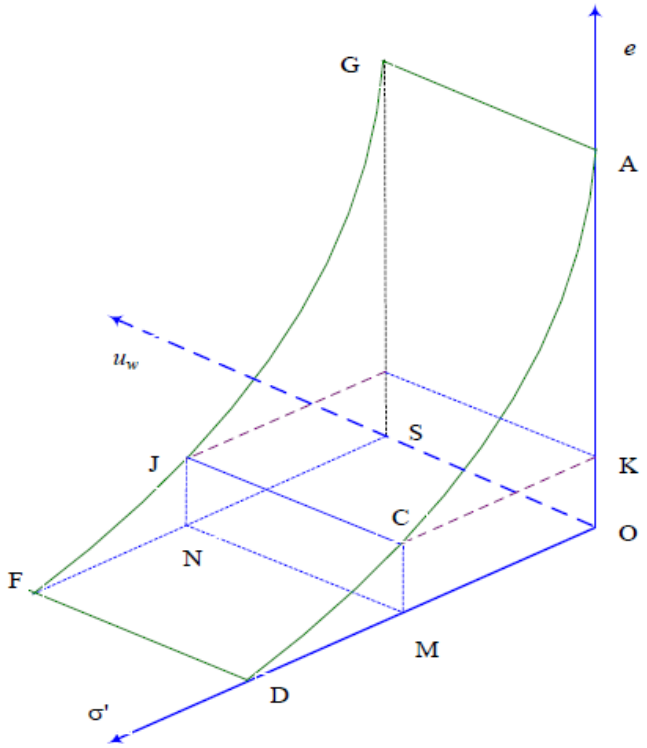

Figure 19 Void ratio constitutive surface for a saturated soil (Zhang 2004)

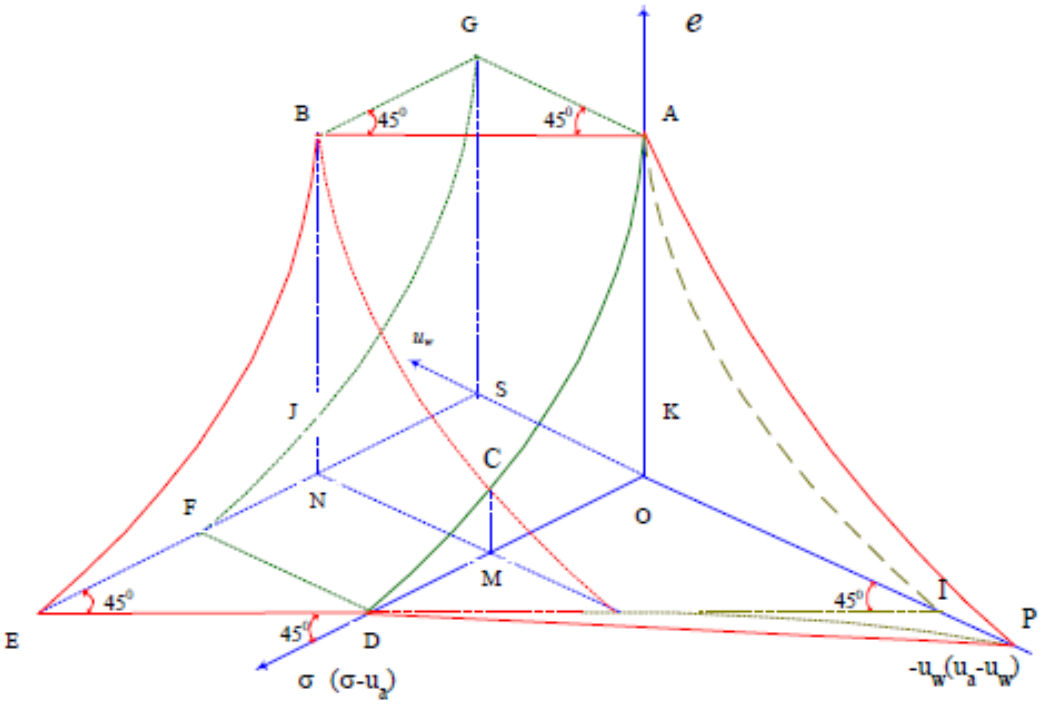

Figure 20 Void ratio constitutive surface for a saturated soil (Zhang 2004)

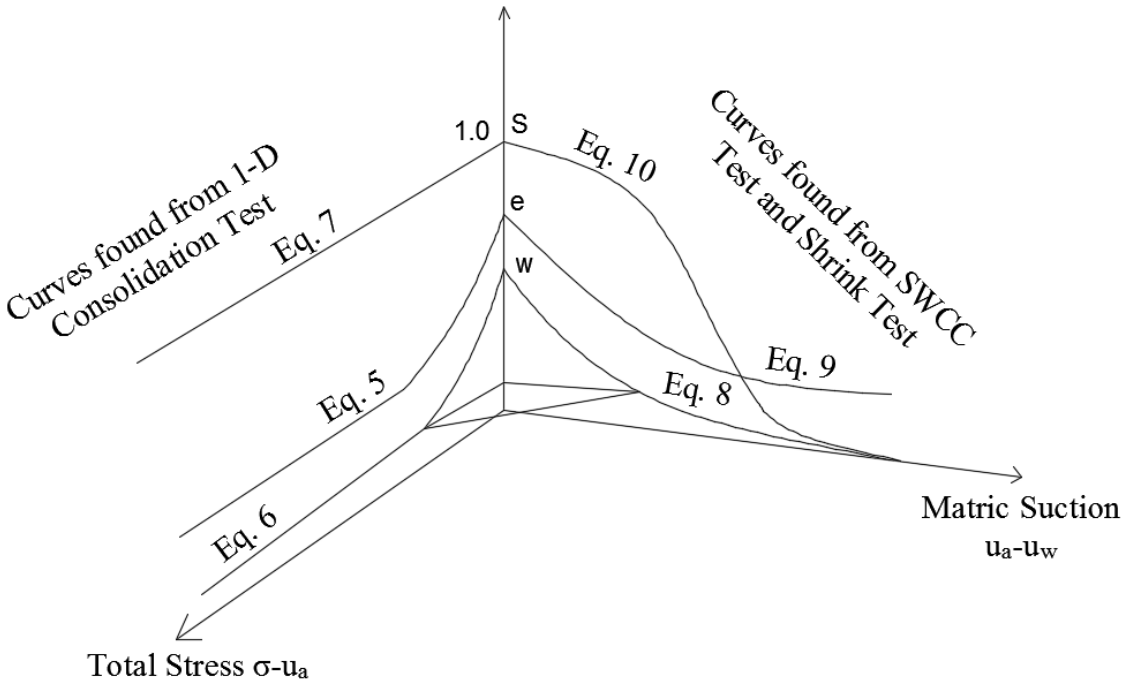

Figure 21 Curves needed for constructing the constitutive surface of an unsaturated soil (Modified after Zhang (2004))

Another assumption was made by taking the constitutive surface as a plane for any particular void ratio (Zhang 2004). Using this assumption, by making a lot planes at various void ratios, the whole constitutive surface can be constructed. Fig. 22 shows the method of constitutive surface construction. From Fig. 22 the straight line a_t and a_m are small segments of void ratio versus net normal stress curve and void ratio versus matric suction curve, respectively. These two segments are assumed to be from the same void ratio range. Using the same procedure for different void ratio changes other planes can be found. Once added together they should provide the whole constitutive surface. At the first glance this method seemed worked. Zhang (2004) stated after a close investigation that in many cases this assumption is not satisfied. For example, in case of unsaturated soils, the net normal stress and matric suction are independent to each other. It means that straight lines a_t and a_m may not be at the same plane. Zhang (2004) proposed a simplified way to construct the constitutive surface. In this method, it is assumed that the constant void ratio curve is a straight line for any void ratio level. Fig. 23 showed the constant void ratio of Madrid clay by Escario (1969) and it matches the assumption.

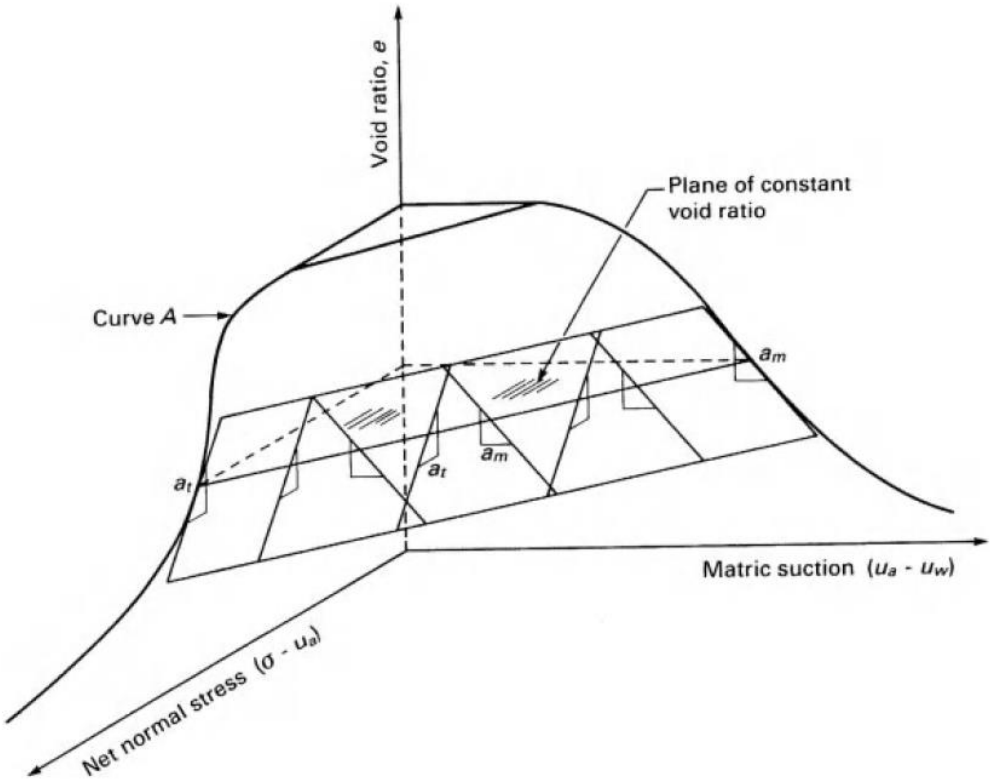

Figure 22 Proposed assumption by Fredlund *et al.* (2012)

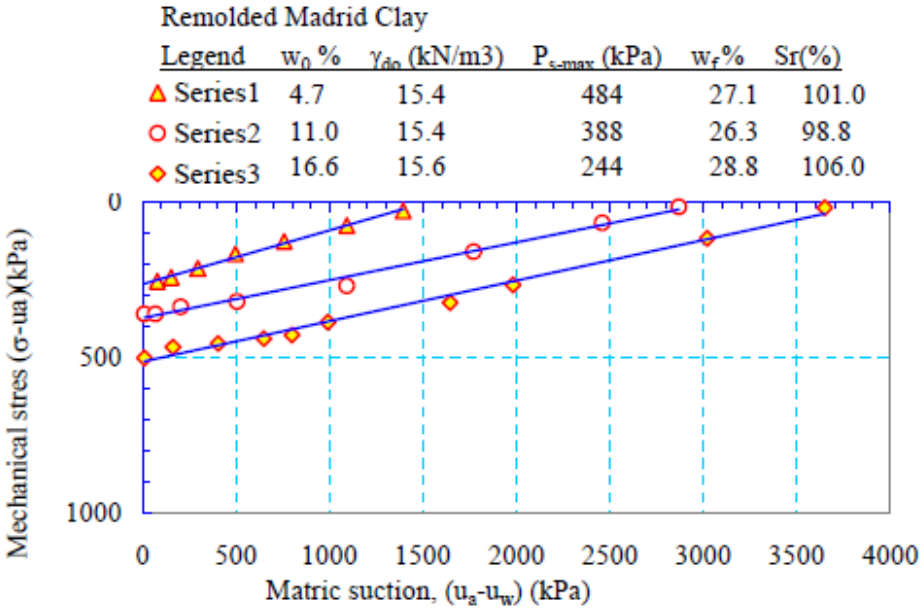

(a)

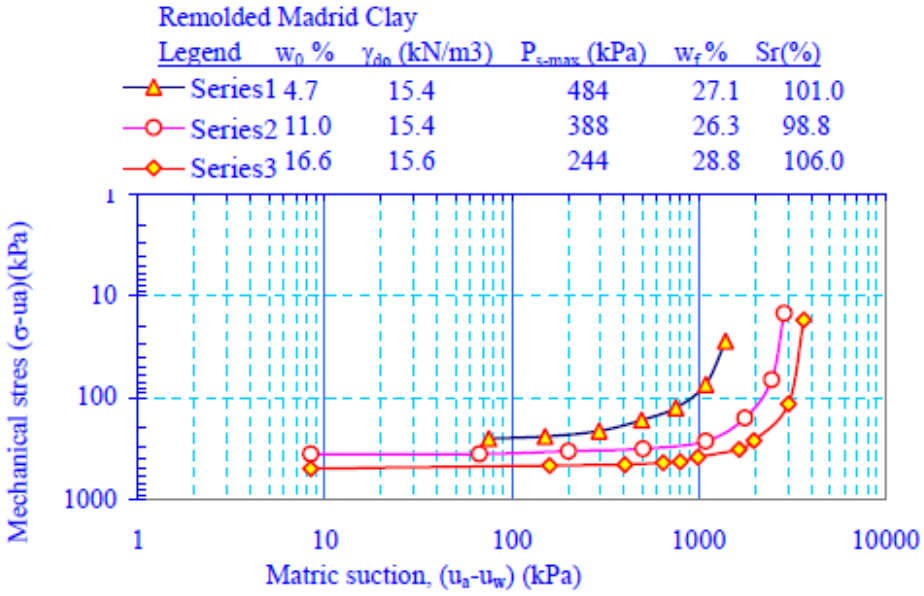

(b)

Figure 23 Constant void ratio curves for some unsaturated soils (a) Cartesian Coordinate; (b) Log-Log coordinate by Zhang (2004) and Escario (1969)

The proposed detailed procedures by Zhang (2004) are given below, which at the end give the same constitutive surface proposed by Fredlund *et al.* (2012):

1. Find the corresponding two points for any void ratio from the void ratio versus net normal mechanical stress curve and the void ratio versus matric suction curve respectively.

2. Connect the two points respectively.

3. Repeat the procedure for all the void ratio levels, finally a surface will be obtained.

A simplified mathematical expression to understand the procedures is given below. Assume the void ratio versus net normal mechanical stress curve and void ratio versus matric suction curve are given in Eqs. 19 and 20, respectively.

$$e = a_1 \times \log_{10} (\sigma - u_a) + a_2 \tag{19}$$

$$e = a_3 \times \log_{10} (u_a - u_w) + a_4 \tag{20}$$

Here, a_1, a_2, a_3 and a_4 are best-fitted constants determined by laboratory test data.

Now if the DP curve from Fig. 21 is assumed to be the DP straight line, the mathematical expression for DP can be found from Eq. 21 and for any void ratio ($e=e_0$) the value of OD and OP can be found from Eqs. 22 and 23, respectively.

$$\frac{\sigma_m - u_a}{OD} + \frac{u_a - u_w}{OP} = 1 \tag{21}$$

$$OD_{e=e_0} = (\sigma_m - u_a)_{(u_a - u_w = 0, e = e_0)} = 10^{\left(\frac{e_0 - a_2}{a_1}\right)} \tag{22}$$

$$OP_{e=e_0} = (u_a - u_w)_{(\sigma_m - u_a = 0, e = e_0)} = 10^{\left(\frac{e_0 - a_4}{a_3}\right)} \tag{23}$$

By combining Eqs. 22 and 23, a mathematical expression for the void ratio constitutive surface can be found as expressed in Eq. 24.

$$\frac{\sigma_m - u_a}{10^{\left(\frac{e_0 - a_2}{a_1}\right)}} + \frac{u_a - u_w}{10^{\left(\frac{e_0 - a_4}{a_3}\right)}} = 1 \tag{24}$$

Zhang (2004) finally concluded the followings:

1. The constant void ratio curve for the void ratio constitutive surface does not necessarily have to be a straight line. If only the constant void ratio curve is a function of both the net normal mechanical stress and matric suction, this method is applicable.

2. Furthermore, it can also be proven that if the mathematical expressions for the void ratio versus net normal mechanical stress curve and the void ratio versus matric suction curve and the constant void ratio are continuous and have continuous first derivatives unlike the discontinues first derivative of the proposed method by Fredlund *et al.* (2012).

6.3.1 CONSTRUCTING 3-D CONSTITUTIVE SURFACE OF MORELAND CLAY

A simplified method was suggested by Zhang (2004) by using six boundary curves to interpolate the whole surface. In previous sections the process of constructing an unsaturated soil constitutive surface is described. Here a detailed process of finding the six boundary curves are described. The boundary curves are given below:

$e = f(\sigma - u_a, u_a - u_w = 0)$ (suction is zero) (25)

$w = f(\sigma - u_a, u_a - u_w = 0)$ (suction is zero) (26)

$S = f(\sigma - u_a, u_a - u_w = 0)$ (suction is zero) (27)

$w = f(u_a - u_w, \sigma - u_a = 0)$ (mechanical stress is zero) (28)

$e = f(u_a - u_w, \sigma - u_a = 0)$ (mechanical stress is zero) (29)

$S = f(u_a - u_w, \sigma - u_a = 0)$ (mechanical stress is zero) (30)

Eqs. 25 through 27 can be found from the consolidation test, showing how the void ratio (e), moisture content (w) and degree of saturation (s) are changing exclusively by the change in net normal stress ($\sigma - u_a$). On the other hand, Eqs. 28 through 30 can be found from the SWCC test, giving the information about how the soil volume changes when only the matric suction ($u_a - u_w$) changes. Eq. 25 is the void ratio versus net normal stress curve when the matric suction is zero and can be found from the consolidation test. In consolidation test the soil sample is submerged into water during the whole time, making the suction zero. Eq. 26 expresses the water content versus net normal stress curve when the matric suction is zero and can be found from the formula $Se=wG_s$. As in the consolidation test the degree of saturation is one and specific gravity (G_s) is a known value for any specific soil, a relation can be easily found between moisture

content and net normal stress. Eq. 27 is the degree of saturation versus mechanical stress curve when the matric suction is zero and is a constant value (=1) during the change process of $\sigma - u_a$. Eq. 28 is the moisture content versus suction curve when the net normal stress is zero and can be found from the SWCC test. In the SWCC test no mechanical stress is applied. Eq. 29, which is the void ratio versus suction curve when the net normal stress is zero, can be found from the modified shrinkage test. Eq. 30 is the degree of saturation versus matric suction curve when the net normal stress is zero and it can be found from the formula $Se=wG_s$.

As a summary to the previous paragraph, to construct the constitutive surface of unsaturated soil the minimum tests are needed as followed: 1) The consolidation test, 2) the SWCC curve and 3) The free shrinkage test. All the tests were performed for the Moreland clay, and described in the previous section of this chapter.

6.3.1.1 $e = f(\sigma - u_a, u_a - u_w = 0)$

Using the consolidation test the e-log (σ) relation was found. Using commercial software Sigmaplot (Systat Software Inc. 2016) regression analysis was done and a mathematical expression for the curve was found. The expression is given in Eq. 31 and the regression curve is showed in Fig. 25.

$$e = 0.80761 + \frac{0.50737}{1+\exp\left(\frac{\log_{10}(\sigma)-2.73049}{0.29184}\right)} \quad (31)$$

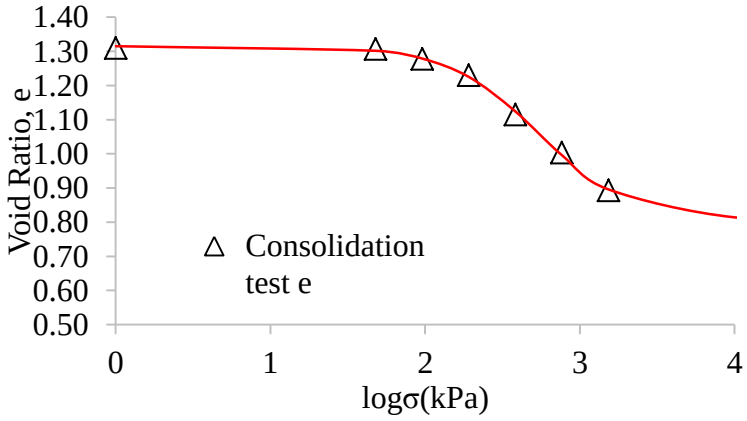

Figure 24 e-log (σ) expression from the consolidation test

6.3.1.2 $w = f(\sigma - u_a, u_a - u_w = 0)$

Using the expression $Se = wG_s$, a relation between moisture content and net mechanical stress can be found. For north Louisiana, expansive soil $G_s = 2.75$. Mathematical expression is given in Eq. 32 and the regression curve is shown in Fig. 26.

$$w = 0.80761 + \frac{0.50737}{1+\exp\left(\frac{\log_{10}(\sigma)-2.12377}{0.22699}\right)} \quad (32)$$

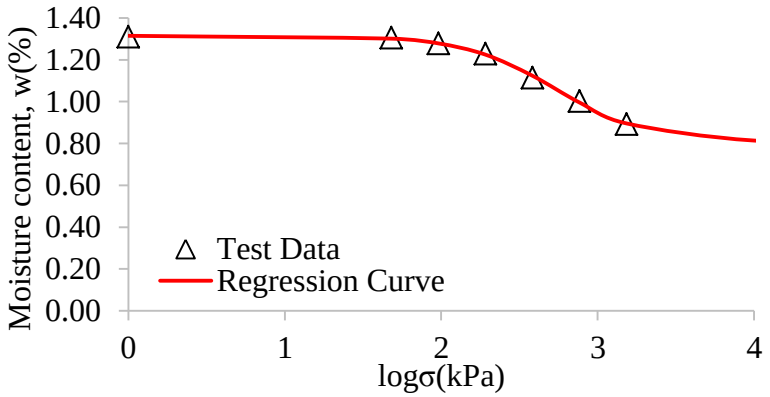

Figure 25 w-log (σ) expression from the consolidation test

6.3.1.3 $S = f(\sigma - u_a, u_a - u_w = 0)$

In the consolidation test the degree of saturation is always one with the change of mechanical stress. The expression is given in Eq. 33 and illustrated in Fig. 27.

$$S = 1 \quad (33)$$

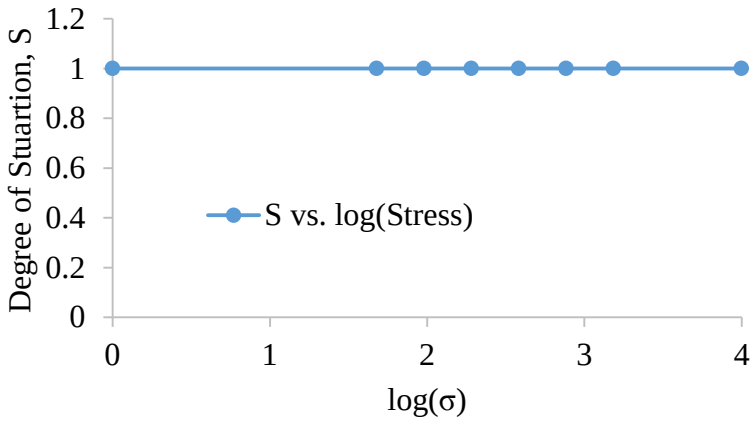

Figure 26 S-log (σ) expression from the consolidation test

6.3.1.4 $w = f(u_a - u_w,\ \sigma - u_a = 0)$

This boundary curve was found from the SWCC curve. The SWCC curve is used to understand the relationship between the volumetric water content and the matric suction. Zhang (2004) suggested using the gravimetric water content instead. The reason behind the suggestion is that, the slope of the gravimetric water content versus the matric suction is referred as specific water capacity. The SWCC test was performed between 1 kPa and 1000000 kPa as shown in Fig. 9. In Fig. 9 two assumptions were made, first, when the soil is fully saturated the suction is zero. The reason behind is that, although theoretically at saturation point the suction is zero but log(0) is not a real number. As the objective is to find the relation between water content (%) versus suction in logarithmic scale, so the suction at fully saturated condition is taken as zero. The logic behind taking the logarithmic suction is to finally plot a 3-D graph between void ratio, logarithmic net normal stress and logarithmic suction, so all the boundary conditions should have either logarithmic mechanical stress or logarithmic suction. Secondly, in Fig. 9 at the oven dried condition the soil suction is assumed to be 1000000 as recommended by Zhang (2004).

Eq. 34 the mathematical expression is given and in Fig. 28 the regression curve is showed. In Fig. 28 the two boundary conditions are marked in blue color.

$$w(\%) = -1.68865 + \frac{52.50339}{1+\exp\left(\frac{\log_{10}(u_a - u_w) + 1.91858}{20.18804}\right)} \tag{34}$$

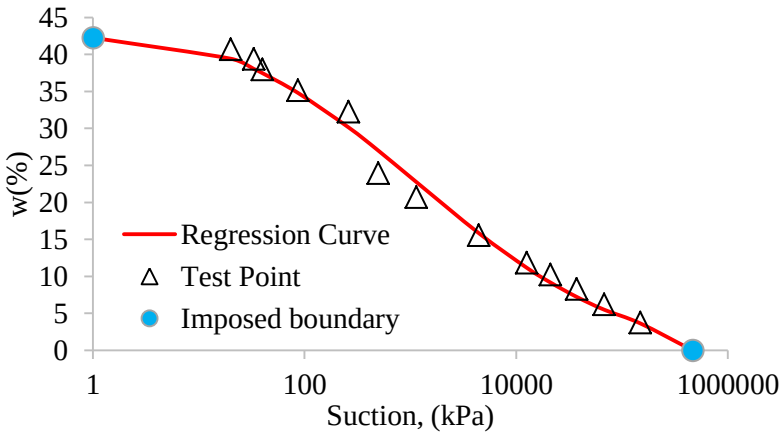

Figure 27 w-log (u_a-u_w) expression from the SWCC test

6.3.1.5 $S = f(u_a - u_w,\ \sigma - u_a = 0)$

The free shrinkage test was performed as per Briaud *et al.* (2003) and showed previously in Fig. 11 and later modified after Zhang (Zhang 2004) in Fig. 12. The Moreland clay has a shrinkage limit 9%, so when the water content went below 9%, it is assumed the void ratio is the same as shown in Fig. 12. As the void ratio is constant below the shrinkage limit, a linear relation can be found between degree of saturation S and water content w, when w < 9% and found to be S = 7.22*w. After considering this phenomenon an expression between w and e can be found and showed in Eq. 35 and expression between S and w is given by Eqs. 36 and 37.

$$e = 0.22218 + \frac{1.14759}{1+\exp\left(\frac{-w+0.22661}{0.07171}\right)} \tag{35}$$

$$S = -2.85551 + \frac{10.49865}{1+\exp\left(\frac{-w+3.51076}{5.24136}\right)} \text{ (When, } w \geq 9\%) \tag{36}$$

$$S = 7.22 * w \text{ (When, } w < 9\%) \tag{37}$$

6.3.1.6 $e = f(u_a - u_w,\ \sigma - u_a = 0)$

Eq. 34 gives the relation between w (%) and log (u_a-u_w) and Eq. 35 gives the relation between e and w. Combining these two equations an expression between e and log(u_a-u_w) can be found and given in Eq. 38 and the curve is showed in Fig. 29.

$$e = 0.347128 + \frac{0.992809}{1+\exp\left(\frac{\log_{10}(u_a-u_w)-2.766902}{0.682210}\right)} \tag{38}$$

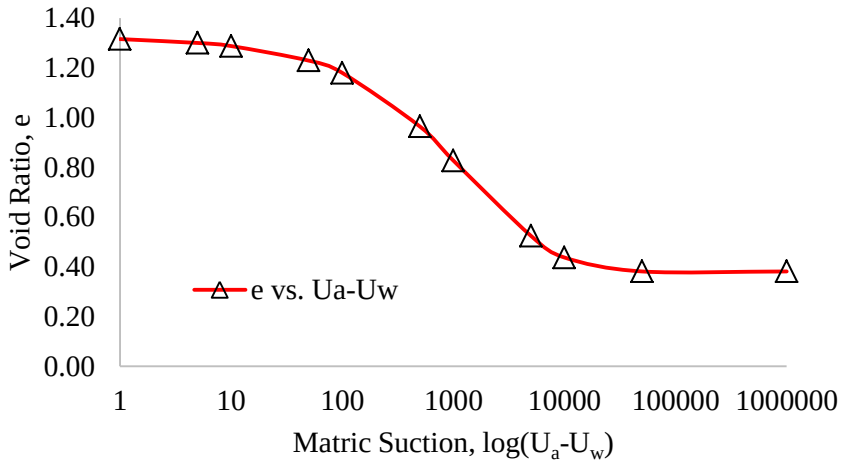

Figure 28 e-log (U_a-U_w) expression from the SWCC test

6.3.1.7 Combining e = f ($\sigma - u_a$, $u_a - u_w$ =0) and e = f ($u_a - u_w$, $\sigma - u_a$ =0)

Once the all six boundary conditions equations were found, Eq. 31 and 38 were combined to find the 3-D constitutive equation of Moreland clay. Eqs. 39 to 43 show the details of the combining process.

$$e = 0.80761 + \frac{0.50737}{1+\exp\left(\frac{\log_{10}(\sigma_v)-2.73049}{0.29184}\right)} \quad (39)$$

$$\log_{10}(\sigma_v) = 0.29184\left(\frac{0.50737}{(e-0.80761)} - 1\right) + 2.73049 \quad (40)$$

$$e = 0.347128 + \frac{0.992809}{1+\exp\left(\frac{\log_{10}(u_a-u_w)-2.66902}{0.682210}\right)} \quad (41)$$

$$\log_{10}(u_a - u_w) = 0.682210\left(\frac{0.992809}{(e-0.347128)} - 1\right) + 2.66902 \quad (42)$$

$$\frac{\sigma_V - U_a}{10^{\left(0.29184\left(\frac{0.50737}{(e-0.80761)}-1\right)+2.73049\right)}} + \frac{U_a - U_w}{10^{\left(0.682210\left(\frac{0.992809}{(e-0.347128)}-1\right)+2.66902\right)}} = 1 \quad (43)$$

Using any net normal stress (σ-u_a) and matric suction (u_a-u_w), the void ratio can be found using iterative method from Eq. 43. Sigmaplot (Systat Software Inc. 2016) was used to plot the constitutive surface of the Moreland clay. Fig. 30 shows the void ratio constitutive surface where, the curve at the void ratio vs. suction axis represents the SWCC and the curve at the void ratio vs. mechanical stress axis represents the consolidation test curve. Some published void ratio constitutive surfaces from different areas of the world are illustrated in Figs. 31, 32 and 33. From the figures, it is for certain that the constitutive surfaces are unique for each soil and each surface gives a visual idea about how the void ratio change affects the matric suction and mechanical stress of the soil.

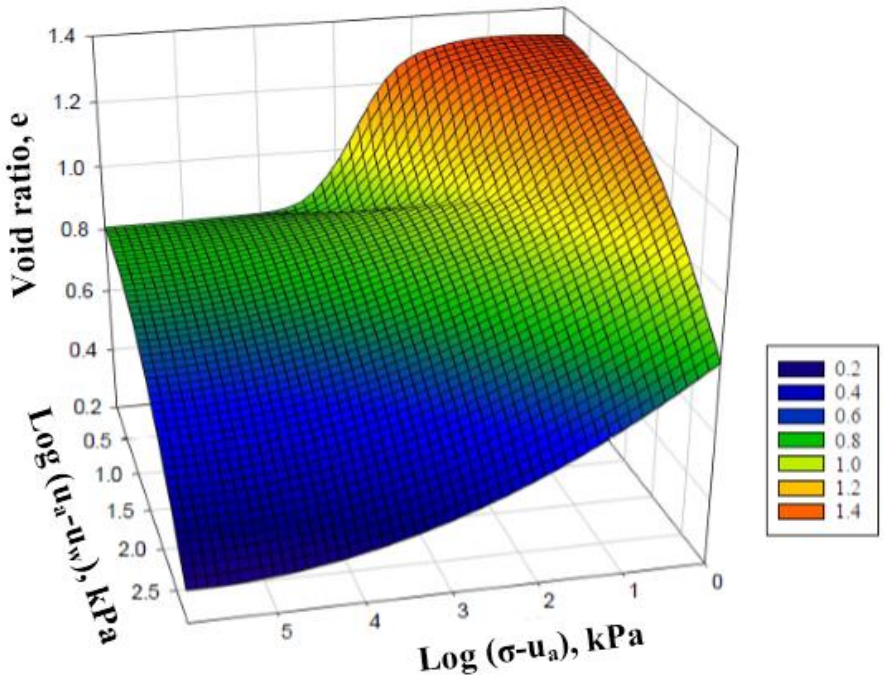

Figure 29 The void ratio constitutive surface of the Moreland clay

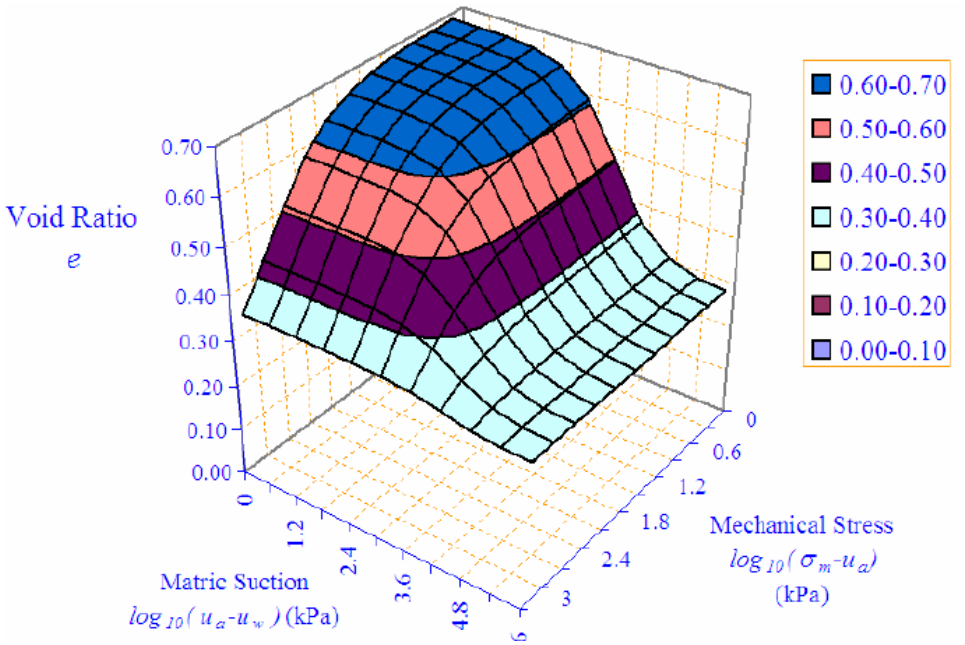

Figure 30 The void ratio constitutive surface of the Texas expansive soil (Zhang 2004)

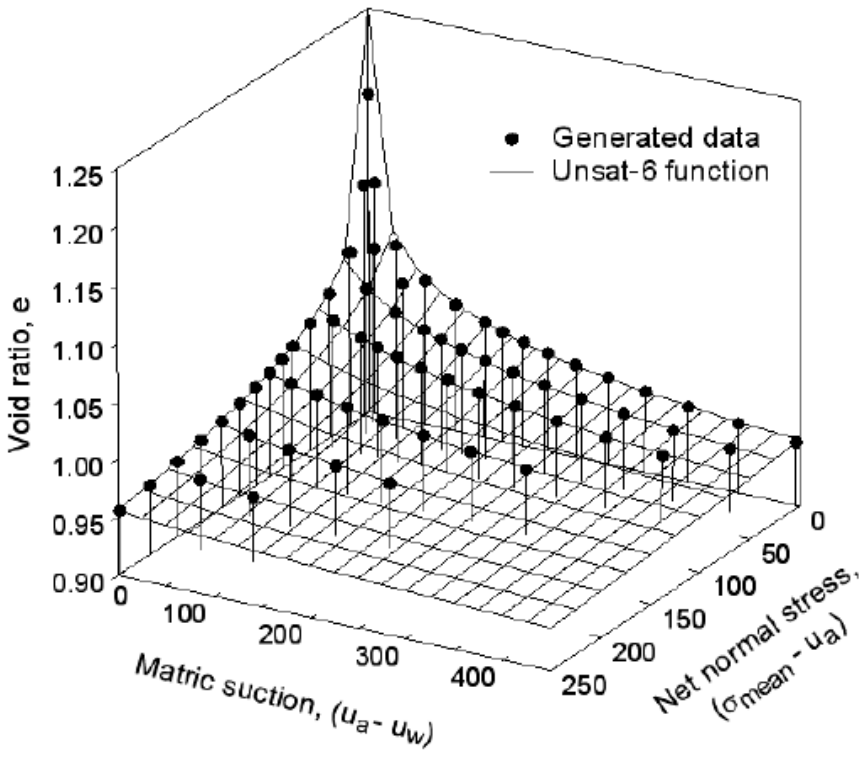

Figure 31 The void ratio constitutive surface of the Regina soil (Hung 2002)

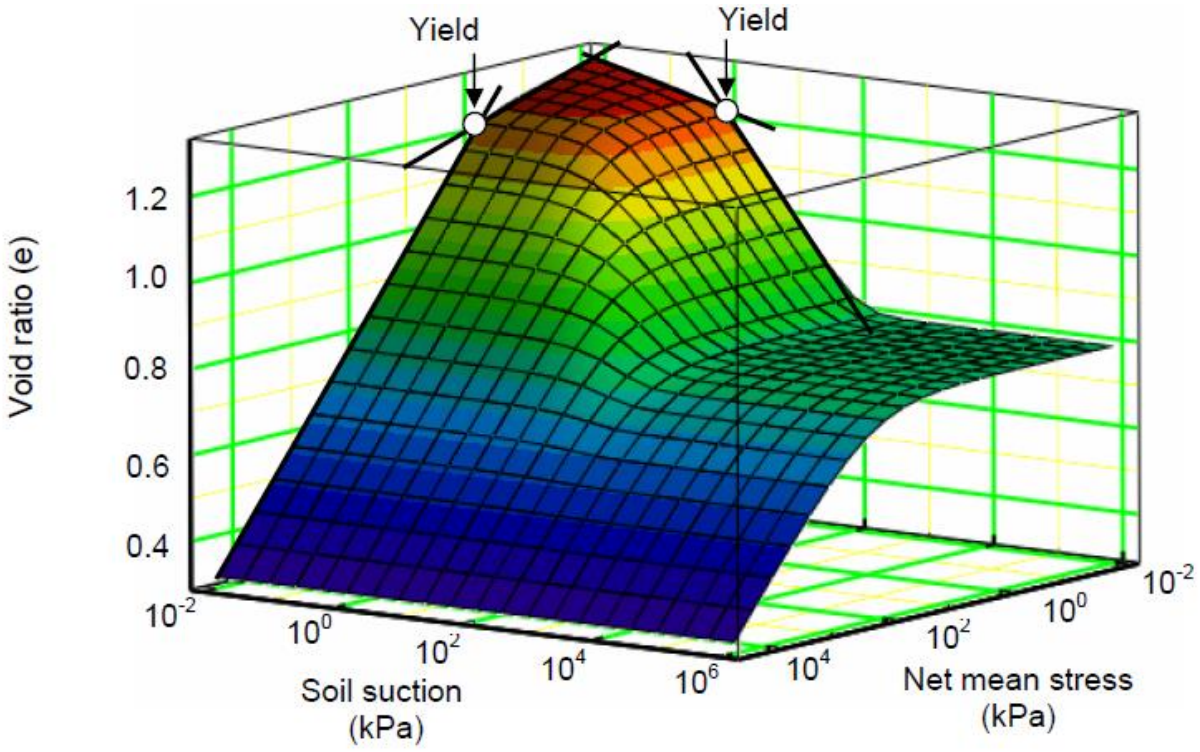

Figure 32 The void ratio constitutive surface of the artificial silt soil (Pham 2005)

7. DEVELOPMENT OF AN ANALYTIC METHOD TO DETERMINE HEAVE/SHRINKAGE-INDUCED PAVEMENT STRESSES

7.1 INTRODUCTION

To analyze structures on expansive soil it requires the knowledge of understanding the properties of structures as well as the properties of the soil. Generally the properties of the soil are difficult to obtain (Tsudik 2012). Different soils behave differently under applied load. This method is mainly based on Winkler foundation model. Winkler (1867) first proposed modelling the soil as an elastic medium. In the Winkler foundation model soil is replaced with springs that behaves the same under applied load as real soils. Because of its simplicity the Winkler model is the most popular soil model used by practicing engineers (Tsudik 2012). Many scientists like Hetényi (1946), Umansky (1933) and others used the Winkler foundation as the base of their research, where some researchers tried to improve the soil models mentioned above by recommending the use of new soil models. Some notable research include that Pasternak (1954) proposed a soil model with two coefficients of subgrade reaction and Reissner (1958) recommended a soil model that simplified analysis of foundations supported on the elastic half-space.

In this section, a new one-dimensional analytical method is proposed for modelling granular fills/pavement/beam on expansive soil with or without a surcharge load using the Winkler foundation model. In the research, since the Winkler Foundation theory is applied to analyze pavement, the pavement is referred to as the beam, which is equivalent to the pavement resting on expansive soil unless otherwise specified.

7.2 DESCRIPTION OF WINKLER FOUNDATION MODEL

Winkler foundation model consists of an infinite numbers of closely spaced unconnected linear-elastic springs whose behavior resembles that of a liquid base (Melerski 2006). These springs are defined my subgrade modulus (k_s). Closed form solutions for a simple problem has been proposed by many researchers (Dodge 1964; Hetényi 1946; Miranda and Nair 1966; Ting 1982;

Yin 2000). The mechanism behind the model is that the maximum displacement will occur under the load. The Winkler foundation model has some assumptions as mentioned below:

1. The load applied to the soil surface produces settlements of the soil only under the applied load and does not produce any settlements and stresses outside of the loaded area.

3. The soil can resist compression as well as tension stresses.

4. The shape and size of the foundation do not affect the settlement of the soil.

These assumptions are not always true as described in the following paragraphs. The limitations of Winkler model are given below:

1. When a load is applied to the soil it produces settlement under the applied load and outside of the loaded area.

2. Soil does not resist any tension stresses even a small amount.

3. Settlement of the soil is not only the function of applied load also the shape and size of the foundation.

In spite of these limitations mentioned above researchers such as Klepikov (1967) proved that analysis based on Winkler foundation produces realistic results that are practically close enough to results obtained from soil testing and observations of settlements of real structures.

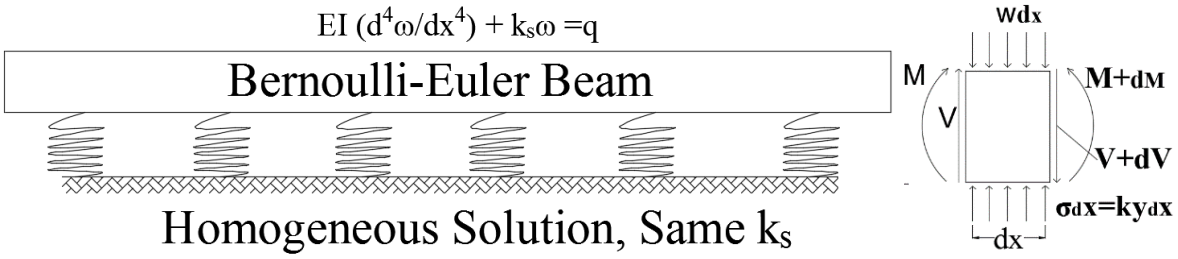

Figure 33 Loaded beam supported on elastic foundation

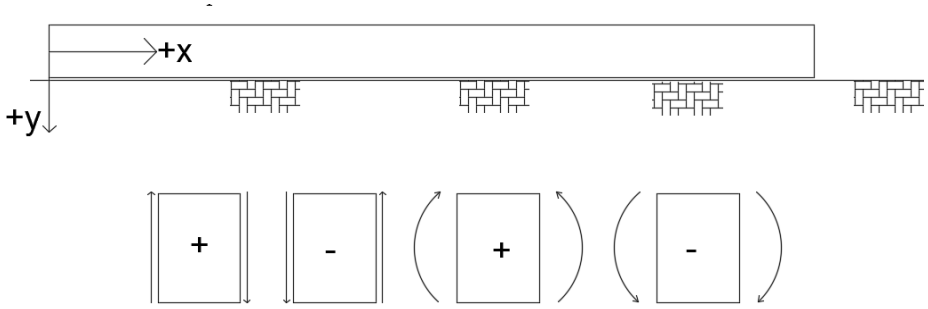

Figure 34 Sign convention for deflection, shear force and bending moment

For a loaded beam of a unit width and length L supported by elastic foundation as shown in Fig. 34, the relation between foundation reactions (R) at any point along the beam is directly proportional to the vertical displacement (w). Here, k_s is constant of proportionality also known as subgrade modulus.

$$R = k_s * w \tag{44}$$

Now if a small piece of beam is considered, x-distance from the left with a length δx as illustrated in Fig. 34. The shear force on that beam is considered V and bending moment as M. From Fig. 35 Eq. 45 can be found using the equilibrium condition.

$$V - (V + \delta V) + k_s w \delta x - q \delta x = 0 \tag{45}$$

$$\frac{\delta V}{\delta x} = k_s w - q \tag{46}$$

In the limit

$$\frac{dV}{dx} = k_s w - q \tag{47}$$

Using the relation between shear force and bending moment

$$V = \frac{dM}{dx} \tag{48}$$

$$\frac{d^2 M}{dx^2} = k_s w - q \tag{49}$$

Using the relation between bending moment and bending stiffness of the beam

$$EI\left(\frac{d^2 w}{dx^2}\right) = -M \tag{50}$$

From Eq. 49 and 50

$$\frac{d^2}{dx^2} EI\left(\frac{d^2w}{dx^2}\right) = k_s w - q \qquad (51)$$

7.3 THE CONCEPT OF VIRTUAL LOAD

If a pavement represented as a beam is resting on a regular (unexpansive) soil, it will only deflect by the introduction of an external load. Fig. 36 (a) and (b) shows the deflection of the beam on the regular soil. Beam deflection on a regular soil can be measured using the Winkler foundation model. Fig. 36 (c) shows beam deflection due to volume change of the subgrade expansive soil. This expansive-soil-induced beam deflection can be represented by the introduction of a virtual load on the beam with the subgrade considered as a regular soil. Fig. 36 (d) shows the virtual load on a beam with a regular soil as a subgrade. The virtual load makes the beam deflected, which is equivalent to the real deflection induced by the volume change of the expansive soil subgrade. The advantage of this transformation is that this virtual load imposed beam-regular subgrade soil system can be analyzed using the Winkler foundation model.

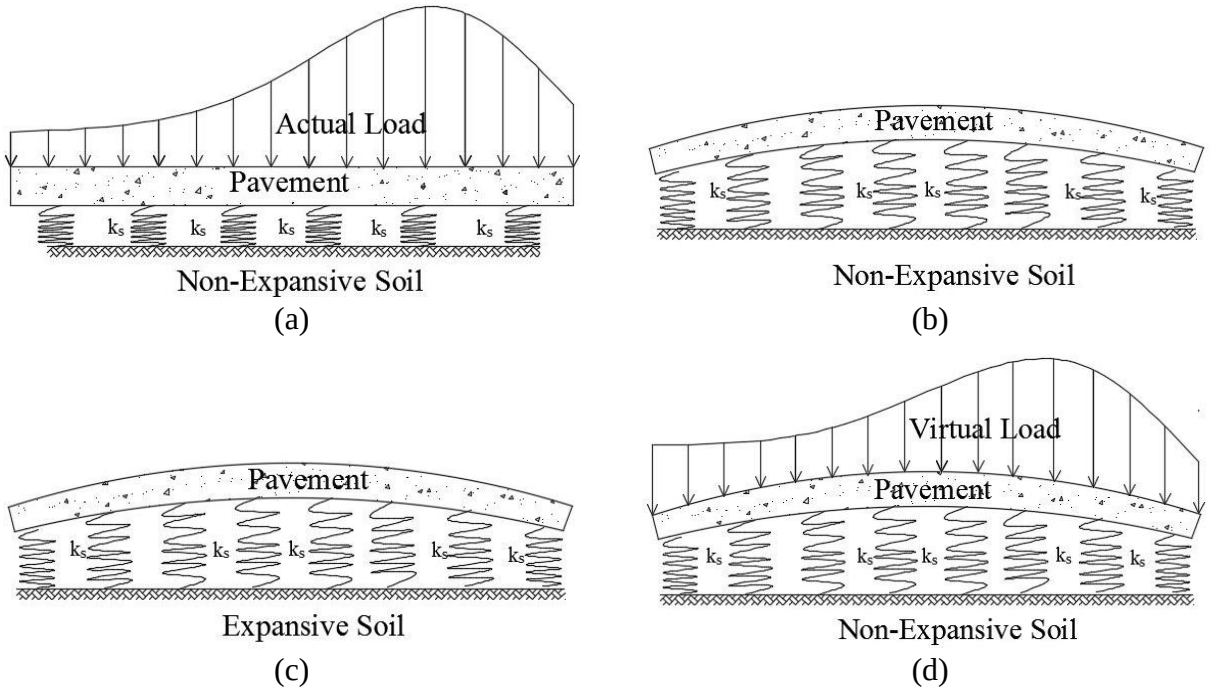

Figure 35 (a) Pavement on a Regular Soil, (b) Pavement Deflection Due to External,Load, (c) Pavement Deflection Due to Expansive Soil's Volume Change, and (d) Proposed Virtual Load Soil Model

The virtual load distribution is not known; thus, it is expressed as a form of Fourier series. The model will be established in the following steps: 1) consider the virtual load as a form of Fourier series in the combination of a few Fourier terms; 2) find the beam deflections at multiple points across the pavement from shoulder to shoulder, which are calculated from the heave or settlement prediction of the expansive subgrade soil; 3) find a closed-form solution of beam-like pavement deflection as a function of the only regression constants; 4) using regression analysis, find the Fourier constants, and the virtual load is thereby known; 5) once q (virtual load) is known, find the deflection, rotation, shear force and bending moment of the beam, using the closed-form solution of the Winkler foundation model; 6) again find the deflection, rotation, shear force and moment of the beam because of the self-weight and the external load (if any) by using the regular closed-form solution of the Winkler foundation, and 7) finally, using the super position theorem, find the combined deflection, rotation, shear force and moment of the beam.

7.4 ANALYTICAL METHOD TO FIND A CLOSED FORM SOLUTION OF PAVEMENT DUE TO ANY KNOWN LOAD (q) USING THE WINKLER FOUNDATION THEORY

From Eq. 51

$$EI\frac{d^4w}{dx^4} + k_s w = q \tag{52}$$

Let us consider a finite beam (beam width of L and bending stiffness EI) subjected to any form of pressure loading. The pressure q (e.g., self-weight, external load) can be expressed as a function of x, that is

$$q = f(x) \text{ for } 0 < x < L \tag{53}$$

Where, f(x) can be expressed in a Fourier cosine series

$$q = A_n \cos\left(\frac{n\pi x}{L}\right) \tag{54}$$

Let's assume the particular integral is

$$w_P = a_n \cos\left(\frac{n\pi x}{L}\right) \tag{55}$$

From Eq. 52

$$\left(\frac{n\pi}{L}\right)^4 a_n \cos\left(\frac{n\pi x}{L}\right) + \frac{k_s}{EI} a_n \cos\left(\frac{n\pi x}{L}\right) = \frac{A_n \cos\left(\frac{n\pi x}{L}\right)}{EI}$$

$$\left(\frac{n\pi}{L}\right)^4 a_n + \frac{k_s}{EI} a_{n_n} = \frac{A_n}{EI}$$

$$a_n = \frac{A_n}{k_s + EI\left(\frac{n\pi}{L}\right)^4} \tag{56}$$

Taking four terms in Fourier series

$$q(x) = \sum_{n=0}^{4} A_n \cos\left(\frac{n\pi x}{L}\right)$$

$$q\,(x) = A_0 + \sum_{n=1}^{4} A_n \cos\left(\frac{n\pi x}{L}\right) \tag{57}$$

Where,

$$A_0 = \frac{1}{L}\int_0^L f(x)dx \quad \text{and} \quad A_0 = \frac{2}{L}\int_0^L f(x)\cos\left(\frac{n\pi x}{L}\right)dx \tag{58}$$

7.4.1 BEAM DEFLECTION $W_P(X)$ EQUATION DUE TO LOAD q

A Homogeneous solution of beam for any type of load types (e.g., uniformly distributed load (UDL), point load, concentrated moment) is given in Eq. 59 and particular solution which is the function of load type is given in Eq. 60.

$$w_H(x) = e^{\beta x}\{C_1 \cos(\beta x) + C_2 \sin s(\beta x)\} + e^{-\beta x}\{C_3 \cos(\beta x) + C_4 \sin(\beta x)\} \tag{59}$$

$$w_{PA}(x) = A_0 + \sum_{n=1}^{4} A_n \cos\left(\frac{n\pi x}{L}\right) \tag{60}$$

Here, C_1, C_2, C_3, and C_4 are four constants to be determined by the four given boundary conditions.

The solution of Eq. 51 is the summation of the homogeneous solution and the particular solution. Eqs. 61 to 62 show the steps for the beam deflection equation.

$$w_B(x) = w_H(x) + w_{PA}(x) \tag{61}$$

$$EI\frac{d^4w}{dx^4} + k_s w = A_0 + \sum_{n=1}^{4} A_n \cos\left(\frac{n\pi x}{L}\right) \tag{62}$$

$$w_B(x) = e^{\beta x}\{C_1\cos(\beta x) + C_2\,\text{sins}(\beta x)\} + e^{-\beta x}\{C_3\cos(\beta x) + C_4\sin(\beta x)\} + \frac{A_0}{k_s} + \sum_{n=1}^{4} a_n \cos\left(\frac{n\pi x}{L}\right) \tag{63}$$

Where,

$$a_n = \frac{A_n}{k_s + EI\left(\frac{n\pi}{L}\right)^4} \tag{64}$$

$$\beta = \sqrt[4]{\frac{k_s}{4EI}} \tag{65}$$

After rearranging Eq. 66 as a matrix form

$$[w_B(x)] = [e^{\beta x}\cos(\beta x) \quad e^{\beta x}\sin(\beta x) \quad e^{-\beta x}\cos(\beta x) \quad e^{-\beta x}\sin(\beta x)] * \begin{bmatrix} C_1 \\ C_2 \\ C_3 \\ C_4 \end{bmatrix} + \frac{A_0}{k_s} + \left[\cos\left(\frac{\pi x}{L}\right) \quad \cos\left(\frac{2\pi x}{L}\right) \quad \cos\left(\frac{3\pi x}{L}\right) \quad \cos\left(\frac{4\pi x}{L}\right)\right] * \begin{bmatrix} a_1 \\ a_2 \\ a_3 \\ a_4 \end{bmatrix} \tag{66}$$

7.4.2 PAVEMENT ROTATION Φ(x) EQUATION DUE TO Q LOAD

Eqs. 67 to72 show the steps for the beam rotation derivations.

$$\phi(x) = \frac{dw(x)}{dx} \tag{67}$$

$$\phi(x) = e^{\beta x}\{C_1\beta\cos(\beta x) + C_2\beta\sin(\beta x)\} + e^{\beta x}\{C_2\beta\cos(\beta x) - C_1\beta\sin(\beta x)\} - e^{-\beta x}\{C_3\beta\cos(\beta x) + C_4\beta\sin(\beta x)\} + e^{-\beta x}\{C_4\beta\beta\cos(\beta x) - C_3\beta\sin(\beta x)\} - \sum_{n=1}^{4}\left(\frac{n\pi}{L}\right)a_n\sin\left(\frac{n\pi x}{L}\right) \tag{68}$$

$$\phi(x) = e^{\beta x}\{(C_1\beta + C_2\beta)\cos(\beta x) + (-C_1\beta + C_2\beta)\sin(\beta x)\} + e^{-\beta x}\{(-C_3\beta + C_4\beta)\cos(\beta x) + (-C_3\beta - C_4\beta)\sin(\beta x)\} - \sum_{n=1}^{4}\left(\frac{n\pi}{L}\right)a_n\sin\left(\frac{n\pi x}{L}\right) \tag{69}$$

$$\phi\,(x) = e^{\beta x}\{C_5\cos(\beta x) + C_6\sin(\beta x)\} + e^{-\beta x}\{C_7\cos(\beta x) + C_8\sin(\beta x)\} - \sum_{n=1}^{4}\left(\frac{n\pi}{L}\right)a_n\sin\left(\frac{n\pi x}{L}\right) \quad (70)$$

Where,

$$C_5 = C_1\beta + C_2\beta$$

$$C_6 = -C_1\beta + C_2\beta$$

$$C_7 = -C_3\beta + C_4\beta$$

$$C_8 = -C_3\beta - C_4\beta$$

$$\begin{bmatrix} C_5 \\ C_6 \\ C_7 \\ C_8 \end{bmatrix} = \begin{bmatrix} \beta & \beta & 0 & 0 \\ -\beta & \beta & 0 & 0 \\ 0 & 0 & -\beta & \beta \\ 0 & 0 & -\beta & -\beta \end{bmatrix} * \begin{bmatrix} C_1 \\ C_2 \\ C_3 \\ C_4 \end{bmatrix} \quad (71)$$

$\phi\,(x) =$

$$[e^{\beta x}\cos(\beta x) \quad e^{\beta x}\sin(\beta x) \quad e^{-\beta x}\cos(\beta x) \quad e^{-\beta x}\sin(\beta x)] * \begin{bmatrix} \beta & \beta & 0 & 0 \\ -\beta & \beta & 0 & 0 \\ 0 & 0 & -\beta & \beta \\ 0 & 0 & -\beta & -\beta \end{bmatrix} * \begin{bmatrix} C_1 \\ C_2 \\ C_3 \\ C_4 \end{bmatrix} - \sum_{n=1}^{4}\left(\frac{n\pi}{L}\right)a_n\sin\left(\frac{n\pi x}{L}\right) \quad (72)$$

7.4.3 PAVEMENT MOMENT M(x) EQUATION DUE TO q LOAD

Equations 73 to 78 show the steps of the beam moment equation derivation.

$$M\,(x) = -EI\frac{d\phi(x)}{dx} \quad (73)$$

$$\frac{d\phi(x)}{dx} = e^{\beta x}\{(C_1\beta^2 - C_1\beta^2 + 2C_2\beta^2)\cos(\beta x) + (C_2\beta^2 - C_2\beta^2 - 2C_1\beta^2)\sin(\beta x)\} + e^{-\beta x}\{(C_3\beta^2 - C_3\beta^2 - 2C_4\beta^2)\cos(\beta x) + (C_4\beta^2 - C_4\beta^2 + 2C_3\beta^2)\sin(\beta x)\} - \sum_{n=1}^{4}\left(\frac{n\pi}{L}\right)^2 a_n\cos\left(\frac{n\pi x}{L}\right) \quad (74)$$

$$\frac{d\phi(x)}{dx} = e^{\beta x}\{2C_2\beta^2\cos(\beta x) - 2C_1\beta^2\sin(\beta x)\} + e^{-\beta x}\{-2C_4\beta^2\cos(\beta x) + 2C_3\beta^2\sin(\beta x)\} - \sum_{n=1}^{4}\left(\frac{n\pi}{L}\right)^2 a_n\cos\left(\frac{n\pi x}{L}\right) \quad (75)$$

$$\frac{d\phi(x)}{dx} = e^{\beta x}\{C_9\cos(\beta x) + C_{10}\sin(\beta x)\} + e^{-\beta x}\{C_{11}\cos(\beta x) + C_{12}\sin(\beta x)\} - \sum_{n=1}^{4}\left(\frac{n\pi}{L}\right)^2 a_n\cos\left(\frac{n\pi x}{L}\right) \quad (76)$$

Where,

$$C_9 = 2C_2\beta^2$$

$$C_{10} = -2C_1\beta^2$$

$$C_{11} = -2C_4\beta^2$$

$$C_{12} = 2C_3\beta^2$$

$$\begin{bmatrix} C_9 \\ C_{10} \\ C_{11} \\ C_{12} \end{bmatrix} = \begin{bmatrix} 0 & 2\beta^2 & 0 & 0 \\ -2\beta^2 & 0 & 0 & 0 \\ 0 & 0 & 0 & -2\beta^2 \\ 0 & 0 & 2\beta^2 & 0 \end{bmatrix} * \begin{bmatrix} C_1 \\ C_2 \\ C_3 \\ C_4 \end{bmatrix} \quad (77)$$

$$M(x) = -EI * \left\{ [e^{\beta x}\cos(\beta x) \quad e^{\beta x}\sin(\beta x) \quad e^{-\beta x}\cos(\beta x) \quad e^{-\beta x}\sin(\beta x)] * \begin{bmatrix} 0 & 2\beta^2 & 0 & 0 \\ -2\beta^2 & 0 & 0 & 0 \\ 0 & 0 & 0 & -2\beta^2 \\ 0 & 0 & 2\beta^2 & 0 \end{bmatrix} * \begin{bmatrix} C_1 \\ C_2 \\ C_3 \\ C_4 \end{bmatrix} - \sum_{n=1}^{4}\left(\frac{n\pi}{L}\right)^2 a_n\cos\left(\frac{n\pi x}{L}\right) \right\} \quad (78)$$

7.4.4 PAVEMENT SHEAR V(x) EQUATION DUE TO q LOAD

Equations 79 to 84 show the steps of beam shear equation derivation.

$$V(x) = \frac{dM(x)}{dx} \tag{79}$$

$V(x) =$

$$EI\Big[e^{\beta x}\{(C_1\beta^3 - C_2\beta^3 + 3C_2\beta^3 - 3C_1\beta^3)\cos(\beta x) + (C_2\beta^3 + C_1\beta^3 - 3C_1\beta^3 - 3C_2\beta^3)\sin(\beta x)\} + e^{-\beta x}\{(-C_3\beta^3 - C_4\beta^3 + 3C_3\beta^3 + 3C_4\beta^3)\cos(\beta x) + (-C_4\beta^3 + C_3\beta^3 - 3C_3\beta^3 + 3C_4\beta^3)\sin(\beta x)\} - 2q_0\sum_{n=1}^{4}\left(\frac{n\pi}{L}\right)^3 a_n \sin\left(\frac{n\pi x}{L}\right)\Big] \tag{80}$$

$$V(x) = EI\Big[e^{\beta x}\{(2C_2\beta^3 - 2C_1\beta^3)\cos(\beta x) + (-2C_1\beta^3 - 2C_2\beta^3)\sin(\beta x)\} + e^{-\beta x}\{(2C_3\beta^3 + 2C_4\beta^3)\cos(\beta x) + (-2C_3\beta^3 + 2C_4\beta^3)\sin(\beta x)\} - 2q_0\sum_{n=1}^{4}\left(\frac{n\pi}{L}\right)^3 a_n \sin\left(\frac{n\pi x}{L}\right)\Big] \tag{81}$$

$$V(x) = EI\Big[e^{\beta x}\{C_{13}\cos(\beta x) + C_{14}\sin(\beta x)\} + e^{-\beta x}\{C_{15}\cos(\beta x) + C_{16}\sin(\beta x)\} - 2q_0\sum_{n=1}^{4}\left(\frac{n\pi}{L}\right)^3 a_n \sin\left(\frac{n\pi x}{L}\right)\Big] \tag{82}$$

Where,

$$C_{13} = -2C_1\beta^3 + 2C_2\beta^3$$

$$C_{14} = -2C_1\beta^3 - 2C_2\beta^3$$

$$C_{15} = 2C_3\beta^3 + 2C_4\beta^3$$

$$C_{16} = -2C_3\beta^3 + 2C_4\beta^3$$

$$\begin{bmatrix} C_{13} \\ C_{14} \\ C_{15} \\ C_{16} \end{bmatrix} = \begin{bmatrix} -2\beta^3 & 2\beta^3 & 0 & 0 \\ -2\beta^3 & -2\beta^3 & 0 & 0 \\ 0 & 0 & 2\beta^3 & 2\beta^3 \\ 0 & 0 & -2\beta^3 & 2\beta^3 \end{bmatrix} * \begin{bmatrix} C_1 \\ C_2 \\ C_3 \\ C_4 \end{bmatrix} \tag{83}$$

$V(x) =$

$EI *$

$$\left[[e^{\beta x}\cos(\beta x) \quad e^{\beta x}\sin(\beta x) \quad e^{-\beta x}\cos(\beta x) \quad e^{-\beta x}\sin(\beta x)] * \begin{bmatrix} 2\beta^3 & -2\beta^3 & 0 & 0 \\ 2\beta^3 & 2\beta^3 & 0 & 0 \\ 0 & 0 & -2\beta^3 & -2\beta^3 \\ 0 & 0 & 2\beta^3 & -2\beta^3 \end{bmatrix} * \begin{bmatrix} C_1 \\ C_2 \\ C_3 \\ C_4 \end{bmatrix} - 2q_0 \sum_{n=1}^{4} \left(\frac{n\pi}{L}\right)^3 a_n \sin\left(\frac{n\pi x}{L}\right) \right] \quad (84)$$

7.4.5 DETERMINATION OF CONSTANT C_1 TO C_{16}

Using boundary condition x= 0, V=0, M =0 and x=L, V=0, M =0 in Eqs. 78 and 84; matrix [M][C] = [R] can be found (Eq. 85). Matrix **M** is a function of basic parameters such as β, L, k_s, E and I, where R matrix is a function of parameters for load **q**. Once all the parameters mentioned above are known, using matrix $[C] = [M]^{-1}[R]$ (Eq. 86) constants C_1 to C_4 can be found. Once C_1 to C_4 is known using Eqs. 71, 77 and 83, constants C_5 to C_{16} can be found. Eq. 111 shows the final matrix solution of the beam deflection. Following the same procedure matrix solutions can be developed for rotation, moment and shear force.

$$[\boldsymbol{M}][\boldsymbol{C}] = [\boldsymbol{R}]$$

$$\begin{bmatrix} 0 & 2\beta^2 & 0 & -2\beta^2 \\ 2*\beta^3 & -2*\beta^3 & -2*\beta^3 & -2*\beta^3 \\ -2\beta^2\, e^{\beta L} sin(\beta L) & 2\beta^2 e^{\beta L} cos(\beta L) & 2\beta^2\, e^{-\beta L} sin(\beta L) & -2\beta^2 e^{-\beta L} cos(\beta L) \\ 2\beta^3 * e^{\beta L}\{cos(\beta L) + sin(\beta L)\} & 2\beta^3 * e^{\beta L}\{sin(\beta L) - cos(\beta L)\} & -2\beta^3 * e^{-\beta L}\{cos(\beta L) - sin(\beta L)\} & -2\beta^3 * e^{-\beta L}\{cos(\beta L) + sin(\beta L)\} \end{bmatrix} \begin{bmatrix} C_1 \\ C_2 \\ C_3 \\ C_4 \end{bmatrix} =$$

$$\begin{bmatrix} \sum_{n=1}^{4} \left(\frac{n\pi}{L}\right)^2 a_n \\ 0 \\ \sum_{n=1}^{4} \left(\frac{n\pi}{L}\right)^2 a_n (-1)^n \\ 0 \end{bmatrix} \tag{85}$$

$$[\boldsymbol{C}] = [\boldsymbol{M}]^{-1}[\boldsymbol{R}] = [\boldsymbol{D}][\boldsymbol{R}]$$

$$\begin{bmatrix} C_1 \\ C_2 \\ C_3 \\ C_4 \end{bmatrix} =$$

$$\begin{bmatrix} 0 & 2\beta^2 & 0 & -2\beta^2 \\ 2*\beta^3 & -2*\beta^3 & -2*\beta^3 & -2*\beta^3 \\ -2\beta^2\, e^{\beta L} sin(\beta L) & 2\beta^2 e^{\beta L} cos(\beta L) & 2\beta^2\, e^{-\beta L} sin(\beta L) & -2\beta^2 e^{-\beta L} cos(\beta L) \\ 2\beta^3 * e^{\beta L}\{cos(\beta L) + sin(\beta L)\} & 2\beta^3 * e^{\beta L}\{sin(\beta L) - cos(\beta L)\} & -2\beta^3 * e^{-\beta L}\{cos(\beta L) - sin(\beta L)\} & -2\beta^3 * e^{-\beta L}\{cos(\beta L) + sin(\beta L)\} \end{bmatrix}^{-1} \begin{bmatrix} \sum_{n=1}^{4} \left(\frac{n\pi}{L}\right)^2 a_n \\ 0 \\ \sum_{n=1}^{4} \left(\frac{n\pi}{L}\right)^2 a_n (-1)^n \\ 0 \end{bmatrix}$$

(86)

$$[D] = \begin{bmatrix} 0 & 2\beta^2 & 0 & -2\beta^2 \\ 2*\beta^3 & -2*\beta^3 & -2*\beta^3 & -2*\beta^3 \\ -2\beta^2\, e^{\beta L} sin(\beta L) & 2\beta^2 e^{\beta L} cos(\beta L) & 2\beta^2\, e^{-\beta L} sin(\beta L) & -2\beta^2 e^{-\beta L} cos(\beta L) \\ 2\beta^3 * e^{\beta L}\{cos(\beta L) + sin(\beta L)\} & 2\beta^3 * e^{\beta L}\{sin(\beta L) - cos(\beta L)\} & -2\beta^3 * e^{-\beta L}\{cos(\beta L) - sin(\beta L)\} & -2\beta^3 * e^{-\beta L}\{cos(\beta L) + sin(\beta L)\} \end{bmatrix}^{-1} =$$

$$\frac{1}{Det\ of\ M}\begin{bmatrix} b_{11} & b_{12} & b_{13} & b_{14} \\ b_{21} & b_{22} & b_{23} & b_{24} \\ b_{31} & b_{32} & b_{33} & b_{34} \\ b_{41} & b_{42} & b_{43} & b_{44} \end{bmatrix} \quad (87)$$

After performing the matrix operation the coefficients from b_{11} to b_{44} can be found

$$b_{11} = 8\beta^8 e^{-2\beta L}\{sin^2(\beta L) + cos^2(\beta L)\} + 8\beta^8\{-2 * sin(\beta L) * cos(\beta L) - cos^2(\beta L) + sin^2(\beta L)\} \quad (88)$$

$$b_{12} = -8\beta^7 e^{-2\beta L}\{-cos^2(\beta L) - sin^2(\beta L)\} - 8\beta^7 * \{cos^2(\beta L) + sin^2(\beta L) - 2 * sin(\beta L) * cos(\beta L)\} \quad (89)$$

$$b_{13} = 8\beta^8 e^{-\beta L}\{3 * sin(\beta L) - cos(\beta L)\} \quad (90)$$

$$b_{14} = -8\beta^7 e^{-\beta L}\{2 * sin(\beta L) + cos(\beta L)\} + 8\beta^7 e^{\beta L} cos(\beta L) \quad (91)$$

$$b_{21} = 8\beta^8 e^{-2\beta L}\{cos^2(\beta L) + sin^2(\beta L)\} + 8\beta^8\{-cos^2(\beta L) - 3 * sin^2(\beta L) - 2 * sin(\beta L) * cos(\beta L)\} \quad (92)$$

$$b_{22} = 16\beta^7 sin^2(\beta L) \quad (93)$$

$$b_{23} = 8\beta^8 e^{\beta L}\{sin(\beta L) + cos(\beta L)\} + 8\beta^8 e^{-\beta L}\{-sin(\beta L) + cos(\beta L)\} \quad (94)$$

$$b_{24} = -8\beta^7 e^{-\beta L} * sin(\beta L) + 8\beta^7 e^{\beta L} * sin(\beta L) \quad (95)$$

$$b_{31} = -8\beta^8\{-2 * sin(\beta L) + cos(\beta L) + cos^2(\beta L) - sin^2(\beta L)\} + 8\beta^8 e^{2\beta L}\{sin^2(\beta L) + cos^2(\beta L)\} \quad (96)$$

$$b_{32} = 8\beta^7\{sin^2(\beta L) + cos^2(\beta L) + 2 * sin(\beta L) + cos(\beta L)\} - 8\beta^7 e^{2\beta L}\{cos^2(\beta L) + sin^2(\beta L)\} \quad (97)$$

$$b_{33} = -32\beta^8 e^{\beta L} sin(\beta L) + 8\beta^8 e^{-\beta L}\{sin(\beta L) + cos(\beta L)\} \quad (98)$$

$$b_{34} = -8\beta^7 e^{-\beta L} cos(\beta L) - 8\beta^7 e^{\beta L}\{2sin(\beta L) - cos(\beta L)\} \quad (99)$$

$$b_{41} = 8\beta^8\{3 * sin^2(\beta L) - 2 * sin(\beta L) * cos(\beta L) + cos^2(\beta L)\} - 8\beta^8 e^{2\beta L}\{cos^2(\beta L) + sin^2(\beta L)\} \quad (100)$$

$$b_{42} = 16\beta^7 sin^2(\beta L) \quad (101)$$

$$b_{43} = -8\beta^8 e^{-\beta L}\{-sin(\beta L) + cos(\beta L)\} + 8\beta^8 e^{\beta L}\{sin(\beta L) + cos(\beta L)\} \quad (102)$$

Lets assume,

$$[E] = [e^{\beta x}cos(\beta x) \quad e^{\beta x}sin(\beta x) \quad e^{-\beta x}cos(\beta x) \quad e^{-\beta x}sin(\beta x)] \tag{103}$$

$$[F] = \begin{bmatrix} \left(\frac{\pi}{L}\right)^2 & \left(\frac{2\pi}{L}\right)^2 & \left(\frac{3\pi}{L}\right)^2 & \left(\frac{4\pi}{L}\right)^2 \\ 0 & 0 & 0 & 0 \\ -\left(\frac{\pi}{L}\right)^2 & \left(\frac{2\pi}{L}\right)^2 & -\left(\frac{3\pi}{L}\right)^2 & \left(\frac{4\pi}{L}\right)^2 \\ 0 & 0 & 0 & 0 \end{bmatrix} \tag{104}$$

$$[G] = \left[cos\left(\frac{\pi x}{L}\right) \quad cos\left(\frac{2\pi x}{L}\right) \quad cos\left(\frac{3\pi x}{L}\right) \quad cos\left(\frac{4\pi x}{L}\right)\right] \tag{105}$$

So,

$$\begin{bmatrix} C_1 \\ C_2 \\ C_3 \\ C_4 \end{bmatrix} = [D] \begin{bmatrix} \sum_{n=1}^{4} \left(\frac{n\pi}{L}\right)^2 a_n \\ 0 \\ \sum_{n=1}^{4} \left(\frac{n\pi}{L}\right)^2 a_n(-1)^n \\ 0 \end{bmatrix} = [D] * \begin{bmatrix} \left(\frac{\pi}{L}\right)^2 & 4\left(\frac{\pi}{L}\right)^2 & 9\left(\frac{\pi}{L}\right)^2 & 16\left(\frac{\pi}{L}\right)^2 \\ 0 & 0 & 0 & 0 \\ -\left(\frac{\pi}{L}\right)^2 & 4\left(\frac{\pi}{L}\right)^2 & -9\left(\frac{\pi}{L}\right)^2 & 16\left(\frac{\pi}{L}\right)^2 \\ 0 & 0 & 0 & 0 \end{bmatrix} \begin{bmatrix} a_1 \\ a_2 \\ a_3 \\ a_4 \end{bmatrix} =$$

$$[\mathrm{D}][\mathrm{F}] \begin{bmatrix} \mathrm{a}_1 \\ \mathrm{a}_2 \\ \mathrm{a}_3 \\ \mathrm{a}_4 \end{bmatrix} \tag{106}$$

$$\begin{bmatrix} \mathrm{C}_1 \\ \mathrm{C}_2 \\ \mathrm{C}_3 \\ \mathrm{C}_4 \end{bmatrix} = [\mathrm{D}][\mathrm{F}] \begin{bmatrix} \mathrm{a}_1 \\ \mathrm{a}_2 \\ \mathrm{a}_3 \\ \mathrm{a}_4 \end{bmatrix} \tag{107}$$

From deflection Eq. 66,

$$[\mathrm{w_B(x)}] = \left[[\mathrm{E}] * [\mathrm{F}] * [\mathrm{D}]\right] * \begin{bmatrix} \mathrm{a}_1 \\ \mathrm{a}_2 \\ \mathrm{a}_3 \\ \mathrm{a}_4 \end{bmatrix} + \frac{\mathrm{A_0}}{\mathrm{k_s}} + [\mathrm{G}] * \begin{bmatrix} \mathrm{a}_1 \\ \mathrm{a}_2 \\ \mathrm{a}_3 \\ \mathrm{a}_4 \end{bmatrix} \tag{108}$$

$$[\mathrm{w_B(x)}] = \left[[\mathrm{E}] * [\mathrm{F}] * [\mathrm{D}] + [\mathrm{G}]\right] * \begin{bmatrix} \mathrm{a}_1 \\ \mathrm{a}_2 \\ \mathrm{a}_3 \\ \mathrm{a}_4 \end{bmatrix} + \frac{\mathrm{A_0}}{\mathrm{k_s}} \tag{109}$$

Lets Assume,

$$\left[[\mathrm{E}] * [\mathrm{F}] * [\mathrm{D}] + [\mathrm{G}]\right] = [\mathrm{H}_1 \quad \mathrm{H}_2 \quad \mathrm{H}_3 \quad \mathrm{H}_4] \tag{110}$$

$$[w_B(x)] = \begin{bmatrix} \frac{1}{k_s} & H_1 & H_2 & H_3 & H_4 \end{bmatrix} \begin{bmatrix} A_0 \\ a_1 \\ a_2 \\ a_3 \\ a_4 \end{bmatrix} \quad (111)$$

Here are the steps of the solution in a systematic order for a known load:

1. Using the beam theory a closed-form beam deflection, rotation, moment and shear force equations were developed where pressure load q (e.g., self weight, UDL) is expressed as a Fourier series.

2. Using the boundary condition x= 0, V=0, M =0 and x=L, V=0, M =0, [M][C] = [R] matrix was developed.

3. Using $[C] = [M]^{-1}[R]$ matrix constants C_1 through C_4 can be found.

4. Using the values of C_1 to C_4, C_5 to C_{16} can be determined.

5. Using Eqs. 66, 72, 78 and 84 deflection, rotation, shear and moment can be found.

7.5 PROPOSED EXPANSION OF THE CLOSED FORM WINKLER SOLUTION TO EXPANSIVE SOIL

In section 7.4, deflection, rotation, moment and shear force of a moment on a beam under a known load q has been derived. If the load is not known but the deflection of the beam due to an unknown load is known (e.g., deflection of the beam caused by the volume change of expansive soil below the beam), an analytical method has been proposed to find an equivalent virtual load q(x), which will create deflection of a beam resting on regular soil as same as the deflection of that beam resting on an expansive soil. If the structural property of the beam is known then the only unknowns are C_1 to C_4 which are a fuction of A_0 and a_1 through a_4, where A_0 and a_1 through a_4 are Fourier constants of load q(x). So basically, in Eq. 111 the only unknowns are fourier constants of load q(x). In a known deflection with an unknown load situation, these Fourier constants can be found by employing regression analysis with the predicted soil heave/shrinkage (w_p) of the expansive soil. There are a number of empirical equations available to predict soil heave/shrinkage (w_p) as described in section 5.

Here are the steps of the solution in a systematic order for a known soil heave/shrinkage:

1. Predict the heave/shrinkage at different points of the beam $w_p(x)$, using different soil volume change equations, as described in section 5.

2. Using the closed-form Winkler solution, find the equation of deflection of the beam $w_B(x)$. The only unknown of the deflection equation (Eq. 111) will be the Fourier constants.

3. Using regression analysis between $w_P(x)$ and $w_B(x)$, find the Fourier constants. Now load q(x) is known as are the C_1 to C_4 constants since they are a function of Fourier constants.

4. Now follow from steps 4 to 5 of the "Steps of the solution in a systematic order for a known load".

7.6 THE COMBINED SOLUTION USING SUPERPOSITION METHOD

Using superposition theorem the combined effect on the beam can be found. For example, in case of soil heave, the combined beam deflection can be found from Eq. 112 and for soil shrinkage the combined deflection can be found from Eq. 113.

$$w_C(x) = w_q(x) + w_w(x) + w_H(x) \quad (112)$$

or

$$w_C(x) = w_q(x) + w_w(x) + w_S(x) \quad (113)$$

Where,

$w_C(x)$ = Combined beam deflection

$w_q(x)$ = Beam deflection due to external load q

$w_w(x)$ = Beam deflection due to self-weight

$w_H(x)$ = Beam deflection due to soil heave

$w_S(x)$ = Beam deflection due to soil shrinkage

In the same way, the combined rotation, moment and shear force can be found. Generally, self-weight of a pavement is minimal, and its contribution to deflection, rotation, moment and shear can be ignored. Once the bending moment and shear force are known, bending stress and shear stress at every section can be found using Eqs. 114 and 115.

$$\sigma(x) = \frac{M(x)y}{I} \quad (114)$$

$$\tau(x) = \frac{V(x)Q(x)}{It} \quad (115)$$

Here,

σ = bending stress of a beam at a section x- distance from the side;

τ = shear stress of a beam at a section x- distance from the side;

M = total bending moment of a beam at a section x- distance from the side;

V = total shear force of a beam at a section x- distance from the side;

y = distance from the neutral axis to the top/bottom fiber of the beam at a section x- distance from the side;

I = the second moment of inertia of a beam at a section x- distance from the side;

Q = the first moment of area of the top/bottom portion of the cross-sectional area at a section x- distance from the side;

t = thickness of the section.

7.7 A PARAMETRIC STUDY OF THE PROPOSED METHOD

Once the model is developed, a parametric study is carried out. In the parametric study, two extreme situations are considered: 1) extreme heave and 2) extreme shrinkage.

7.7.1 DEFINING STRUCTURAL PROPERTIES OF THE BEAM

A beam is considered resting on expansive soil, as shown in Fig. 37. The structural properties of the beam are defined in Table 8. Young's modulus E_{Clay} for soft clay can be defined from its undrained shear strength C_u from Eq. 116 (Yin 2000). Korenev (1962) suggested k_s values for different types of soil as shown in Table 8. Here, Eq. 117 was used to find the subgrade modulus k_s (Bowles 1996; Selvadurai 2013; Vesic 1961). From Table 8 the k_s value for analyzing soil heave/shrinkage (B=10 m) and beam's self-weight (B=10 m) was found to be 2.67×10^2 kN/m^3. For this case study Young's modulus E is taken to be E = 50,000 kPa. Here, L is the width of the pavement, r is the distance from the edge of the pavement to the starting of the load, B is the

width of the load and finally h is the height of the pavement. Expansive soil induced virtual load and pavement self-weight is present to the whole cross-section, for that reason measuring the stress of pavement by expansive soil and self-weight of pavement the value of r is equal zero while the value of B is taken the same as L.

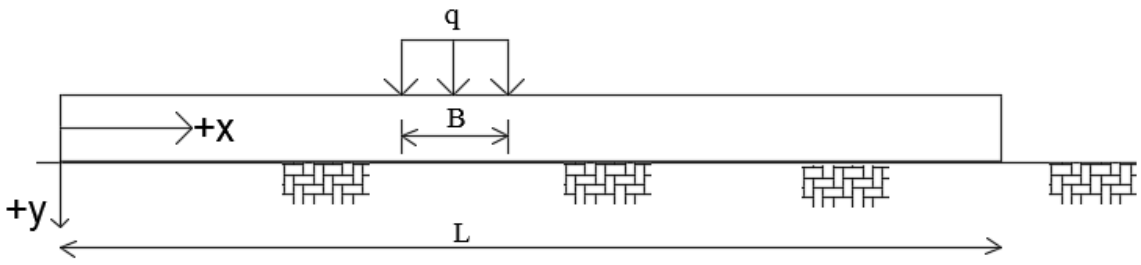

Figure 36 A typical loaded beam

$$E_{Clay} = (200 \sim 500) * C_u \quad (116)$$

$$k_s = \frac{E_{Clay}}{B(1-\upsilon^2)} \quad (117)$$

Table 8 Structural properties of the beam

Parameters	Expansive Soil
r (m)	0
B (m)	10
L (m)	10
h (m)	0.584
q_w (kPA)	--
k_s (kN/m^3)	2.67×10^2
E (kN/m^3)	50000
υ	0.5
y_c (m)	0.292
EI (kN-m)	830.756

Table 9 Modulus of subgrade reaction k_s

General description of the soil	Type of Soil	k_s (kg/cm^3)
Lower density soil	Quicksand, filled-up sand, wet soft clay	0.1-0.5
Average density soil	Sandy ballast, loose gravel, wet clay	0.5-5
Compact solid soil	High density sand, gravel, dry clay	5-10
Very solid compacted soil	Compacted sandy clay, stiff clay	10-20
Stiff soil	Soft rocky soil, limestone, sandstone	20-100
Rocky soil	Rock	100-1500
Reinforced soil	Pile foundation	5-15

7.7.2 DEFINING SOIL PROPERTIES AND SOIL HEAVE PREDICTION

A road (FM2) in Texas was constructed over expansive soils. TxDOT installed horizontal and vertical moisture content sensors underneath the pavement. A year-long readings were taken by the TxDOT. Figs. 38 and 39 show the section of the Texas FM2 pavement. The Texas FM2 road was modeled using VADOSE/W program subject to weather changes in the year, and heave/shrinkage distribution underneath the pavement and shoulder regions was found (Ikra 2017b). After taking the readings, moisture content distributions at different location were plotted for horizontal sensors and vertical sensors. Fig. 40 shows the horizontal moisture distribution underneath the pavement where Fig. 41 shows the vertical moisture content distribution in the ditch. From the thirty-year climate data of the pavement location the driest month was found July and the wettest month was found September as showed in Fig. 42. Theoretically moisture distribution of the date close to July and September from Figs. 40 and 41 should be taken to replicate the extreme shrinkage and extreme heave conditions.

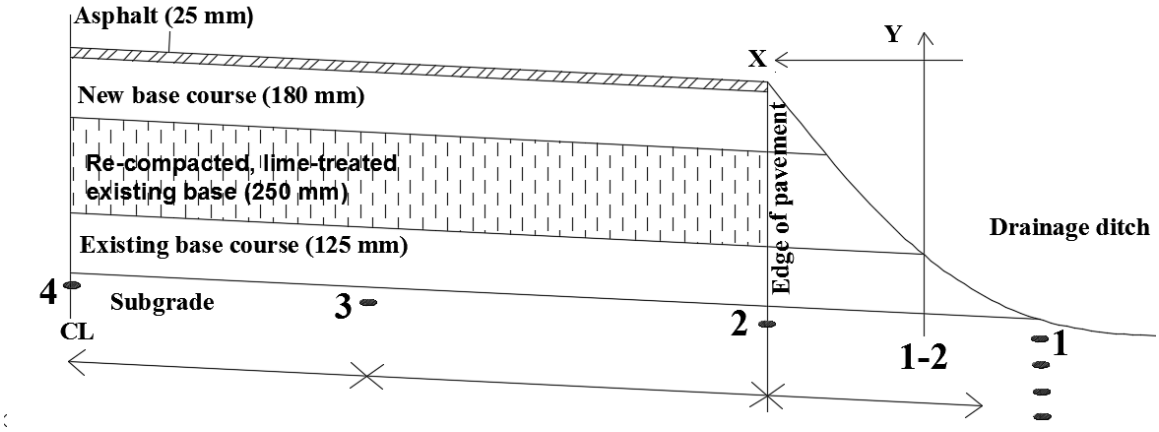

Figure 37 Placement of horizontal moisture sensors at FM 2 site (Modified after Gupta (2009))

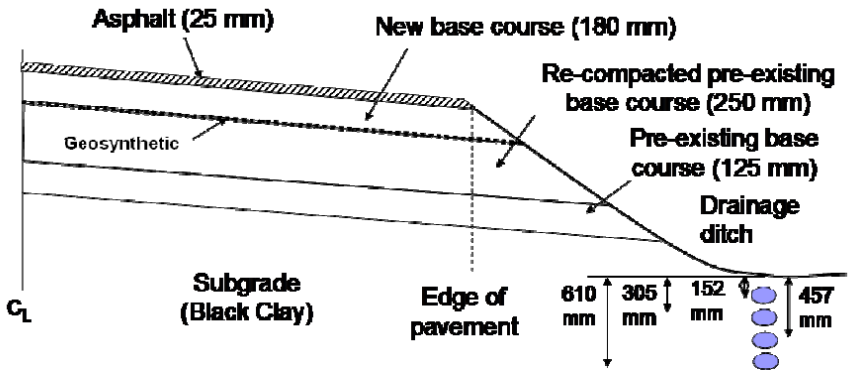

Figure 38 Placement of vertical moisture sensors at FM 2 site (Modified after Gupta (2009))

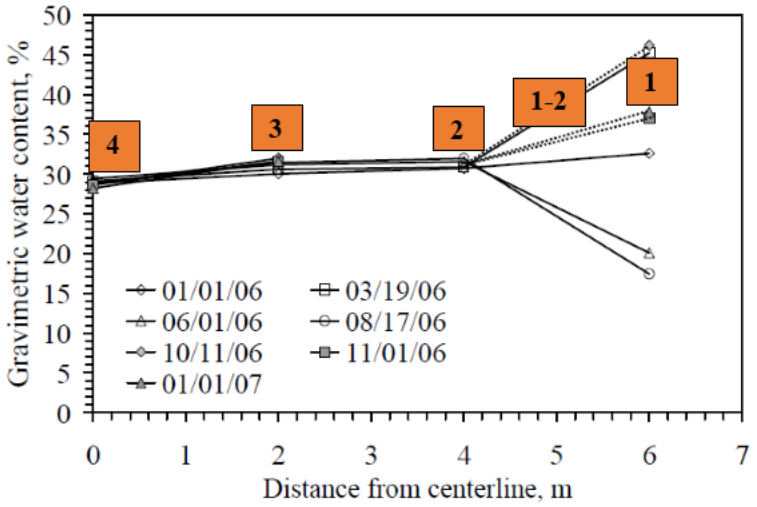

Figure 39 Continuous horizontal moisture data from four sensors (Modified after Gupta (2009))

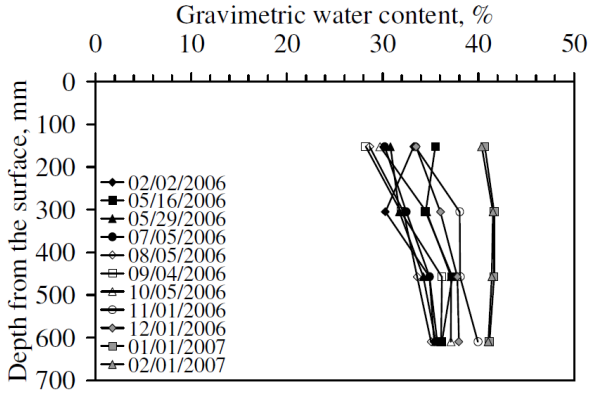

Figure 40 Continuous vertical moisture data from four sensors (Gupta 2009)

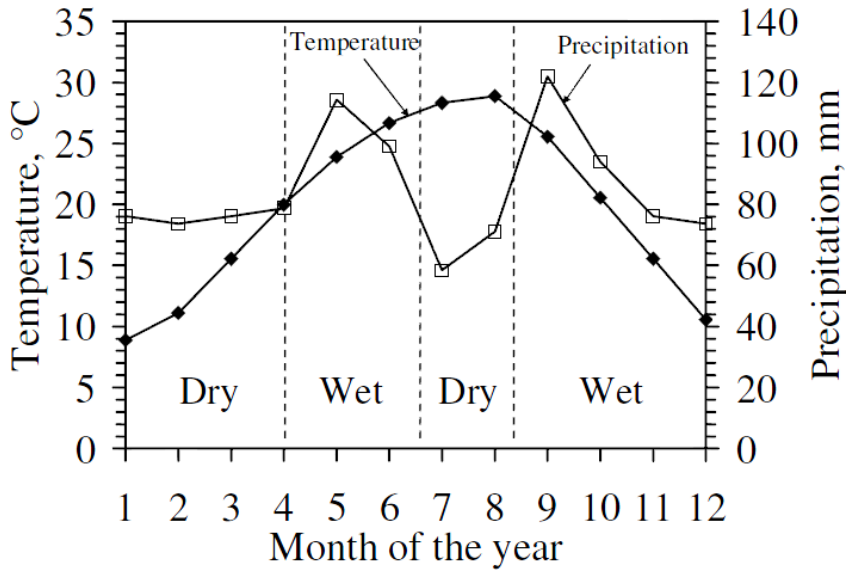

Figure 41 Wet and dry season at the site based on the 30-year average climate data (Gupta 2009)

Ikra (2017b) used VADOSE/W to simulate the moisture distribution and calculate the heave underneath the Texas FM2 pavement. She used Daily weather data (from February 2, 2006 to February 1, 2007) from the station College Station, Bryan District of Texas to obtain the temperature, precipitation, relative humidity of the FM 2 site. All those data showed the driest day was July 17th and the wettest day was January 20th. Fig. 43 shows the model which later she verified using the moisture distribution through the ditch profile found from the model at different dates with the measured moisture distribution found from Fig. 41 on those same dates.

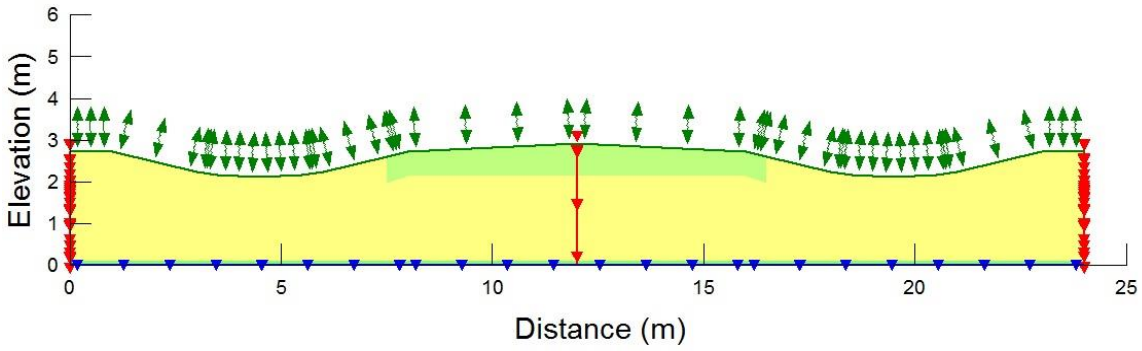

Figure 42 A Model Geometry used in the VADOSE/W Simulation (Ikra 2017b)

In this analysis, the moisture content variations that led to the extreme heave and extreme shrinkage at the ditch (station 1) and the edge of the paved section (station 2) were taken from

the VADOSE/W software. The soil heave and shrinkage at the edge of the shoulder (station 1-2) were calculated from the average heave and shrinkage of station 1 and station 2. At the pavement center, there was no moisture content change and it is assumed no soil volume change at station 4 as shown in Fig. 40. Finally, soil heave and shrinkage at the station 3 between stations 2 and 4 were obtained by taking a linear interpolation as shown in Table 10.

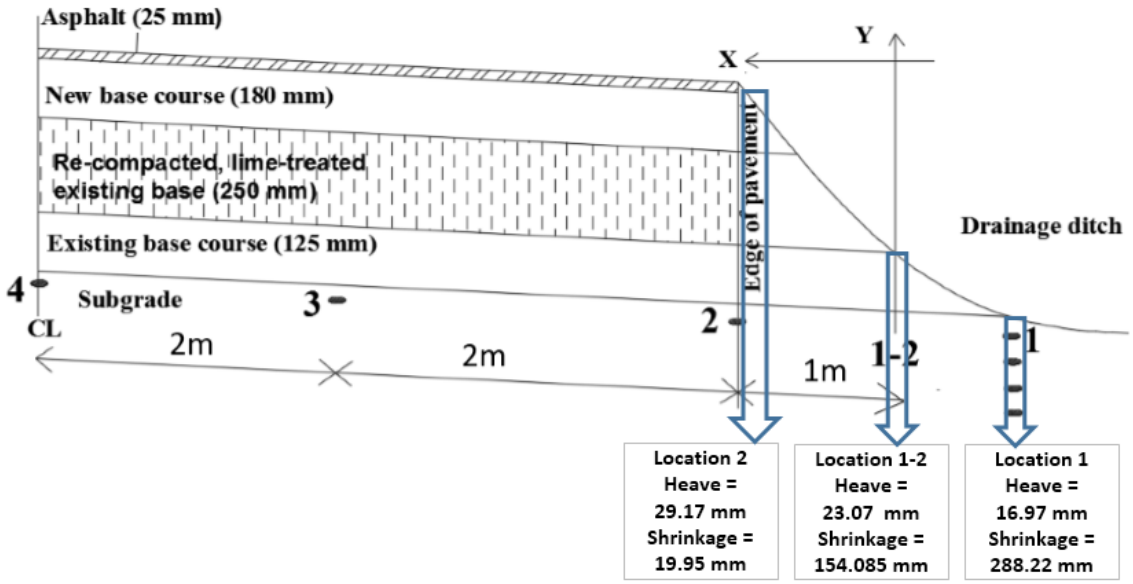

Figure 43 Soil extreme heave and shrinkage during the one-year period from the VADOSE/W Simulation

Table 10 Distribution of moisture content and soil deflection at the cross-section of FM 2 site

Moisture sensor station	Distance from the edge of the pavement	Extreme-heave condition	Extreme-shrinkage condition
		Calculated heave (m) at different locations	Calculated shrinkage (m) at different locations
1	Ditch	0.01697	0.2882
1-2	0.0	0.02307	0.1541
	0.3	0.02510	0.1094
	0.7	0.02714	0.0647
2	1.0	0.02917	0.0200
	1.3	0.02674	0.0168
	1.7	0.02431	0.0137
	2.0	0.02188	0.0106
	2.3	0.01945	0.0075
	2.7	0.01702	0.0043
3	3.0	0.01459	0.0012
	3.3	0.01215	0.0010
	3.7	0.00972	0.0008
	4.0	0.00729	0.0006
	4.3	0.00486	0.0004
	4.7	0.00243	0.0002
4 (Center)	5.0	0.00000	0.0000

Moisture sensor station	Distance from the edge of the pavement	Extreme-heave condition	Extreme-shrinkage condition
		Calculated heave (m) at different locations	Calculated shrinkage (m) at different locations
	5.3	0.00243	0.0002
	5.7	0.00486	0.0004
	6.0	0.00729	0.0006
	6.3	0.00972	0.0008
	6.7	0.01215	0.0010
3	7.0	0.01459	0.0012
	7.3	0.01702	0.0043
	7.7	0.01945	0.0075
	8.0	0.02188	0.0106
	8.3	0.02431	0.0137
	8.7	0.02674	0.0168
2	9.0	0.02917	0.0200
	9.3	0.02714	0.0647
	9.7	0.02510	0.1094
1-2	10.0	0.02307	0.1541
1	Ditch	0.01697	0.2882

7.7.3 STRUCTURAL ANALYSIS OF PAVEMENT DUE TO EXTREME SOIL HEAVE AND SHRINKAGE

At first, the extreme soil heave/shrinkage is calculated from section 7.7.2. Once the heave/shrinkage values (w_p) is known then following the closed-form solution as described in section 7.4, the virtual load q(x) is found. Later the virtual load is used to find the deflection, rotation, bending moment, shear force, bending stress and shear stress of the pavement. Table 11 shows the extreme-heave condition and Table 12 shows the extreme-shrinkage condition deflection, rotation, bending moment, shear force, bending stress and shear stress at 31 locations of the 10-m pavement cross-section of the FM 2 road. A series of figures are plotted using the values of Tables 11 to 12. Fig. 45 shows soil-heave-induced effects on the pavement, and Fig. 46 shows the shrinkage effect on the pavement. Table 13 shows the percent change of deflection, bending stress and shear stress between extreme heave and extreme-shrinkage conditions in the FM 2 road. From Table 13, it can be concluded that shrinkage has a more severe effect on the pavement than extreme-heave condition. Texas FM2 Pavement deflection increased by 369% and bending stress increased by 289%, but shear stress decreased by 422% in the extreme-shrinkage condition compared to the extreme-heave condition. The maximum bending moment is found about 30 kPa during the extreme shrinkage condition. This peak value is found at 2.2-m from the shoulder edge. From the pictures of pavement, the longitudinal cracks occur and propagates in between 1-m to 2.5-m. The location of the cracks found from the analytical solution would converge more with the field investigation if the whole cross-section including the shoulders of the pavement, is not taken as a paved section.

Table 11 Pavement structural analysis due to virtual load (extreme heave)

	Soil heave induced pavement properties					
x	$W_B(x)$, m	$\phi(x)$	M(x), kN-m/m	V(x), kN/m	σ (x), kPa	τ (x), kPa
0.00	-2.6E-02	1.2E-05	6.1E-16	2.9E-17	1.1E-14	7.4E-17
0.33	-2.6E-02	4.6E-05	-2.5E-01	-3.0E+00	-4.4E+00	-7.6E+00
0.67	-2.6E-02	2.8E-04	-9.6E-01	-5.3E+00	-1.7E+01	-1.4E+01
1.00	-2.6E-02	8.5E-04	-2.0E+00	-6.5E+00	-3.4E+01	-1.7E+01
1.33	-2.5E-02	1.9E-03	-3.0E+00	-6.1E+00	-5.3E+01	-1.6E+01
1.67	-2.4E-02	3.3E-03	-3.9E+00	-4.2E+00	-6.9E+01	-1.1E+01
2.00	-2.3E-02	4.9E-03	-4.4E+00	-1.1E+00	-7.7E+01	-2.8E+00
2.33	-2.1E-02	6.7E-03	-4.2E+00	2.9E+00	-7.4E+01	7.3E+00
2.67	-1.8E-02	8.2E-03	-3.4E+00	6.9E+00	-6.0E+01	1.8E+01
3.00	-1.6E-02	9.3E-03	-2.0E+00	1.0E+01	-3.4E+01	2.7E+01
3.33	-1.2E-02	9.7E-03	3.2E-03	1.3E+01	5.6E-02	3.3E+01
3.67	-9.1E-03	9.3E-03	2.2E+00	1.3E+01	3.9E+01	3.4E+01
4.00	-6.2E-03	8.0E-03	4.4E+00	1.2E+01	7.7E+01	3.1E+01
4.33	-3.9E-03	5.8E-03	6.2E+00	9.3E+00	1.1E+02	2.4E+01
4.67	-2.4E-03	3.1E-03	7.4E+00	5.0E+00	1.3E+02	1.3E+01
5.00	-1.9E-03	-9.3E-08	7.8E+00	-2.0E-04	1.4E+02	-5.0E-04
5.33	-2.4E-03	-3.1E-03	7.4E+00	-5.0E+00	1.3E+02	-1.3E+01
5.67	-3.9E-03	-5.8E-03	6.2E+00	-9.3E+00	1.1E+02	-2.4E+01
6.00	-6.2E-03	-8.0E-03	4.4E+00	-1.2E+01	7.7E+01	-3.1E+01
6.33	-9.1E-03	-9.3E-03	2.2E+00	-1.3E+01	3.9E+01	-3.4E+01
6.67	-1.2E-02	-9.7E-03	3.0E-03	-1.3E+01	5.3E-02	-3.3E+01
7.00	-1.6E-02	-9.3E-03	-2.0E+00	-1.0E+01	-3.4E+01	-2.7E+01
7.33	-1.8E-02	-8.2E-03	-3.4E+00	-6.9E+00	-6.0E+01	-1.8E+01
7.67	-2.1E-02	-6.7E-03	-4.2E+00	-2.9E+00	-7.4E+01	-7.3E+00
8.00	-2.3E-02	-4.9E-03	-4.4E+00	1.1E+00	-7.7E+01	2.8E+00
8.33	-2.4E-02	-3.3E-03	-3.9E+00	4.2E+00	-6.9E+01	1.1E+01
8.67	-2.5E-02	-1.9E-03	-3.0E+00	6.1E+00	-5.3E+01	1.6E+01
9.00	-2.6E-02	-8.5E-04	-2.0E+00	6.5E+00	-3.4E+01	1.7E+01
9.33	-2.6E-02	-2.8E-04	-9.6E-01	5.3E+00	-1.7E+01	1.4E+01
9.67	-2.6E-02	-4.6E-05	-2.5E-01	3.0E+00	-4.4E+00	7.6E+00
10.00	-2.6E-02	-1.2E-05	-1.3E-09	-2.2E-04	-2.2E-08	-5.6E-04
Max	***-1.9E-03***	***9.7E-03***	***7.8E+00***	***1.3E+01***	***1.4E+02***	***3.4E+01***
Min	***-2.6E-02***	***-9.7E-03***	***-4.4E+00***	***-1.3E+01***	***-7.7E+01***	***-3.4E+01***

Table 12 Pavement structural analysis due to self-weight (extreme shrinkage)

	Pavement self-weight induced pavement properties					
x	$W_B(x)$, m	$\phi(x)$	M(x), kN-m/m	V(x), kN/m	σ (x), kPa	τ (x), kPa
0.00	1.2E-01	-6.3E-02	0.0E+00	2.1E-15	0.0E+00	5.3E-15
0.33	1.0E-01	-6.3E-02	-1.2E+00	-2.8E+01	-2.2E+01	-7.3E+01
0.67	7.9E-02	-6.2E-02	-5.0E+00	-5.1E+01	-8.7E+01	-1.3E+02
1.00	5.9E-02	-5.9E-02	-1.1E+01	-6.6E+01	-1.9E+02	-1.7E+02
1.33	4.0E-02	-5.3E-02	-1.7E+01	-7.0E+01	-3.1E+02	-1.8E+02
1.67	2.4E-02	-4.5E-02	-2.4E+01	-6.4E+01	-4.2E+02	-1.6E+02
2.00	1.1E-02	-3.4E-02	-2.9E+01	-4.9E+01	-5.0E+02	-1.3E+02
2.33	1.5E-03	-2.2E-02	-3.0E+01	-2.7E+01	-5.4E+02	-7.0E+01
2.67	-3.9E-03	-1.0E-02	-2.9E+01	-3.4E+00	-5.1E+02	-8.6E+00
3.00	-5.4E-03	7.2E-04	-2.4E+01	1.9E+01	-4.2E+02	4.9E+01
3.33	-3.7E-03	9.0E-03	-1.7E+01	3.6E+01	-2.9E+02	9.3E+01
3.67	2.2E-04	1.4E-02	-7.3E+00	4.5E+01	-1.3E+02	1.2E+02
4.00	5.1E-03	1.5E-02	2.2E+00	4.5E+01	3.8E+01	1.2E+02
4.33	9.7E-03	1.2E-02	1.0E+01	3.6E+01	1.8E+02	9.2E+01
4.67	1.3E-02	6.9E-03	1.6E+01	2.0E+01	2.8E+02	5.1E+01
5.00	1.4E-02	-1.6E-07	1.8E+01	-6.8E-04	3.1E+02	-1.7E-03
5.33	1.3E-02	-6.9E-03	1.6E+01	-2.0E+01	2.8E+02	-5.1E+01
5.67	9.7E-03	-1.2E-02	1.0E+01	-3.6E+01	1.8E+02	-9.2E+01
6.00	5.1E-03	-1.5E-02	2.2E+00	-4.5E+01	3.8E+01	-1.2E+02
6.33	2.2E-04	-1.4E-02	-7.3E+00	-4.5E+01	-1.3E+02	-1.2E+02
6.67	-3.7E-03	-9.0E-03	-1.7E+01	-3.6E+01	-2.9E+02	-9.3E+01
7.00	-5.4E-03	-7.2E-04	-2.4E+01	-1.9E+01	-4.2E+02	-4.9E+01
7.33	-3.9E-03	1.0E-02	-2.9E+01	3.4E+00	-5.1E+02	8.6E+00
7.67	1.5E-03	2.2E-02	-3.0E+01	2.7E+01	-5.4E+02	7.0E+01
8.00	1.1E-02	3.4E-02	-2.9E+01	4.9E+01	-5.0E+02	1.3E+02
8.33	2.4E-02	4.5E-02	-2.4E+01	6.4E+01	-4.2E+02	1.6E+02
8.67	4.0E-02	5.3E-02	-1.7E+01	7.0E+01	-3.1E+02	1.8E+02
9.00	5.9E-02	5.9E-02	-1.1E+01	6.6E+01	-1.9E+02	1.7E+02
9.33	7.9E-02	6.2E-02	-5.0E+00	5.1E+01	-8.7E+01	1.3E+02
9.67	1.0E-01	6.3E-02	-1.2E+00	2.8E+01	-2.2E+01	7.3E+01
10.00	1.2E-01	6.3E-02	-1.0E-08	-1.7E-03	-1.8E-07	-4.4E-03
Max	***1.2E-01***	***6.3E-02***	***1.8E+01***	***7.0E+01***	***3.1E+02***	***1.8E+02***
Min	***-5.4E-03***	***-6.3E-02***	***-3.0E+01***	***-7.0E+01***	***-5.4E+02***	***-1.8E+02***

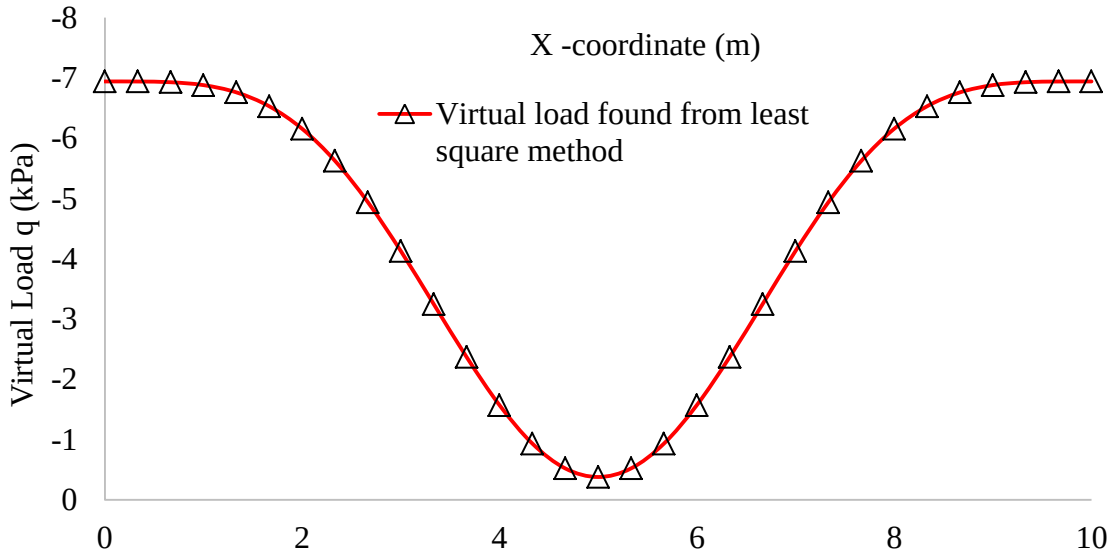

(a) Virtual Load

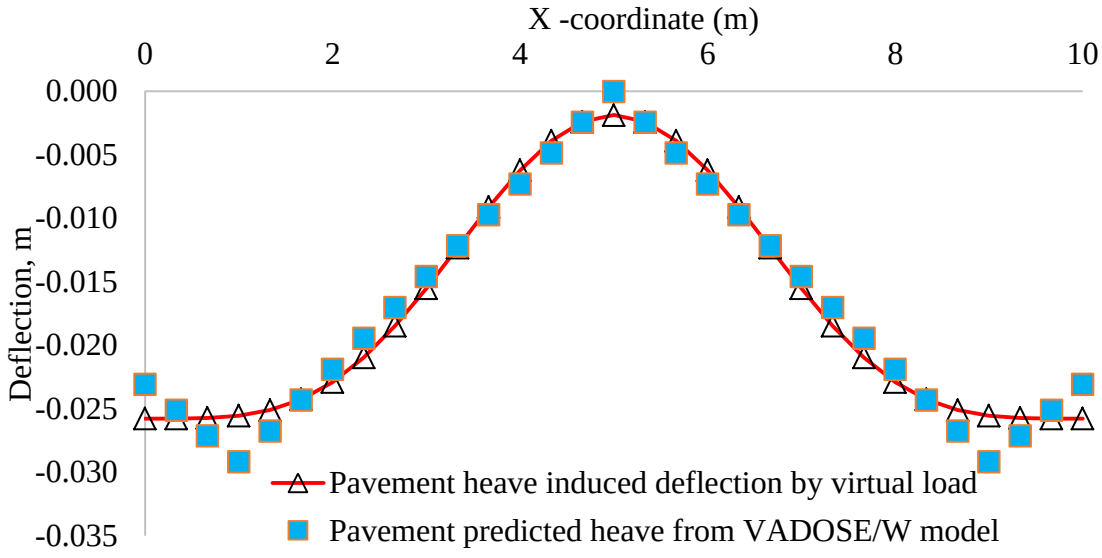

(b) Pavement Deflection

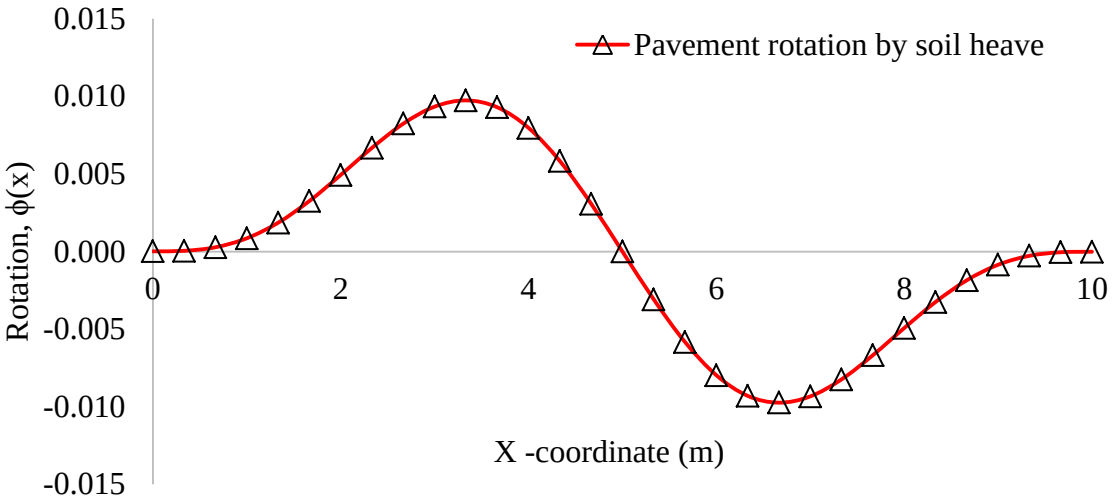

(c) Pavement Rotation

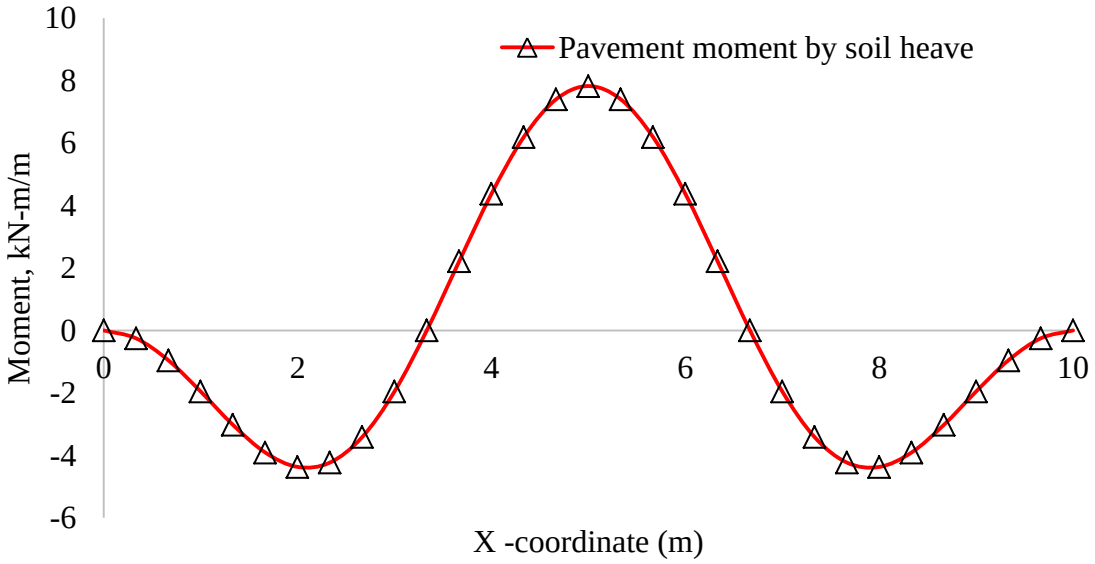

(d) Pavement Bending Moment

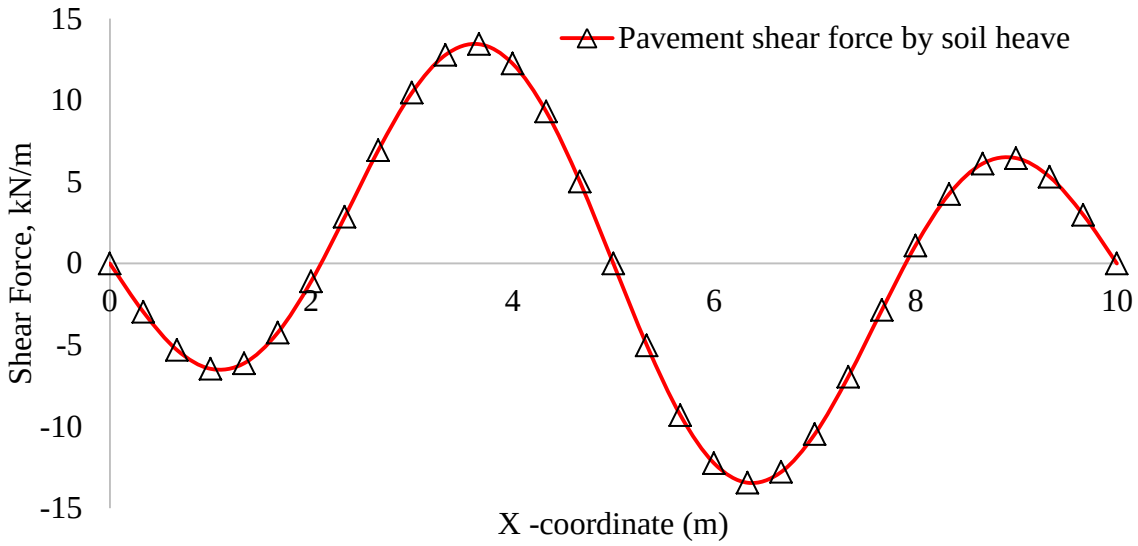

(e) Pavement Shear Force

Figure 44 Extreme-Heave Condition

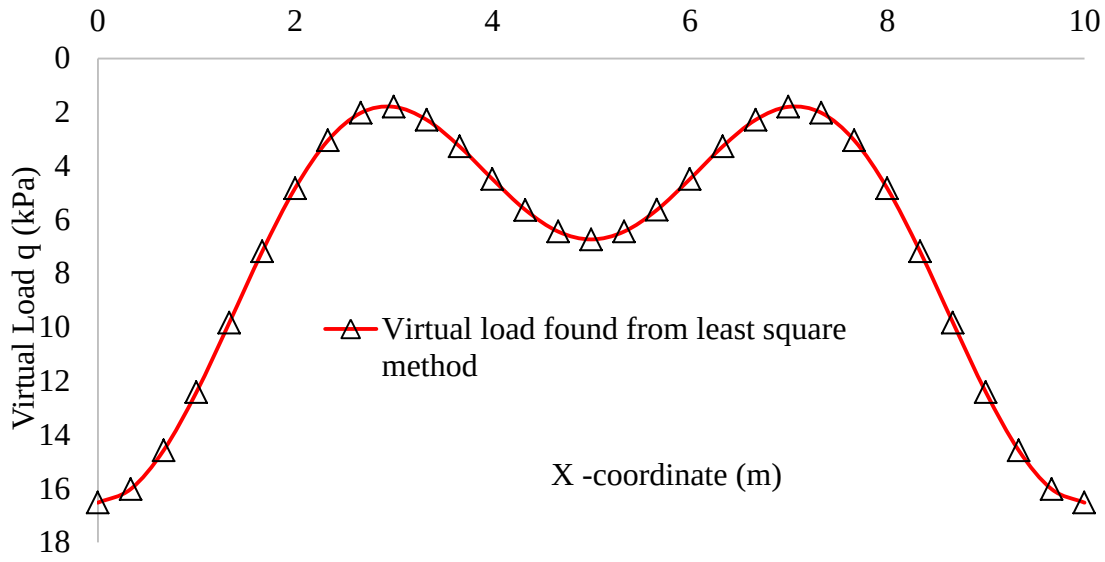

(a) Virtual Load

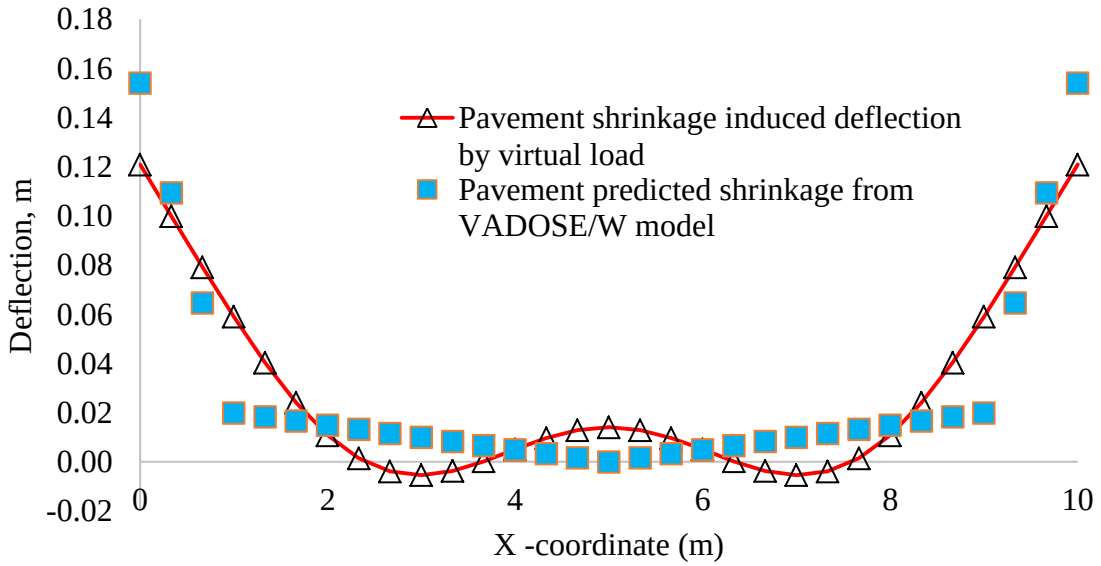

(b) Pavement Deflection

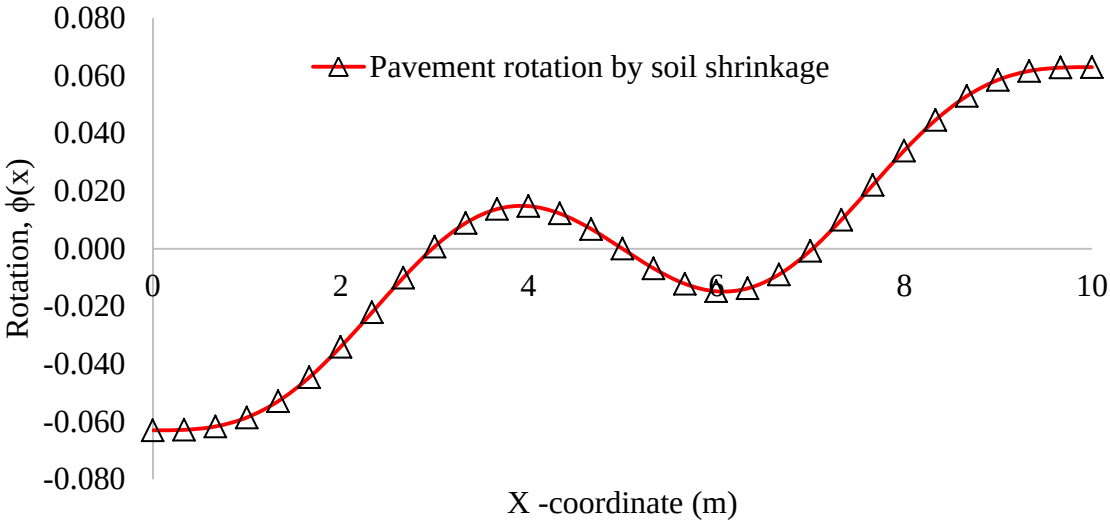

(c) Pavement Rotation

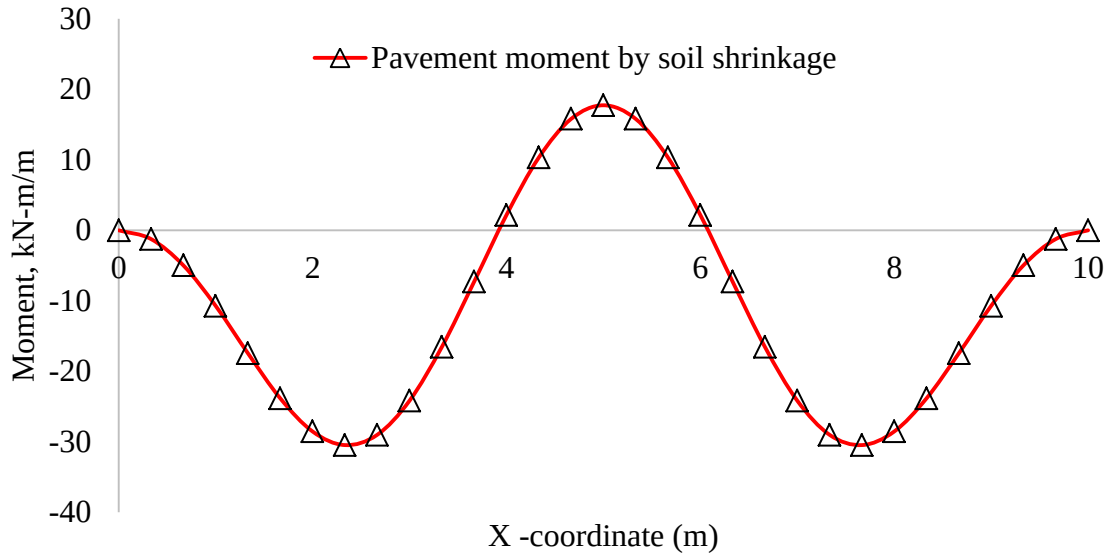

(d) Pavement Bending Moment

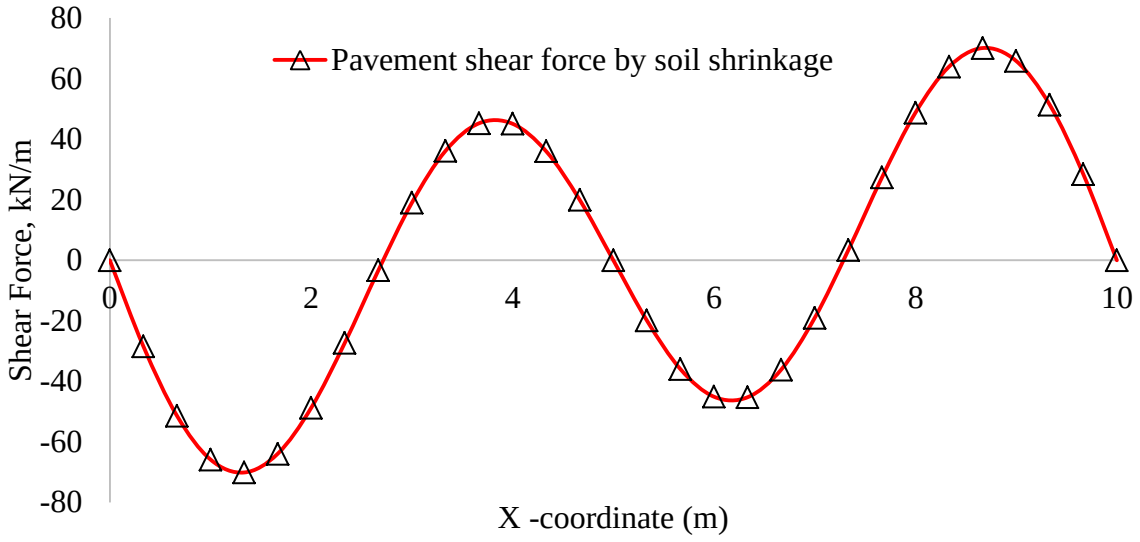

(e) Pavement Shear Force

Figure 45 Extreme-Shrinkage Condition

Table 13 Changes in pavement deformation under extreme conditions

	Maximum $W_B(x)$, (m)		Maximum σ (x), kPa		Maximum τ (x), kPa	
	Extreme heave	Extreme shrinkage	Extreme heave	Extreme shrinkage	Extreme heave	Extreme shrinkage
By virtual load	2.6E-02	1.2E-01	1.4E+02	5.4E+02	3.4E+01	1.8E+02
% Change	369		289		422	

7.8 SUMMARY OF THE PROPOSED ANALYTICAL SOLUTION

A new analytical method for the calculation of the heave/shrinkage-induced stresses in pavement on expansive subgrade soils has been developed. Model validation was performed. Field observations from a country road (FM2) in Texas on expansive soil indicated that initiation and propagation of the cracks in the road had a good match with the location where the maximum bending moment was found. Preliminary results have demonstrated that the closed-form solutions could provide a reliable prediction for the bending moment and shear force in the pavement. As compared with the finite element models, the developed analytical model is

significantly simple and more easily implemented. All the equations and calculations are integrated in the Excel spreadsheet, which is easily implementable in pavement design.

8. SOIL STABILIZATION WITH GEOPOLYMER

8.1 INTRODUCTION

For expansive soils stabilization, the advantage of using geopolymer material over the Portland cement is not well documented. Portland cement if used in construction might have only a design life about 100 years and maybe 150 years for bridge engineering, which is not found in real life, due to the original design and construction errors, potential damages caused by mechanical actions and environmental effects, and changes in functionality, etc. (Fan 2015). Davidovits and James (2009) described in the book titled "Why the pharaohs built the pyramids with fake stones?" that the Egyptians already knew how to build huge concrete blocks which can last for thousands of years and they used geopolymers as a construction material. The American Coal Ash Association (ACAA) in its coal combustion products (CCP) production & use survey for 2014 (American Coal Ash Association 2014) reported an annual fly ash (FA) production of approximately 51 million tons in USA, among them only 23 million was put to a productive use, leaving 28 million to be placed in storage lagoons at a significant cost. Fly ash disposal costs are expected to increase due to pending government regulations aimed at regulating fly ash disposal. Storage lagoons, commonly used as long-term storage facilities, also pose a potential environmental hazard in case of a spill such as the one that took place in Kingston, Tennessee on December 22, 2008 when an ash storage lagoon failed releasing 2.6 million cubic yards of ash into Emory river near a residential area (Diaz and Allouche 2010). In recent years the new application of geopolymers as a soil stabilizer has been emerged. Using cementitious materials to stabilize soil is the most common practiced procedure in the industry in dealing with weak and/or defective (e.g., presence of expansive soil) subgrade.

From different literature reviews the most common technologies that are employed to alleviate the harmful effects of expansive soils are: 1) Soil Cap- using the cut and fill method to replace expansive soil with non-expansive soil up to a certain depth; 2) Drainage- providing adequate draining around the structures to promote a rapid runoff; 3) Size of slab on ground- increasing the size of slab on ground will decrease the chances of moisture content propagation underneath

the structure; 3) Design of slab on ground- increasing the thickness of slab on ground and reinforcing it to resist the subgrade movement-induced stress; 3) Special slab on ground- using waffle mat system will allow the soil to slide in to the waffle boxes when it swells; 4) Geosynthetics- placing geosynthetics (i.e., geotextile, geogrid, etc.) inside the subgrade soil; 5) Mechanical stabilization- compacting the subgrade soil will reduce expansive soil's seasonal movement and 6) Admixture stabilization- Different pozzolanic agent (i.e., cement, lime, fly ash, etc.) and industrial waste (i.e., slag, sludge ash, rice husk, crushed concrete powder etc.) can be used to stabilize expansive soil (al-Swaidani *et al.* 2016; Arulrajah *et al.* 2016; Dang *et al.* 2016; Dhakal 2009; Etim *et al.* 2017; Gurbuz 2015; Jaditager and Sivakugan 2017; Kumar and Sharma 2004; Kumar Yadav *et al.* 2017; Latifi *et al.* 2017; Mahvash *et al.* 2017; Miao *et al.* 2017; Mohammadinia *et al.* 2016a; Mohammadinia *et al.* 2016b; Ojuri *et al.* 2017; Sabat 2012a; Sabat 2012b). Other than the methods mentioned above, one of the new emerging technologies is to use fly ash-based geopolymer cement (GPC) to stabilize expansive soil. It has properties similar to cement (e.g., high strength and strength-gain rate, superior resistance to corrosion, heat and chemical attack and low permeability) with a lesser carbon footprint than cement (Davidovits 1993). According to Davidovits (1991), for every ton of Portland cement produced, one ton of carbon dioxide is released into the atmosphere, making it a serious concern to the global greenhouse gas effect. One of the impressive things about geopolymer is that it can be produced either by naturally occurring raw materials (e.g., clay, mica, etc.) or by making use of industrial byproducts (e.g., fly ash and rice husk ash). One of the major problems is lack of awareness and because Portland cement is used so widely, geopolymer is still perceived to be more of a laboratory product use of fly ash or fly ash combining with cement or lime to stabilize expansive soil (Islam 2013). Understanding the benefit of geopolymer compared to traditional stabilizer (i.e., cement and lime), the department of transportation (DOT) in various states (e.g., Texas, Oklahoma, Indiana, Arkansas) already accepted the direct use of fly ash or fly ash combining with cement or lime to stabilize expansive soil (AHTD 2014; INDOT 2008; ODOT 2009; TxDOT 2005a; TxDOT 2005b). After a close observation of the 2006 and 2016 specifications at Louisiana Department of Transportation and Development (LADOTD) (LADOTD 2006; LADOTD 2016), it can be concluded that 1) percentage of cement using as a soil stabilizer has been significantly reduced over the years, 2) there is no specification for using fly ash as a soil stabilizer, and 3) there is no stabilization standard for soils with a plasticity index (PI) value

higher than 35 (e.g. Moreland clay). This research will try to fill in the knowledge gap of the LADOTD specification.

In this section, the soil stabilization using geopolymer was investigated. A series of soil samples were prepared with different concentrations of geopolymer and cement, respectively, and let them to stabilize for 7, 14 or 30 days, respectively. Finally, experiments were conducted to evaluate their stabilization performance with different concentrations and time.

Various states established their own criteria for modification and stabilization. In the following paragraphs soil stabilization standards and specifications of Louisiana and its neighboring states will be discussed briefly.

Louisiana - From Tables 14 and 15, it is seen that the 2016 LADOTD specification required cement or lime far less than that was required in their 2006 specification. According to Tables 14 and 15 it can be concluded that 1) Cement percentage has been significantly reduced, 2) There is no specification for GPC based soil stabilization and 3) There is no stabilization standards for soils with PI value higher than 35 (e.g., Moreland clay).

Table 14 The 2016 LADOTD specification (LADOTD 2016)

Plasticity Index, (PI)	Lime/Cement (% Volume)
0-15	6%Cement
16-25	6%lime + 6%Cement
26-35	9%Lime + 6%Cement

Table 15 The 2006 LADOTD specification (LADOTD 2006)

Plasticity Index, (PI)	Lime/Cement (% Volume)
0-15	9%Cement
16-25	6%lime + 9%Cement
26-35	9%Lime + 9%Cement

Texas – According to 2005 TxDOT there is a standard and specification for subgrade and base stabilization by either cement, Lime or Fly ash. Fig. 47 shows the subgrade stabilization specification and Fig. 48 shows base stabilization specification.

Oklahoma – According to Oklahoma D.O.T stabilization additive shall be determined by the AASHTO group classification. Fig. 49 shows the stabilization table.

New Mexico – According to NMDOT published "Standard Specifications for Highway and Bridge Construction" manual the subgrade in accordance with the State Materials Bureau's mix design (NMDOT 2014). Unfortunately, there is no detail information was found about the percentage of cement or lime has to be used.

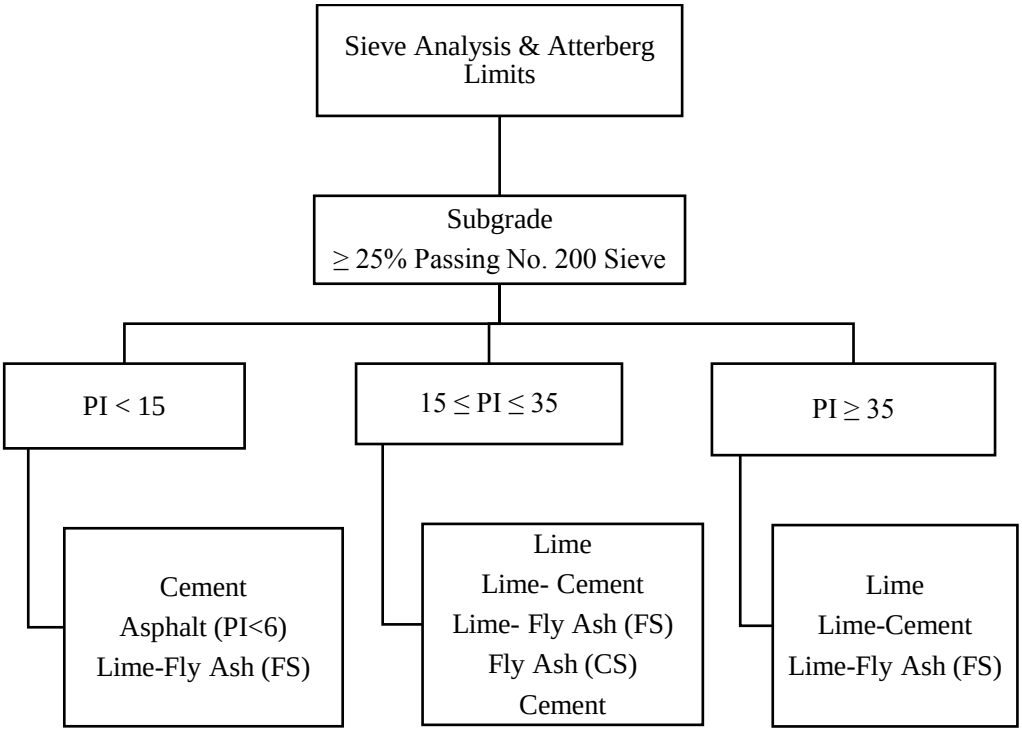

Figure 46 Subgrade stabilization (TxDOT 2005a)

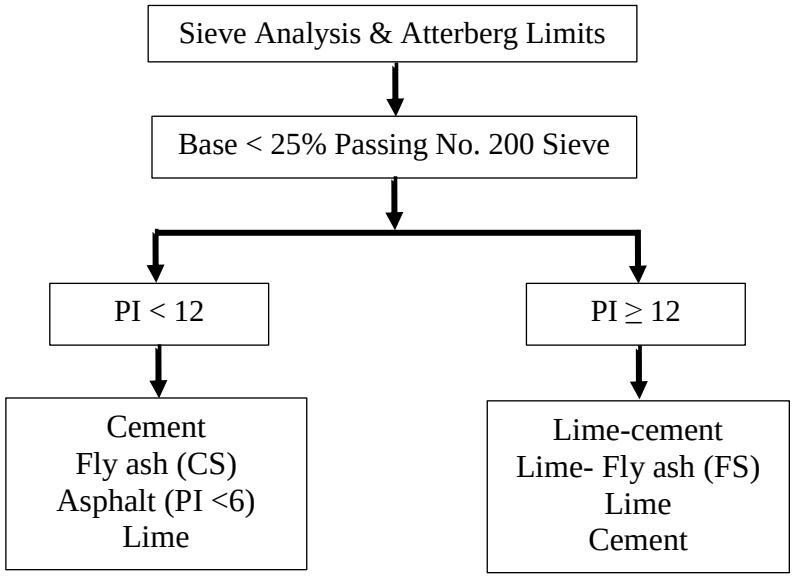

Figure 47 Base stabilization (TxDOT 2005c)

SOIL STABILIZATION TABLE												
ADDITIVE (Expressed as a percentage added on oven dry basis)	SOIL GROUP CLASSIFICATION - AASHTO M145											
	A-1		A-2				A-3	A-4	A-5	A-6	A-7	
	A-1-a	A-1-b	A-2-4	A-2-5	A-2-6	A-2-7					A-7-5	A-7-6
PORTLAND CEMENT	4	4	4	4	4	4	5	√	√	√		
FLY ASH					12	12	13	14	14	14		
CEMENT KILN DUST (Pre-Calciner Plants)	5	5	5	5	5	5	6	√	√			
CEMENT KILN DUST (Other Type Plants)	10	10	10	11	11	11	12	12	12			
HYDRATED LIME*										4	5**	5**

Figure 48 Oklahoma DOT Soil stabilization table (ODOT 2009)

Arkansas – According to Arkansas State Highway and Transportation Department, if lime is used to stabilize subgrade soil then the mixture shall not contain more than 8% by weight lime. For base course treatment if done by cement then the mixture shall not contain more than 4% by weight cement. Fly ash may be used as a partial replacement of cement but not more than 25%. (AHTD 2014)

Indiana – According to Indiana D.O.T cement, lime or fly ash can be used to stabilize the subgrade soil as shown in Table 16 (INDOT 2008).

Table 16 Selection of stabilizer on soil properties by INDOT

Treatment	Soil property	Additive type	Suggested amount
Stabilization	PI>10 and clay content (2μ) >10%	Lime (quick lime)	If lime or lime byproduct is used :4% - 7% If cement is used: 4% to 6% If Fly ash Class C is used: 10% to 16%
	PI < 10 and < 20% passing # 200 sieve	Cement	
Modification	PI ≥ 5 and > 35% passing #200 sieve.	Lime	
	5<PI<20 and >35% passing #200 sieve	Lime fly ash blends	
	PI < 5 and ≤ 35% passing # 200 sieve	Cement and/or Fly ash (C class)	

8.2 GEOPOLYMER

Geopolymers are made up with aluminosilicate-based cementitious materials. They have properties similar to cement (e.g., high strength and strength gain rate, superior resistance to corrosion, heat and chemical attack, and low permeability) with lesser carbon footprint than cement (Davidovits 1993).

According to Davidovits (Davidovits 1991), for every ton of Portland cement produced one ton of carbon dioxide is released into the atmosphere, making it a serious concern to the global greenhouse gas effect. One of the impressive thing about geopolymer is it can be produced either by naturally occurring raw materials (e.g., clay, mica, etc.) or by making use of industrial byproducts (e.g., fly ash and rice husk ash). One of the major problem is due to lack of awareness and several other reasons geopolymer is still perceived more of a laboratory product due to the wide spread use of Portland cement. (Islam 2013)

8.3 GEOPOLYMER CHEMISTRY

Fly ash-based geopolymer in the presence of activator solution creates geopolymeric chains which refer to as geopolymerization. The empirical formula developed by Davidovits (1991) for alumino silicate can be written as $M_n\{-(SiO_2)_z\text{-}AlO_2)_n.wH_2O$ where M can be any number of cation (e.g., Na^+, K^+, Ca^{++} , Ba^{++}, NH_4^+, H_3O^+) and n is the degree of polymerization. The letter z represents 1, 2, or 3, determining the resulting geopolymer net. For the case of Z=1 the net will be of the polysialate type, if Z=2 the net will be a poly (sialate-siloxo) and, if Z=3 the net will be a poly (sialate- disiloxo) (Islam 2013). Fig. 50 presents the structural model proposed by Davidovits (1993). Scientists Hua Xu and Deventer (2000) described the three main steps of geopolymerization, which are: i) Dissolution of silicon and aluminum species from the source material through the action of highly alkaline solution. ii) Transportation of species and formation of monomers and iii) Polycondensation and growth of polymeric structures resulting in the hardening of the material. These steps typically overlap each other under thermal curing and are hard to recognize in the reaction process (Islam 2013).

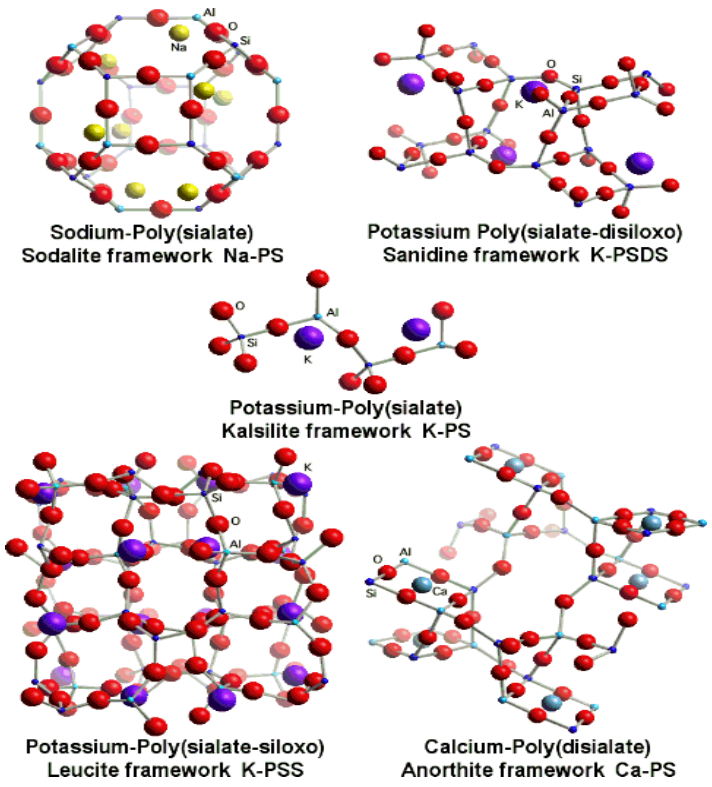

Figure 49 The structural model of geopolymer proposed by Davidovits (1993)

8.4 IMPORTANT DEFINITION OF GEOPOLYMER

Fly ash: Fly ash is defined by the American Concrete Institute, ACI 116R, as "the finely divided residue that results from the combustion of ground or powdered coal and that is transported by flue gases from the combustion zone to the particle removal system" (Edouard 2011). Fly ash, which is transported along with the flue gases and captured by pollution control devices, namely, electro precipitators or bughouses and occasionally by scrubber systems is a very fine and powdery material made of spherical shaped particles that are in the range of a few microns to 100 µm (Islam 2013). Typically, a small portion of the chemical composition is arranged in crystalline form, mainly quartz and mullite, and the rest are amorphous with no particular arrangement due to rapid cooling after leaving the boiler (Diaz and Allouche 2010). FA is classified according to ASTM standard C618 into three different groups:

Class F fly ash- is generally found as a byproduct of the burning of either lignite (or sub bituminous) coal and anthracite (or bituminous) coal. The minimum requirement of summation of silicon, aluminum, and iron oxide is seventy percent with a LOI and calcium oxide maximum value 6% and 10%, respectively. (Islam 2013)

Class C fly ash – is generally found from lignite, sub bituminous, anthracite and bituminous coal. This slightly cementitious nature fly ash has a requirement of a maximum summation of silicon, aluminum and iron oxide to 50%, maximum LOI 6% and minimum calcium oxide as 10%.(Islam 2013)

Class N fly ash – is generally found from raw or calcine natural pozzolans such as opaline cherts, shales, volcanic ashes, pumicites, and various materials. It has a requirement of a minimum 70% sum of 70% of silicon, aluminum, and iron oxide with a maximum LOI 10% (Islam 2013).

Add-water geopolymer: Generally, geopolymer is used with its caustic activators which may cause safety issues. For this reason, add water geopolymer was developed in the construction industry which performs like ordinary Portland cement (OPC). In this research to produce add water geopolymer METSO® 2048 from PQ® was used.

8.5 SOIL STABILIZATION EXPERIMENT DESIGN

There is no standardized method about the soil stabilization with geopolymer so far. In this research, an experiment was designed to evaluate the Moreland clay stabilization with geopolymers. For this four batches of soil sample were produced where each batch of the Moreland clay were mixed with either 5%, 10%, 20% geopolymers cement (GPC) or 10% Portland cement by weight. Each batch consists of 3 samples.

The procedure of producing GPC is described as below:

1) 60 gm METSO® beats were mixed with 100 gm water to make a solution (Fig. 51a)

2) 100 gm FA was taken.

3) 100 gm FA then mixed with 13 gm METSO® solution creating 0.13 GPC (Fig. 51b)

Figure 50 (a) METSO® solution (b) 0.13 GPC

Soil sample preparation description:

1) 500 gm of the Moreland clay passing sieve 40 was mixed with either 5%, 10%, 20% GPC and 10% cement by weight, respectively.

2) To make a thorough mixture, additional water was added. To find the minimum water to be added water was added little by little and found the minimum moisture content needed to make a thorough soil paste for the soil and GPC mixture. In every batch, the same moisture content was

maintained so that the final results can be comparable with each other. The moisture content was found 27% and different amount of water was added in the samples with 5%, 10%, 20% GPC and 10% Cement, respectively, to make sure every batch had 27% moisture content.

3) Once the soil batches were produced, they were placed in tubes like containers in three layers with 30 tamping in each layer under plastic covers to get air dried (Fig. 52).

4) The curing period was taken as 7-day, 14-day and 30-day periods, respectively.

5) After curing the soil samples were taken out from the containers and again placed in the consolidation rings in three layers with 30 tamping for each layer.

6) Perform consolidation tests of the twelve samples (Fig. 53).

Figure 51 Stabilized Moreland clay samples under curing process

Figure 52 Consolidation tests of the stabilized Moreland clay samples

8.5.1 CONSOLIDATION TEST OF THE STABILIZED SOILS

Figs. 54 to 56 show the results of the consolidation test of all the twelve Moreland clay samples. Finally, the relations between compression index (C_c) and swelling index (C_s) with curing time were showed in Figs. 57 and 58.

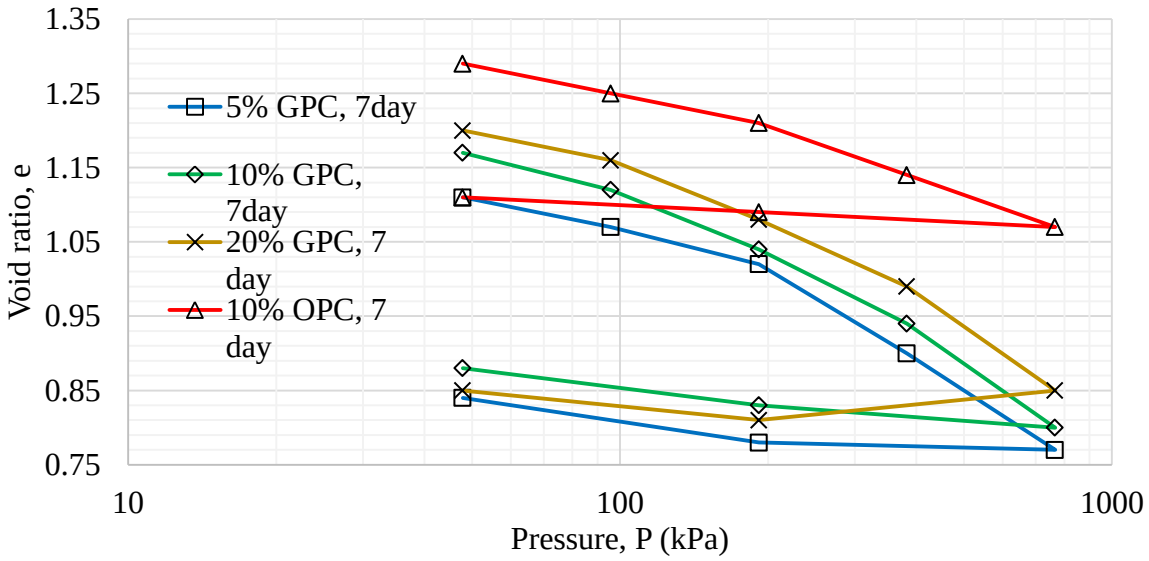

Figure 53 Seven-day soil stabilization

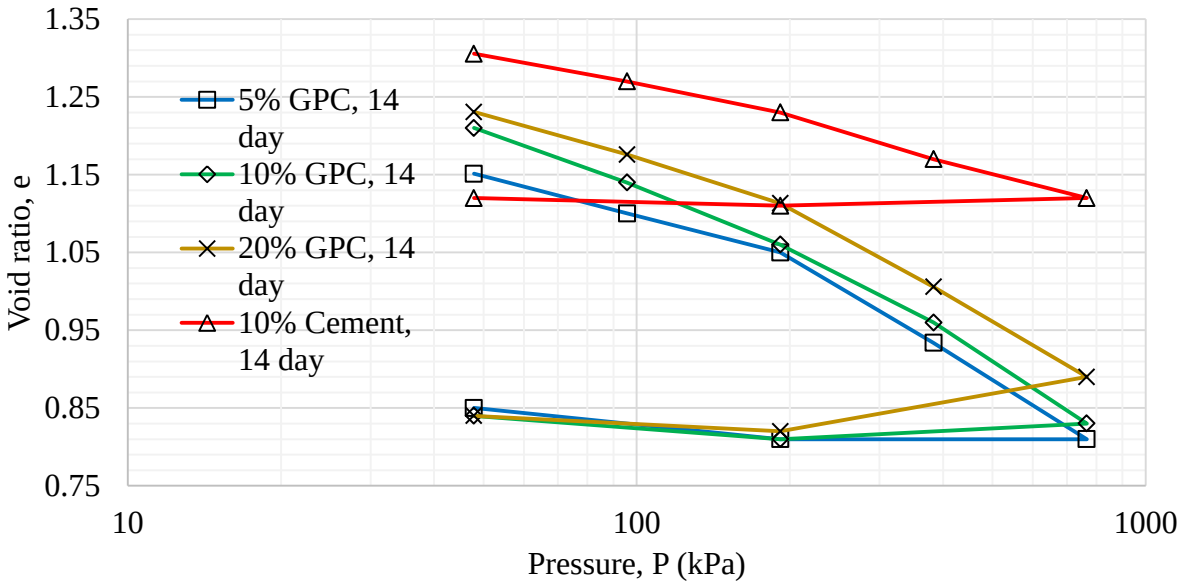

Figure 54 Fourteen-day soil stabilization

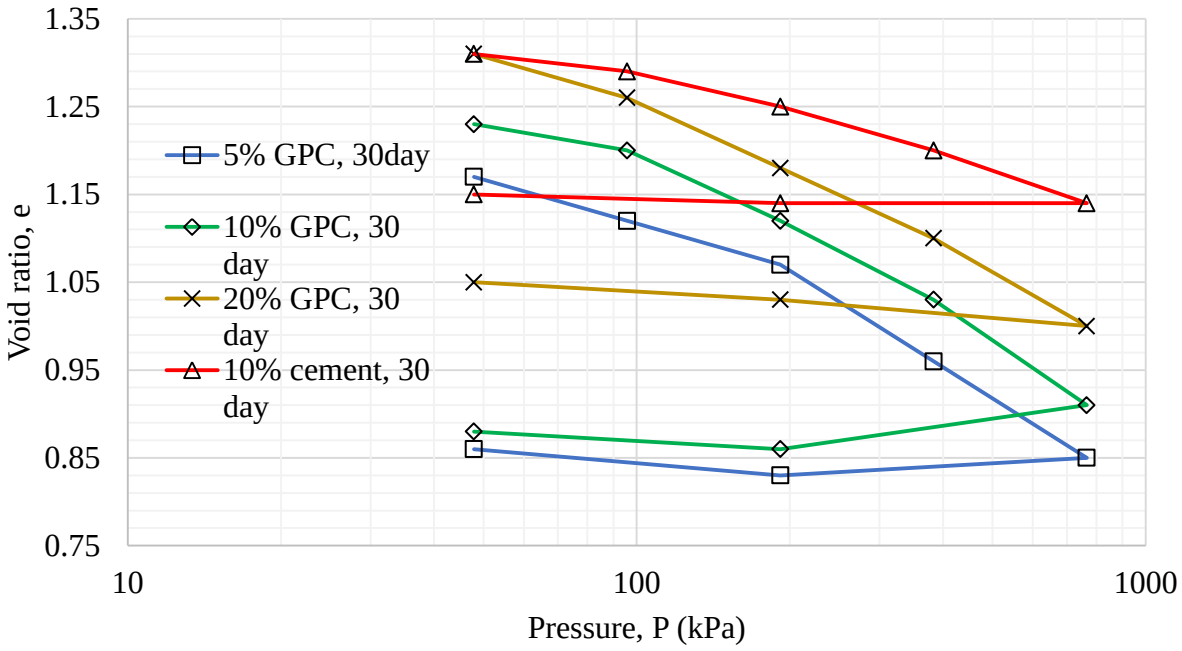

Figure 55 Thirty-day soil stabilization

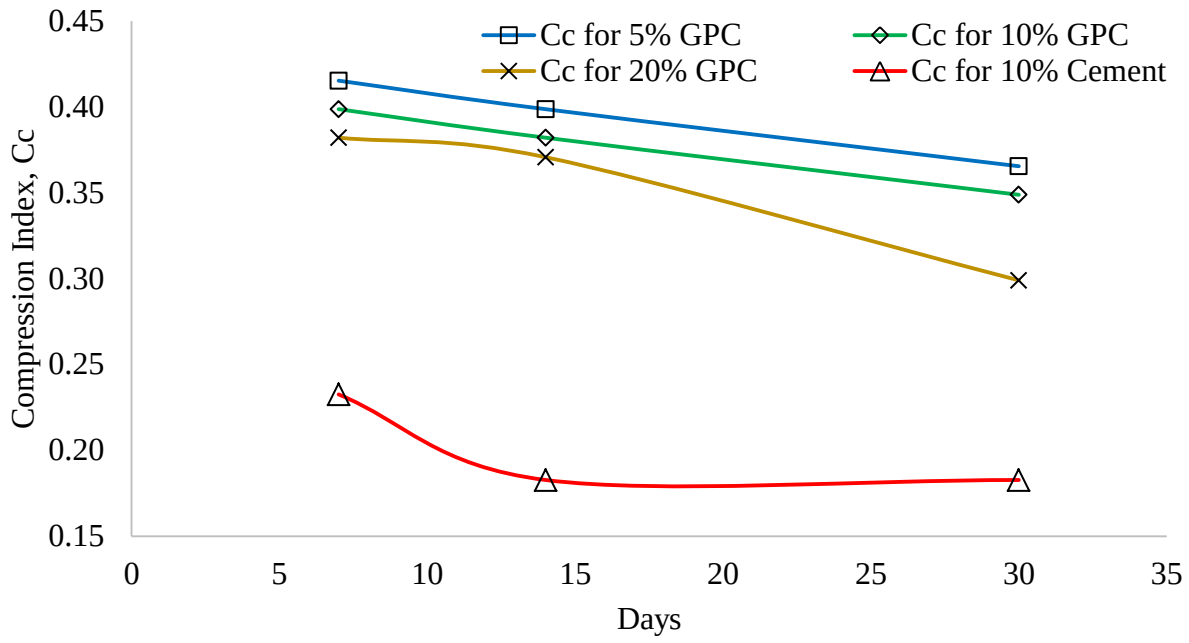

Figure 56 Relation between the compression index and curing time

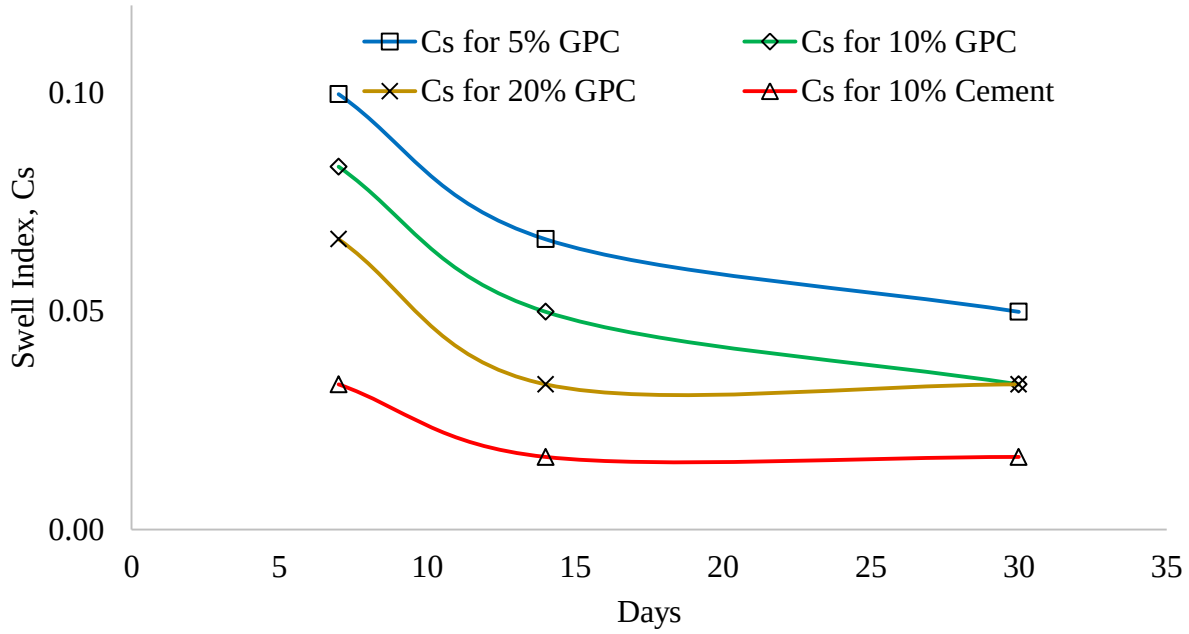

Figure 57 Relation between the swelling index and curing time

8.6 SUMMARY OF THE EXPANSIVE SOIL STABILIZATION

The following conclusions can be made from Figs. 54 to 58:

1) As the GPC percentage is increased the soil became more stabilized and lesser void ratio changed under the same pressure.

2) At any curing time cement stabilizes soil better than GPC. Even 20% GPC-stabilized expansive soil under a specific load has a void ratio greater than the 10% cement-stabilized soil.

3) On average 10% GPC-stabilized soil had a compression index 90% more than that of 10% cement-stabilized soil.

4) On average 10% GPC-stabilized soil has a compression index 77% more than that of 20% cement-stabilized soil.

5) On average 10% GPC stabilized soil has a compression index 150% more than that of 10% cement-stabilized soil.

6) On average 10% GPC stabilized soil has a compression index 100% more than that 20% cement-stabilized soil.

9. CONCLUSIONS AND RECOMMENDATIONS

The focus of this study was to have a better understanding of shrink-swell properties of the Moreland clay, to develop an analytical solution for expansive soil to the heave/shrinkage-induced stresses on pavement and finally as a solution of this problem to find an innovative way to stabilize expansive soil with GPC.

The following conclusions can be drawn from the research:

1. For the first time the swell-shrink properties of the Moreland clay were investigated through a various geotechnical lab experiments.
2. Given the laboratory experimental results, the Moreland clay found in northern Louisiana is identified as a very expansive soil in nature using different identification methods, as compared to the expansive soils found in many other places around the world.
3. An empirical equation was proposed for the unsaturated shear strength of the Moreland clay.
4. As part of the characterization, a three-dimensional constitutive surface describing the volume change behavior was constructed, which will shed lights on how the volume changes with the imposed pressure and moisture variation.

5. A map to show distribution of expansive soils and their degrees of expansion severity over Louisiana based on the calculated swelling potential was plotted using the ArcGIS software. A conclusion may be drawn from the map that the southern Louisiana soil has more swelling potential compared to the soil in northern Louisiana. It must be noted that the map is not to give a real measurement of soil heave, but to offer a general idea regarding the distribution of expansive soils based on swelling degrees over Louisiana.
6. A new analytical method for the calculation of the stress in the pavement induced from heave/shrinkage of expansive soil was developed. To the authors' knowledge, it is for the first time that the deflection, rotation, shear force and bending moment of a pavement due to the volume change of expansive subgrade can be calculated without any use of complicated finite element analysis. Model validation was performed. Field observations from a country road (FM 2) on expansive soil in Texas indicated that initiation and propagation of the cracks in the road had a good match with the location where the maximum bending moment was found. Preliminary results have demonstrated that the closed-form solutions could provide a reliable prediction for the bending moment and shear force in the pavement. As compared with the finite element models, the developed analytical model is significantly simple and more easily implemented. All the equations and calculations were integrated in the Excel spreadsheet, which will be easily implementable in pavement design.
7. The Moreland clay stabilization was investigated by employing geo-polymer concrete (GPC) and cement as stabilizer, respectively. Through an extensive laboratory experiments on Moreland clay it may be concluded that cement is a better soil stabilizer than GPC. However, the application of higher percentage of GPC, a satisfactory level of soil stabilization can be achieved as well.

10. IMPLEMENTATION AND TECHNOLOGY TRANSFER

From the very beginning, the research team has stayed closely with Louisiana Transportation Research Center (LTRC), and/or Louisiana Department of Transportation and Development (LADOTD) for special helps in the duration of the project, such as field monitoring and testing data. Local industry has been contacted to identify the location of the Moreland expansive clay sites. Presentations to disseminate the preliminary and final achievements have been made in

LTRC/LADOTD and international conferences to find potential application of the research achievements. The potential technology implementation in industry will be implemented together with the LTRC/LADOTD engineers if a need comes up. If necessary, a detailed steps and sample calculations will be documented for the easy deployment of the achieved results. Recently, LTRC has provided detailed information regarding those pavements (geosynthetic-reinforced or non-geosynthetic-reinforced) on expansive soils that were distressed by the heave/shrinkage of the expansive subgrades. The developed model will be applied in those pavements where cracks were found, and the analyses will be implemented. Partial results were presented in November 2016 at the second Climate Conference at the SPTC at Norman, Oklahoma. Conference and journal papers have been published, reviewed or prepared.

REFERENCES

Abu-Farsakh, Y, M., and Chen, Q. (2012). "Evaluation of the Base/Subgrade Soil under Repeated Loading: Phase II–In-Box and Alf Cyclic Plate Load Tests." Louisiana Transportation Research Center, Baton Rouge, LA, 1-97.

Abu-Farsakh, M., and Nazzal, M. (2009). "Evaluation of the Base/Subgrade Soil under Repeated Loading: Phase 1–Laboratory Testing and Numerical Modeling of Geogrid Reinforced Bases in Flexible Pavement." Louisiana Transportation Research Center, Baton Rouge, LA, 1-139.

AHTD (2014). "Composition." *Cement Treated Base Course*, Arkansas State Highway and Transportation Department, Little Rock, Arkansas.

Al-Homoud, A. S., Basma, A. A., Husein Malkawi, A. I., and Al Bashabsheh, M. A. (1995). "Cyclic Swelling Behavior of Clays." *Journal of Geotechnical Engineering*, 121(7), 562-565.

al-Swaidani, A., Hammoud, I., and Meziab, A. (2016). "Effect of adding natural pozzolana on geotechnical properties of lime-stabilized clayey soil." *Journal of Rock Mechanics and Geotechnical Engineering*, 8(5), 714-725.

American Coal Ash Association (2014). "2014 Coal Combustion Product (CCP) Production & Use Survey Report." <https://www.acaa-usa.org/Portals/9/Files/PDFs/2014ReportFinal.pdf>. (28th September, 2016).

Arulrajah, A., Mohammadinia, A., Phummiphan, I., Horpibulsuk, S., and Samingthong, W. (2016). "Stabilization of Recycled Demolition Aggregates by Geopolymers comprising Calcium Carbide Residue, Fly Ash and Slag precursors." *Construction and Building Materials*, 114, 864-873.

ASTM (2007). "Standard Test Methods for Particle-Size Analysis of Soils." *Annual book of ASTM standards*, ASTM, West Conshohocken, PA.

ASTM (2009). "Standard Test Methods for Soil Exploration and Sampling by Auger Borings." *Annual book of ASTM standards*, ASTM, West Conshohocken, PA.

ASTM (2010a). "Standard Test Method for Laboratory Determination of Water (Moisture) Content of Soil and Rock by Mass." *Annual book of ASTM standards*, ASTM, West Conshohocken, PA.

ASTM (2010b). "Standard Test Methods for Liquid Limit, Plastic Limit, and Plasticity Index of Soils." *Annual book of ASTM standards*, ASTM, West Conshohocken, PA.

ASTM (2010c). "Standard Test Methods for One-Dimensional Consolidation Properties of Soils Using Incremental Loading." *Annual book of ASTM standards*, ASTM, West Conshohocken, PA.

ASTM (2011a). "Standard Test Method for Direct Shear Test of Soils under Consolidated Drained Conditions." *Annual book of ASTM standards*, ASTM, West Conshohocken, PA.

ASTM (2011b). "Standard Test Methods for Classification of Soils for Engineering Purposes (Unified Soil Classification System)." *Annual book of ASTM standards*, ASTM, West Conshohocken, PA.

ASTM (2011c). "Standard Test Methods for Expansion Index of Soil." *Annual book of ASTM standards*, ASTM, West Conshohocken, PA.

ASTM (2014). "Standard Test Methods for Specific Gravity of Soil Solids by Water Pycnometer." *Annual book of ASTM standards*, ASTM, West Conshohocken, PA.

ASTM (2015). "Standard Practice for Thin-Walled Tube Sampling of Fine-Grained Soils for Geotechnical Purposes." *Annual book of ASTM standards*, ASTM, West Conshohocken, PA.

Azam, S., and Chowdhury, R. H. (2013). "Swell-Shrink-Consolidation Behavior of Compacted Expansive Clays." *International Journal of Geotechnical Engineering*, 7(4), 424-430.

Bowles, J. E. (1996). *Foundation Analysis and Design*, McGraw-Hill, New York.

Briaud, J. L., Zhang, X., and Moon, S. (2003). "Shrink Test-Water Content Method for Shrink and Swell Predictions." *Journal of Geotechnical and Geoenvironmental Engineering*, 129(7), 590-600.

Burns, S. F., Hadley, W. O., Mutchler, J. W., Smith, S. M., Siddiqui, A., and Hernandez, M. (1990). "Development of Design Criteria for the Prevention of Slope Failures." Louisiana Tech University, Baton Rouge, LA, 231.

Chao, K.-C. (2007). "Design Principles for Foundations on Expansive Soils." Ph.D. Dissertation, Colorado State University, Fort Collins, Colorado.

Chen, F. H. (1975). *Foundations on Expansive Soils*, Elsevier Scientific Pub. Co., Amsterdam, Netherlands.

Chowdhury, M. R. H. (2013). "Shear Strength Properties of Compacted Expansive Soils." Master of Applied Science in Environmental Systems Engineering, University of Regina, Regina.

Dane, J. H., and Hopmans, J. W. (2002). "Pressure Plate Extractor." *Methods of Soil Analysis: Part 4 Physical Methods*, J. H. Dane, and C. G. Topp, eds., Soil Science Society of America, Madison, WI, 688-690.

Dang, L. C., Fatahi, B., and Khabbaz, H. (2016). "Behaviour of Expansive Soils Stabilized with Hydrated Lime and Bagasse Fibres." *Procedia Engineering*, 143, 658-665.

Das, B. M. (2010). *Principles of Foundation Engineering*, Cengage learning, USA.

Davidovits, J. (1991). "Geopolymers." *Journal of thermal analysis*, 37(8), 1633-1656.

Davidovits, J. (1993). "Carbon-dioxide green-house warming: What future for Portland cement, in: Emerging Technologies." *Symposium on Cement and Concretes in the Global Environment*, Portland Cement Association, Chicago, 21.

Davidovits, J., and James, C. (2009). *Why the Pharaohs Built the Pyramids with Fake Stones*, Geopolymer Institute, Saint-Quentin, France.

Dhakal, S. K. (2009). "Stabilization of Very Weak Subgrade Soil with Cementitious Stabilizers." M.Sc. Thesis, Louisiana State University, Baton Rouge.

Dhowian, A. W. (1990). "Field Performance of Expansive Shale Formation." *Journal of King Abdulaziz University*, 2, 165-182.

Diaz, E. I., and Allouche, E. N. "Recycling of Fly Ash into Geopolymer Concrete: Creation of a Database." *Proc., 2010 IEEE Green Technologies Conference*, 1-7.

Dodge, A. (1964). "Influence functions for beams on elastic foundations." *Journal of the Structural Division*, 90, 63-101.

Edouard, J.-B. (2011). "Experimental Evaluation Of The Durability Of Fly Ash-Based Geopolymer Concrete In The Marine Environment." M.Sc. Thesis, Florida Atlantic University, Boca Raton, Florida.

Erzin, Y., and Erol, O. (2007). "Swell Pressure Prediction by Suction Methods." *Engineering Geology*, 92(3), 133-145.

Escario, V. (1969). "Swelling of Soils in Contact with Water at a Negative Pressure." *Proceedings of the 2nd international conference expansive clay soils,*Texas A&M University, College Station, 207-217.

Etim, R. K., Eberemu, A. O., and Osinubi, K. J. (2017). "Stabilization of black cotton soil with lime and iron ore tailings admixture." *Transportation Geotechnics*, 10, 85-95.

Fan, F. (2015). "Mechanical And Thermal Properties Of Fly Ash-Based Geopolymer Cement." M.Sc. Thesis, Louisiana State University, Baton Rouge, Louisiana.

Fredlund, D. G. "Consolidometer Test Procedural Factors Affecting Swell Properties." *Proc., 2nd International Conference on Expansive Clay Soils*, Texas A & M Press, 435-456.

Fredlund, D. G. (1979). "Appropriate concepts and technology for unsaturated soils." *Canadian Geotechnical Journal*, 16(1), 121-139.

Fredlund, D. G., Morgenstern, N. R., and Widger, R. A. (1978). "The Shear Strength of Unsaturated Soils." *Canadian Geotechnical Journal*, 15(3), 313-321.

Fredlund, D. G., Rahardjo, H., and Fredlund, M. D. (2012). *Unsaturated Soil Mechanics in Engineering Practice*, John Wiley & Sons.

Garven, E. A., and Vanapalli, S. K. (2006). "Evaluation of Empirical Procedures for Predicting the Shear Strength of Unsaturated Soils." *Unsaturated Soils 2006*, 2570-2592.

Groenevelt, P. H., and Grant, C. D. (2004). "A New Model for the Soil-water Retention Curve that Solves the Problem of Residual Water Contents." *European Journal of Soil Science*, 55(3), 479-485.

Grossman, R. B., and Reinsch, T. G. (2002). "Bulk Density and Linear Extensibility." *Methods of Soil Analysis: Part 4 Physical Methods*, J. H. Dane, and C. G. Topp, eds., Soil Science Society of America, Madison, WI, 201-228.

Gupta, R. (2009). "A Study of Geosynthetic Reinforced Flexible Pavement System." Ph.D. Dissertation, The University of Texas at Austin, Austin, TX.

Gurbuz, A. (2015). "Marble powder to stabilise clayey soils in sub-bases for road construction." *Road Materials and Pavement Design*, 16(2), 481-492.

Hetényi, M. (1946). *Beams on Elastic Foundation;: Theory with Applications in the Fields of Civil and Mechanical Engineery*, University of Michigan press, Ann Arbor.

Hua Xu, and Deventer, J. S. J. V. (2000). "The geopolymerisation of alumino-silicate minerals." *International Journal of Mineral Processing*, 59(3), 247-266.

Hung, V. Q. (2002). "Uncoupled and Coupled Solutions of Volume Change Problems in Expansive Soils." Ph.D. Dissertation, University of Saskatchewan, Saskatoon.

Ikra, B. A. (2017a). *Swelling Potential Map for State of Louisiana*, Research Report, Program of Civil Engineering, Louisiana Tech University, Ruston, LA.

Ikra, B. A. (2017b). *Prediction of Moisture Content Changes and Heave Analysis of Expansive Soils Under Extreme Weather*, M.Sc. Thesis, Program of Civil Engineering, Louisiana Tech University, Ruston, LA.

INDOT (2008). "Criteria for Chemical Selection." *Design Procedures for Soil Modification or Stabilization*, Indiana Department of Transportation, Indiana.

Islam, M. R. (2013). "Creation and Analysis of a Fly Ash Database for Facilitating the Standardization of Geopolymer Concrete " M.Sc. Thesis, Louisiana Tech University, Ruston, Louisiana.

Jaditager, M., and Sivakugan, N. (2017). "Infnfluence of Fly Ash–Based Geopolymer Binder on the Sedimentation Behavior of Dredged Mud." *Journal of Waterway, Port, Coastal, and Ocean Engineering*, 143(5).

Jones, D. E., and Holtz, W. G. (1973). "Expansive Soils-The Hidden Disaster." *Civil Engineering, American Society of Civil Engineers*, 87-89.

Jury, W. A., Gardner., W. R., and Gardner., W. H. (1991). *Soil Physics*, John Wiley and Sons., New York.

Khan, M. A., Wang, J. X., and Patterson, W. B. (2017). "A study of the swell-shrink behavior of expansive Moreland clay." *International Journal of Geotechnical Engineering*, 1-13.

Khan, M. A. (2017). *Influence of Moisture Content Distribution in Soil on Pavement and Geothermal Energy*, Ph.D. Dissertation, Program of Civil Engineering, Louisiana Tech University, Ruston, LA.

Klepikov, S. N. (1967). *Analysis of Structures on Elastic Foundation*, Budivelnik, Kiev, Ukraine.

Korenev, B. G. (1962). *Analysis of Plates on Elastic Foundation*, Gosstroiizdat, Moscow, Russia.

Krohn, J. P., and Slosson, J. E. "Assessment of Expansive Soils in The United States." *Proc., 4th International Conference on Expansive Soils*, 596-608.

Kumar, B. R. P., and Sharma, R. S. (2004). "Effect of Fly Ash on Engineering Properties of Expansive Soils." *Journal of Geotechnical and Geoenvironmental Engineering*, 130(7), 764-767.

Kumar Yadav, A., Gaurav, K., Kishor, R., and Suman, S. K. (2017). "Stabilization of alluvial soil for subgrade using rice husk ash, sugarcane bagasse ash and cow dung ash for rural roads." *International Journal of Pavement Research and Technology*, 10(3), 254-261.

LADOTD (2006). "Treatment." *Subgrade Layer*, Louisiana Department of Transportation and Development, Baton Rouge, LA.

LADOTD (2016). "Treatment." *Subgrade Layer*, Louisiana Department of Transportation and Development, Baton Rouge, LA.

Latifi, N., Eisazadeh, A., Marto, A., and Meehan, C. L. (2017). "Tropical residual soil stabilization: A powder form material for increasing soil strength." *Construction and Building Materials*, 147, 827-836.

Lu, L., and Vanapalli, S. K. (2012). "A State-of-the art Review of 1-D Heave Prediction Methods for Expansive Soils." *International Journal of Geotechnical Engineering*, 6(1), 15-41.

Mahvash, S., López-Querol, S., and Bahadori-Jahromi, A. (2017). "Effect of class F fly ash on fine sand compaction through soil stabilization." *Heliyon*, 3(3), e00274.

Marinho, F. A. M., and Oliveira, O. M. (2012). "Unconfined Shear Strength of Compacted Unsaturated Plastic Soils." *Proceedings of the Institution of Civil Engineers - Geotechnical Engineering*, 165(2), 97-106.

Marshall, T. J. (1958). "A Relation between Permeability and Size Distribution of Pores." *Journal of Soil Science*, 9(1), 1-8.

Materials, A. S. f. T. a. (2012). "Standard Test Methods for Laboratory Compaction Characteristics of Soil Using Standard Effort (12400 ft-lbf/ft3 (600 kN-m/m3))." *Annual book of ASTM standards*, ASTM, West Conshohocken, PA.

Matyas, E. L., and Radhakrishna, H. S. (1968). "Volume Change Characteristics of Partially Saturated Soils." *Géotechnique*, 18(4), 432-448.

Melancon, J. L. (1979). "Laboratory Correlation of Soil Swell Potential." Louisiana Department of Transportation and Development, ed., Louisiana Department of Transportation and

Development In Cooperation with U.S. Department of Transportation, Federal Highway Administration, Baton Rouge, LA.

Melerski, E. S. (2006). *Design Analysis of Beams, Circular Plates and Cylindrical Tanks on Elastic Foundations*, Taylor and Francis.

Miao, S., Shen, Z., Wang, X., Luo, F., Huang, X., and Wei, C. (2017). "Stabilization of Highly Expansive Black Cotton Soils by Means of Geopolymerization." *Journal of Materials in Civil Engineering*, 29(10).

Miranda, C., and Nair, K. (1966). "Finite beams on elastic foundation." *Journal of the Structural Division, ASCE*, 92, 131-142.

Mohammadinia, A., Arulrajah, A., Sanjayan, J., Disfani, M. M., Bo, M. W., and Darmawan, S. (2016a). "Stabilization of Demolition Materials for Pavement Base/Subbase Applications Using Fly Ash and Slag Geopolymers: Laboratory Investigation." *Journal of Materials in Civil Engineering*, 28(7).

Mohammadinia, A., Arulrajah, A., Sanjayan, J., Disfani, M. M., Bo, M. W., and Darmawan, S. (2016b). "Strength Development and Microfabric Structure of Construction and Demolition Aggregates Stabilized with Fly Ash–Based Geopolymers." *Journal of Materials in Civil Engineering*, 28(11).

Mualem, Y. (1986). "Hydraulic Conductivity of Unsaturated Soils: Prediction and Formulas." *In Methods of soil analysis. Part 1. Physical and mineralogical methods*, A. Klute., ed., American Society of Agronomy, Inc. and Soil Society of America, Inc., Wisconsin, Madison, U.S.A, 799-823.

Nelson, J. D., Chao, K. C., Overton, D. D., and Nelson, E. J. (2015). *Foundation Engineering for Expansive Soils*, John Wiley & Sons.

Ng, C. W. W., Zhan, L. T., Bao, C. G., Fredlund, D. G., and Gong, B. W. (2003). "Performance of an Unsaturated Expansive Soil Slope Subjected to Artificial Rainfall Infiltration." *Géotechnique*, 53(2), 143-157.

NMDOT (2014). "Material." *Portland Cement or Lime Treated Subgrade*, New Mexico Department of Transportation, Santa Fe, New Mexico.

Nwaiwu, C. M. O., and Nuhu, I. (2006). "Evaluation and Prediction of the Swelling Characteristics of Nigerian Black Clays." *Geotechnical & Geological Engineering*, 24(1), 45-56.

ODOT (2009). "Soil Stabilization Table." *Soil Stabilization Mix Design Procedure*, Oklahoma Department of Transportation, Oklahoma City, OK.

Ojuri, O. O., Adavi, A. A., and Oluwatuyi, O. E. (2017). "Geotechnical and environmental evaluation of lime–cement stabilized soil–mine tailing mixtures for highway construction." *Transportation Geotechnics*, 10, 1-12.

Olive, W. W., Chleborad, A. F., Frahme, C. W., Schlocker, J., Schneider, R. R., and Schuster, R. L. (1989). "Swelling Clays Map of the Conterminous United States." <https://pubs.er.usgs.gov/publication/i1940>. (28th September).

Pasternak, P. L. (1954). *On a New Method of Analysis of an Elastic Foundation by Means of Two Foundation Constants (in Russian) Gosudarstvennoe Izdatelstvo Literaturi po Stroitelstvu i Arkhitekture*, Moscow.

Peck, R. B., Hanson, W. E., and Thornburn, T. H. (1974). *Foundation Engineering*, Wiley New York.

Pham, H. Q. (2005). "A Volume-Mass Constitutive Model for Unsaturated Soils." Ph.D. Dissertation, University of Saskatchewan, Saskatchewan, Canada.

Post Tensioning Institute (2008). *Design of Post-Tensioned Slabs-on-Ground 3rd Edition with 2008 Supplement*, Post Tensioning Institute, Farmington Hills, MI, USA.

Puppala, A. J., Pedarla, A., Hoyos, L. R., Zapata, C., and Bheemasetti, T. V. (2016). "A Semi-Empirical Swell Prediction Model Formulated from 'Clay Mineralogy and Unsaturated Soil' Properties." *Engineering Geology*, 200, 114-121.

Reissner, E. (1958). "A note on deflections of plates on a viscoelastic foundation." *Journal of Applied Mechanics*, 25(1), 144-145.

Rupnow, T. D., Icenogle, P., and Reech, S. (2011). "Evaluation of Cement and Fly Ash Treated Recycled Asphalt Pavement and Aggregates for Base Construction." Louisiana Transportation Research Center, Baton Rouge, LA, 1-68.

Sabat, A. K. (2012a). "Stabilization of Expansive Soil using Waste Ceramic Dust " *Electronic Journal of Geotechnical Engineering*, 17, 3915-3926.

Sabat, A. K. (2012b). "A Study on Some Geotechnical Properties of Lime Stabilised Expansive Soil –Quarry Dust Mixes." *International Journal of Emerging trends in Engineering and Development* 1(2), 42-49.

Scanlon, B. R., Andraski, B. J., and Bilskie, J. (2002). "Bulk Density and Linear Extensibility." *Methods of Soil Analysis: Part 4 Physical Methods*, J. H. Dane, and C. G. Topp, eds., Soil Science Society of America, Madison, WI, 643-670.

Seed, H. B., Woodward Jr, R. J., and Lundgren, R. (1962). "Prediction of Swelling Potential for Compacted Clays." *Journal of the soil mechanics and foundations division*, 88(3), 53-88.

Selvadurai, A. P. S. (2013). *Elastic Analysis of Soil-Foundation Interaction: Development of Geotechnical Engineering*, Elsevier Scientific Publishing Company, New York.

Skempton, A. W. (1953). "The Colloidal Activity of Clays." *Selected Papers on Soil Mechanics*, 106-118.

Snethen, D. R. "Characterization of Expansive Soils using Soil Suction Data." *Proc., 4th International Conference on Expansive Soils*, ASCE, 54-75.

Snethen, D. R. (1986). "Expansive Soils: Where Are We?", National Research Council Communication on Ground Failure Hazards and National Research Council, Washington, D.C., 12–16.

Snethen, D. R., Towsend, F. C., Johnson, l. D., Patrick, D. M., and Vedros, P. J. (1975). "A Review of Engineering Experiences with Expansive Soils in Highway Subgrades." Army Engineer Waterways Experiment Station, Vicksburg, Mississippi, 135.

Systat Software Inc. 2016. SigmaPlot 13, version 13, San Jose, California.

Terzaghi, K., Peck, R. B., and Mesri, G. (1996). *Soil Mechanics in Engineering Practice*, John Wiley & Sons, New York, USA.

Ting, B.-Y. (1982). "Finite Beams on Elastic Foundation with Restraints." *Journal of the Structural Division*, 108(3), 611-621.

Tourtelot, H. A. "Geologic Origin and Distribution of Swelling Clays." *Proc., Workshop on Expansive Clay and Shale in Highway Design and Construction*.

Tsudik, E. (2012). *Analysis of Structures on Elastic Foundations*, J. Ross Publishing.

Tu, H. Y., and Vanapalli, S. K. (2015). "Prediction of 1-D Heave of a Natural Expansive Soil Slope of Zao-Yang in China Using the SWCC-Based and Water Content-Based Models." *Unsaturated Soil Mechanics-from Theory to Practice*, C. W. Zhenghan Chen, De´an Sun, and Xongfu Xu, ed., CRC Press, Guilin, China, 497-502.

TxDOT (2005a). "Additive Selection Criteria." *Subgrade Treatment*, Texas Department of Transportation, Austin, Texas.

TxDOT (2005b). "Additive Selection Criteria." *Base Material treatment*, Texas Department of Transportation, Austin, Texas.

TxDOT (2005c). "Base Material Treatment." *Guidelines for Modification and Stabilization of Soils and Base for Use in Pavement Structures*, TxDOT, Texas.

Umansky, A. A. (1933). *Analysis of Beams on Elastic Foundation*, Central Research Institute of Auto-Transportation, Leningrad, Russia.

Uniform Building Code (1997). "ICBO: Uniform Building Code (1997)." International Conference of Building Officials, Whittier, CA.

USDA (2013). "Web Soil Survey." *Soil Series Extent Mapping Tool*, <http://apps.cei.psu.edu/soiltool/>. (28th September, 2016).

Van Genuchten, M. T. (1980). "A Closed-Form Equation for Predicting the Hydraulic Conductivity of Unsaturated Soils." *Soil science society of America journal*, 44(5), 892-898.

Vanapalli, S. K., Fredlund, D. G., Pufahl, D. E., and Clifton, A. W. (1996). "Model for the Prediction of Shear Strength with Respect to Soil Suction." *Canadian Geotechnical Journal*, 33(3), 379-392.

Vesic, A. S. "Beams on Elastic Subgrade and the Winkler's Hypothesis." *Proc., 5th International Conference on Soil Mechanics and Foundation Engineering*, 845-850.

Wang, L. (2002). "Cementitious Stabilization of Soils in the Presence of Sulfate." Ph.D. Dissertation, Louisiana State University, Baton Rouge.

Winkler, E. (1867). "Die Lehre von der Elustizitat und Festigkeit." *Dominicus, Prague*.

Wu, Z., Chen, X., and Yang, X. (2011). "Finite Element Simulation of Structural Performance on Flexible Pavements with Stabilized Base/Treated Subbase Materials under Accelerated Loading." Louisiana Transportation Research Center, Baton Rouge, LA, 1-133.

Yin, J.-H. (2000). "Closed-Form Solution for Reinforced Timoshenko Beam on Elastic Foundation." *Journal of Engineering Mechanics*, 126(8), 868-874.

Zapata, C., Houston, S., Houston, W., and Dye, H. "Expansion Index and Its Relationship with Other Index Properties." *Proc., 4th International Conference on Unsaturated Soils*, ASCE, 2133-2137.

Zhan, L.-t., Chen, P., and Ng, C. W. W. (2007). "Effect of Suction Change on Water Content and Total Volume of an Expansive Clay." *Journal of Zhejiang University - SCIENCE A*, 8(5), 699-706.

Zhang, X. (2004). "Consolidation Theories for Saturated-unsaturated Soils and Numerical Simulation of Residential Buildings on Expansive Soils." Ph.D. Dissertation, Texas A&M University, College Station, TX.

Zornberg, J. G., Gupta, R., and Ferreira, J. A. Z. (2010). "Field Performance of Geosynthetic Reinforced Pavements over Expansive Clay Subgrades." *9th International Conference on Geosynthetics*Guarujá, Brazil, 1481-1484.